THEORY OF NEUTRON NOISE INDUCED BY SPATIALLY RANDOMLY DISTRIBUTED NOISE SOURCES

Ch. Demazière and I. Pázsit
Department of Reactor Physics
Chalmers University of Technology
SE - 412 96 Göteborg
Sweden
demaz@nephy.chalmers.se ; imre@nephy.chalmers.se

ABSTRACT

In this paper the neutron noise, induced by spatially randomly distributed noise sources is investigated. The prime example of such a case is the neutron noise induced by temperature fluctuations in a PWR core, where the temperature fluctuations in the separate channels (radial positions) are only weakly correlated and their space dependence can only be specified in a statistical sense. Solutions are given for the auto- and cross-spectra of the neutron noise, in terms of the spatial cross-spectra of the noise source (temperature fluctuations). The spatial structure of the neutron noise spectrum is investigated quantitatively as a function of the frequency and the correlation length of the perturbation. The validity of the point kinetic approximation is also investigated. It is found that in the low frequency limit, point kinetics dominates even if the noise source correlation length is zero, i.e. the noise source is completely uncorrelated in space. On the other hand, in systems of realistic sizes and at plateau frequencies, i.e. at around a few Hz, noticeable deviations occur from point kinetics if the source correlation length is much smaller than the system size. The magnitude of this deviation is only a few percents at plateau frequencies in the present 1-D model, but by extrapolation it can be expected to be much larger in realistic 2-D calculations. This latter result bears importance for the determination of the moderator temperature coefficient (MTC) with noise methods, where usually a point kinetic core response is assumed in the evaluation of measurements.

1. INTRODUCTION

In all previous noise work in reactor diagnostics, noise sources have been considered that were temporally random, but spatially deterministic. Localised perturbations such as a vibrating control

rod or an absorber of variable strength, propagating perturbations etc. all belong to this category.

However, there are cases where the spatial distribution of the noise source cannot be given in a deterministic form, only by way of spatial correlations. There are several situations when this is the case. One example is the neutron noise induced by the time- and space-dependent density or material distribution in molten salt systems, that have become potentially interesting recently as one possible candidate for accelerator-driven systems (ADS). A more relevant and timely example is the neutron noise in PWRs, induced by coolant inlet temperature fluctuations and temperature fluctuations generated inside the core. Experimental evidence confirms that the temperature fluctuations are not coherent radially in the core, rather they have a spatial statistical distribution with a relatively short (compared to the core diameter) correlation length[1]. It is then important to know the spatial properties of the neutron noise induced by such sources.

The importance of the latter fact arises because local in-core neutron noise and core-exit temperature fluctuations have been used by several groups in the past few years in order to determine the moderator temperature coefficient (MTC) by noise analysis method[2-16]. In the evaluation of such measurements, it is assumed that the temperature fluctuations are homogeneous (in a horizontal plane) in the core, and as a consequence, that the induced neutron noise can be described by point kinetics. This is the simplest generalisation of local measurements to core-wide parameters (integral quantities), such as the reactivity coefficient.

In the works cited above, it was however found that the MTC values determined from noise measurements were a factor 2 to 5 smaller than the true MTC value, obtained from traditional measurements or core calculations. This means that certain assumptions on which the evaluation of the noise measurement is made are incorrect.

This fact indicates that in order to obtain practical evaluation methods that give quantitatively correct results, the deviation of both the noise source as well as the induced neutron noise from homogeneous (point kinetic) needs to be taken into account. The spatial non-homogeneous property of the perturbation means that the induced reactivity effect will be smaller than the one based on the assumption of homogeneity of the perturbation. The consequences of this fact will be investigated in another communication. In this paper we shall only investigate the second characteristics, namely the deviation from point kinetics of the neutron noise induced by spatially incoherent, random noise sources.

To this end in Section 2 we shall start by specifying the spatial distribution of the noise sources by specifying the radial correlation structure. The axial variation will be neglected due to the axial propagation, and hence the much stronger axial coupling of the source fluctuations. As mentioned earlier, due to the finite dimensions of the system, the correlations cannot be stationary in space. To reduce the generality of the spatial correlations and to use a form that is suitable to physical interpretations, they will be described by a correlation length as well as a magnitude, expressed in form of a variance. In principle, both these functions may be dependent on the position, although in order to represent a physically possible form of the spatial correlations, they both must be relatively slowly varying functions of the position. With this source distribution as input, the auto- and cross-power spectra of the induced space-dependent neutron noise are calculated in a 1-D diffusion model (“exact solution”). In a similar manner, the neutron noise spectra can also be

given in the point kinetic approximation. From a quantitative comparison of the two solutions the validity or accuracy of the point kinetic approximation can be decided as a function of frequency and the correlation length of the perturbation (noise source).

Such a quantitative analysis will be given in Section 3. One novelty of this analysis is that in all work so far, the validity of the various reactor kinetic approximations was investigated on the spatially deterministic neutron response $\delta\phi(\boldsymbol{r}, t)$ or $\delta\phi(\boldsymbol{r}, \omega)$. In the present work such an analysis is performed on the power spectra. The results show that in the limit of low frequencies or long source (perturbation) correlation lengths (i.e. nearly homogenous perturbations) point kinetic behaviour prevails; however at the frequency range of a few Hz which is of practical interest and with correlation lengths much smaller than core radius, significant deviations from point kinetic behaviour may occur. The magnitude of the deviation at such frequencies is only a few per cents in the present study where we use a 1-D model with cross sections extracted from an operating reactor. Earlier investigations with other model problems that were performed in both one and two dimensions indicate that in a 2-D model of the present problem significant deviations from point kinetics are to be expected. In this work such deviations are demonstrated by investigating the results at higher frequencies.

2. GENERAL THEORY

We shall consider a 1-D system, with the spatial co-ordinate representing the radial position in the core. As mentioned in the introduction, the axial dependence of both the noise source and the induced neutron noise will thus be neglected. This is not correct in a real PWR where in addition to the axial propagation of the coolant, there is also generation of additional coolant temperature fluctuation in the core, and thus the axial dependence is not negligible. Nevertheless, the radial dependence of both the perturbation and the neutron noise is much more significant and thus in this study the axial dependence will be neglected.

A one-group diffusion theory approach will be employed in a homogeneous bare reactor, with one group of delayed neutrons. This approach is often quite sufficient to solve diagnostic problems. It can be easily extended to two-group theory as well as to two radial dimensions. The latter of these extensions will be used in a sequel to this work.

2.1 SPECIFICATION OF THE NOISE SOURCE

It will be assumed that the temperature fluctuations induce density fluctuations which in turn give rise to fluctuations of the absorption cross section. In practice, coolant density fluctuations will affect largely the removal cross sections, which are related to neutron moderation, but this effect can only be accounted for in a two-group approach. Thus our primary quantity of the perturbation will be the space- and time-dependent fluctuations of the cross section, $\delta\Sigma_a(\boldsymbol{r}, t)$. It is assumed that $\delta\Sigma_a(\boldsymbol{r}, t)$ is stationary and ergodic in time and has a zero expected value, i.e.

$$\langle \delta\Sigma_a(\boldsymbol{r}, t)\rangle = 0 \qquad \forall \quad r, t \tag{1}$$

where, due to temporal ergodicity, the ensemble average above can be substituted by time averages. Likewise, spectral and correlation analysis can be performed in the time domain and at least formally, the Wiener-Khinchin theorem can be applied when deriving relationships between the auto- and cross-spectra of the induced noise and the noise source.

As seen on the notations, for sake of generality and for reference in later work, we shall keep the 3-D notations in the general theory part. We shall use a one-dimensional notation only when the concrete functional form of the cases studied will be given and the quantitative analysis performed will be described in Section 3.

Unlike in the previous works in reactor diagnostics, however, in the present case the space dependence cannot be given by a deterministic function, thus $\delta\Sigma_a(\boldsymbol{r}, t)$, or its Fourier transform $\delta\Sigma_a(\boldsymbol{r}, \omega)$ cannot be given explicitly. We shall only be able to specify the cross-section fluctuations through the temporal and spatial correlations

$$C(r, \boldsymbol{r}', \tau) \equiv \langle \delta\Sigma_a(\boldsymbol{r}, t)\delta\Sigma_a(\boldsymbol{r}', t + \tau)\rangle \tag{2}$$

As the notations indicate, the process $\delta\Sigma_a(\boldsymbol{r}, t)$ is stationary in time. Due to the final radial extension of the core, no similar stationarity exists for the spatial variables.

To make further progress we assume that $C(r, \boldsymbol{r}', \tau)$ can be factorised in its space and time dependence, and further that $\delta\Sigma_a(\boldsymbol{r}, t)$ is a white noise regarding the temporal variation. This latter assumption means that the power spectrum of the perturbation is constant in frequency. This is certainly acceptable in the frequency domain of interest for MTC determination or even up to plateau frequencies since the temperature fluctuations are of a wide band character. Their cut-off frequency is usually higher than the upper limit of the plateau frequency, which is defined by the upper break frequency of the zero-reactor transfer function $G_0(\omega)$, which is at

$$\omega = \frac{\beta}{\Lambda}. \tag{3}$$

Here, β is the delayed neutron fraction and $\Lambda = (\nu\nu\Sigma_f)^{-1}$ is the prompt neutron generation time.

Thus one assumes

$$C(r, \boldsymbol{r}', \tau) = \delta(\tau)R(r, \boldsymbol{r}') \tag{4}$$

From here it immediately follows that the cross-power spectrum of the perturbation is equal to the spatial part of (4), i.e.

$$CPSD_{\delta\Sigma_a}(r, \boldsymbol{r}', \tau) = R(r, \boldsymbol{r}') \tag{5}$$

Next, it will be assumed that the spatial correlations can be further factorised into a form where one factor depends on the variable

$$\hat{r} = \frac{r + r'}{2} \tag{6}$$

and the other one primarily on $|r - r'|$ as

$$R(r, \boldsymbol{r}') = \sigma^2(\hat{r})\, f(|r - r'|) \tag{7}$$

In this factorisation it is assumed that the dependence on the variable $\hat{r}$ is weak (this will be specified shortly) whereas the dependence of $f(|r - r'|)$ on its argument is strong, such that f is a fast decaying function of the distance $|r - r'|$ on a scale length of the system size. Here in principle it is still possible that a further weak dependence of f on $\hat{r}$ is also allowed, i.e. that the decay of correlations is not uniform in the core everywhere. However this will not be denoted here for brevity, and this possibility will not be used in the quantitative work either. One of the simplest and physically realistic form of f is an exponential decay, i.e.

$$f(|r - r'|) = \frac{1}{l(\hat{r})} e^{-\frac{|r - r'|}{l(\hat{r})}} \tag{8}$$

Here $l(\hat{r})$ is the correlation length of the perturbation, in our case the temperature fluctuations in the radial direction. As an exception here we indicated that in principle, the correlation length can depend on the position in the core. It is clear however that for the above model to have any physical reality, both $\sigma^2(\hat{r})$ and $l(\hat{r})$ must be slowly varying functions of their arguments on a length scale expressed by the local correlation length $l(\hat{r})$ itself.

The above model of temperature fluctuations was taken from an earlier work[17] where it was introduced to describe spatial density correlations in two-phase flow, and later also in fusion plasma transport[18]. Its advantage is that it is non-trivial, lends an intuitive insight into the structure of the perturbation through the concept of the correlation length, and it is functionally simple enough to lead to tractable expressions with a few tunable parameters that can be given physical interpretation.

2.2 CALCULATION OF THE INDUCED NEUTRON NOISE

In one-group diffusion theory, the neutron noise

$$\delta\phi(\boldsymbol{r}, t) = \phi(\boldsymbol{r}, t) - \phi_0(\boldsymbol{r}) \tag{9}$$

with $\phi_0(\boldsymbol{r})$ being the static flux, existing in the system when the perturbation is not present, can be calculated from the time-dependent one-group diffusion equation

$$\frac{1}{v}\frac{\partial\phi(\boldsymbol{r}, t)}{\partial t} = D\nabla^2\phi(\boldsymbol{r}, t) + \nu\Sigma_f(1 - \beta)\phi(\boldsymbol{r}, t) - \Sigma_a(\boldsymbol{r}, t)\phi(\boldsymbol{r}, t) + \lambda C(\boldsymbol{r}, t)\,, \tag{10}$$

$$\frac{\partial C(\boldsymbol{r}, t)}{\partial t} = \beta\nu\Sigma_f\phi(\boldsymbol{r}, t) - \lambda C(\boldsymbol{r}, t)\,. \tag{11}$$

where

$$\Sigma_a(\boldsymbol{r}, t) = \Sigma_a + \delta\Sigma_a(\boldsymbol{r}, t) \tag{12}$$

Here all symbols have their usual meaning. Splitting up both the flux, the precursor density and the time-dependent absorption cross section fluctuations to static and fluctuating quantities as in (9) and (12), neglecting the second order term $\delta\phi(\boldsymbol{r}, t)\delta\Sigma_a(\boldsymbol{r}, t)$, subtracting the static equations and eliminating the delayed neutron precursor density fluctuations with a temporal Fourier transform, one arrives at the equation

$$\nabla^2\delta\Phi(\boldsymbol{r}, \omega) + B^2(\omega)\delta\Phi(\boldsymbol{r}, \omega) = \frac{\delta\Sigma_a(\boldsymbol{r}, \omega)\phi_0(\boldsymbol{r})}{D}, \tag{13}$$

where

$$B^2(\omega) = B_0^2 - \frac{\nu\Sigma_f}{D \cdot G_0(\omega)} = B_0^2\left[1 - \frac{1}{\rho_\infty \cdot G_0(\omega)}\right], \tag{14}$$

with $G_0(\omega)$ being the zero reactor transfer function[19-22]. Introducing the Green's function of (13) as

$$\nabla_r^2 G(\boldsymbol{r}, \boldsymbol{r'}, \omega) + B^2(\omega)G(\boldsymbol{r}, \boldsymbol{r'}, \omega) = \delta(\boldsymbol{r} - \boldsymbol{r'}), \tag{15}$$

the solution of (13) can be written as

$$\delta\phi(\boldsymbol{r}, \omega) = \frac{1}{D}\int G(\boldsymbol{r}, \boldsymbol{r'}, \omega)\phi_0(\boldsymbol{r'})\delta\Sigma_a(\boldsymbol{r}, \omega)d\boldsymbol{r'}. \tag{16}$$

Noise solutions given in the form of equations of the type (16) are usually the basis of studying the spatial structure of the neutron noise induced by a specific perturbation as well as studying the accuracy of the reactor kinetic approximations such as the point kinetic and the adiabatic approximations[19]. In our case however we need to turn to the auto- and cross-power spectra of the neutron noise since the perturbation $\delta\Sigma_a(\boldsymbol{r}, \omega)$ is not known, only its cross-spectrum (5). With a formal application of the Wiener-Khinchin theorem, which connects the Fourier transform of a stochastic process with its power spectrum, one can derive the following relationship for the auto- and cross-spectra of the neutron noise from (16) and (5):

$$APSD_{\delta\phi}(\boldsymbol{r}, \omega) = \frac{1}{D^2}\int G^*(\boldsymbol{r}, \boldsymbol{r'}, \omega)\phi_0(\boldsymbol{r'})G(\boldsymbol{r}, \boldsymbol{r''}, \omega)\phi_0(\boldsymbol{r''})R(r', r'')d\boldsymbol{r'}d\boldsymbol{r''} \tag{17}$$

and

$$CPSD_{\delta\phi}(\boldsymbol{r}_1, \boldsymbol{r}_2, \omega) = \frac{1}{D^2}\int G^*(\boldsymbol{r}_1, \boldsymbol{r'}, \omega)\phi_0(\boldsymbol{r'})G(\boldsymbol{r}_2, \boldsymbol{r''}, \omega)\phi_0(\boldsymbol{r''})R(r', r'')d\boldsymbol{r'}d\boldsymbol{r''} \tag{18}$$

Eqns (17) and (18) constitute the full formal solution of the problem. These expressions will be quantitatively evaluated in the next session with a concrete form of the Green's function and for various forms of $R(r, r')$, i.e. $\sigma^2(\hat{r})$ and $f(|r - r'|)$.

As is also known from the literature, the point kinetic approximations of (17) and (18) can be obtained from the frequency domain solution of the point kinetic equations as

$$\delta\phi^{\text{p.k.}}(\boldsymbol{r}, \omega) = \phi_0(\boldsymbol{r})\rho(\omega)G_0(\omega) \tag{19}$$

with $\rho(\omega)$ being the Fourier-transformed reactivity effect of the perturbation. From (19) one readily obtains

$$APSD_{\delta\phi}^{\text{p.k.}}(\boldsymbol{r}, \omega) = \phi_0^2(\boldsymbol{r}) \cdot APSD_\rho(\omega) \cdot \left|G_0(\omega)\right|^2 \tag{20}$$

and

$$CPSD_{\delta\phi}^{\text{p.k.}}(\boldsymbol{r}, \boldsymbol{r}', \omega) = \phi_0(\boldsymbol{r})\phi_0(\boldsymbol{r}') \cdot APSD_\rho(\omega) \cdot \left|G_0(\omega)\right|^2 \tag{21}$$

The auto-power spectral density $APSD_\rho(\omega)$ of the reactivity fluctuations can be obtained from the first order perturbation formula

$$\rho(t) = -\frac{\int \phi_0^2(\boldsymbol{r})\delta\Sigma_a(\boldsymbol{r}, t)d\boldsymbol{r}}{\nu\Sigma_f \int \phi_0^2(\boldsymbol{r})d\boldsymbol{r}} \tag{22}$$

from where it follows that

$$APSD_\rho(\omega) = \frac{\int \phi_0^2(\boldsymbol{r})\phi_0^2(\boldsymbol{r}')R(r, r')d\boldsymbol{r}d\boldsymbol{r}'}{\left[\nu\Sigma_f \int \phi_0^2(\boldsymbol{r})d\boldsymbol{r}\right]^2} \tag{23}$$

Eqns (20), (21) and (23) will be used in the quantitative evaluation of the validity of the point kinetic approximation through a comparison with eqns (17) and (18).

From (23) it is seen that as long as the spatial correlations are positive, as is assumed e.g. in (8), there is a non-zero reactivity effect of the perturbation. This is valid even in the case when the correlation length tends to zero, i.e. the perturbation is completely uncorrelated in space so that one has

$$f(|r - r'|) = \delta(|r - r'|) \tag{24}$$

in which case one obtains

$$APSD_\rho(\omega) = \frac{\int \phi_0^4(\boldsymbol{r})\sigma^2(\hat{r})d\boldsymbol{r}}{\left[\nu\Sigma_f \int \phi_0^2(\boldsymbol{r})d\boldsymbol{r}\right]^2} > 0 \tag{25}$$

An explicit relationship between the full solutions (17)-(18) and the point kinetic versions (20) and (21) can be found if the Green's functions is expanded with respect to spatial static eigenfunctions $\phi_k(r)$, obeying

$$\nabla^2\phi_k(r) + B_k^2\phi_k(r) = 0 \tag{26}$$

From (15) and (26) it is easy to show that $G(\boldsymbol{r}, \boldsymbol{r}', \omega)$ can be written as

$$G(\boldsymbol{r}, \boldsymbol{r}', \omega) = \sum_k A_k(\omega)\phi_k(r)\phi_k(r') \tag{27}$$

with

$$A_k(\omega) = \frac{1}{[B^2(\omega) - B_k^2]\int \phi_k^2(\boldsymbol{r})d\boldsymbol{r}} \tag{28}$$

In view of (14), it is seen that

$$A_0(\omega) = \frac{DG_0(\omega)}{\nu\Sigma_f\int \phi_0^2(\boldsymbol{r})d\boldsymbol{r}} \tag{29}$$

and a substitution of (27) into (17) and (18) shows that the first term of the arising series, with $k = l = 0$, yields the point kinetic approximations (20) and (21). Thus, for instance for the noise auto-spectrum one will have

$$\begin{aligned} APSD_{\delta\phi}(\boldsymbol{r}, \omega) &= APSD^{\text{p.k.}}{}_{\delta\phi}(\boldsymbol{r}, \omega) \\ &+ \sum_{k+l>0} \phi_k(r)\phi_l(r)A_k^*(\omega)A_l(\omega)\int \phi_k(r')\phi_l(r'')\phi_0(r')\phi_0(r'')R(r', r'')d\boldsymbol{r}'d\boldsymbol{r}'' \end{aligned} \tag{30}$$

and a similar expression can be obtained for $CPSD_{\delta\phi}(\boldsymbol{r}, r', \omega)$. However, in the quantitative analysis a compact analytical solution for the Green's function will be used and the validity of the point kinetic approximation will be decided by a direct comparison of (17) and (18) with (20) and (21).

Since, as (25) shows, the reactivity effect is larger than zero, from (30) it is seen that in the limit $\omega \to 0$ the point kinetic approximation becomes exact. This is because A_0 diverges with $\omega \to 0$, whereas the A_i for $i > 0$ do not. Likewise, for $l \to \infty$, i.e. homogeneous perturbation, the reactor response will be point kinetic. The question to be investigated in the next Section is thus how the point kinetic approximation deteriorates with increasing frequency and decreasing correlation lengths.

3. QUANTITATIVE ANALYSIS OF THE NOISE IN 1-D SYSTEM

The quantitative evaluation of the noise formulas was made in a 1-D homogeneous model. A bare core with dimensions $2a = 300$ cm is used. As for the material parameters, the following values were used:

Table I: Material Constants

$\nu\Sigma_f$ (cm^{-1})	Σ_a (cm^{-1})	D (cm)	λ (s)	β (pcm)	v (m/s)
0.0234	0.0227	6.15	0.0852	530	19800

With these data, $\$_\infty \equiv \rho_\infty / \beta = 5.45$. These data were obtained from two-group power reactor data, condensed to one group.

Regarding the cross-spectrum

$$CPSD(x, x', \omega) = R(x, x') = \sigma^2(\hat{x}) f(|x - x'|) \tag{31}$$

of the noise source, the following forms will be considered. For the spatial decay the form

$$f(|x - x'|) = e^{-\frac{|x - x'|}{l}} \tag{32}$$

is selected with a constant (space-independent) correlation length l. Various values of l will be used in the calculations. As mentioned earlier, for $l = \infty$ only the case $\sigma(\hat{x}) = const$ has a physical meaning. For such cases, as it is well-known, the induced reactor noise will be exactly point kinetic, since the perturbation cannot excite higher order flux eigenfunctions. This can also be seen in eqn. (30), where for $\sigma(\hat{x}) = const$ and $f = const$, the second term on the r.h.s is zero due to orthogonality of the eigenfunctions. The case $l = \infty$ is thus uninteresting and will not be shown below. In the quantitative work, the values $l = a$, $l = a/10$ and $l = a/100$ were used.

Regarding the function $\sigma(\hat{x})$, the space-dependent strength of the fluctuations, we will investigate 3 different forms:

$$\text{a) } \sigma(\hat{x}) = 1 \tag{33}$$

$$\text{b) } \sigma(\hat{x}) = \cos B_0 \hat{x}; \tag{34}$$

$$\text{c) } \sigma(\hat{x}) = \frac{1}{1 - \left(\frac{x}{(a + \delta a)}\right)^2}; \ \delta a = a/5 \tag{35}$$

The choice of the forms above is motivated by the following. Version a) is the simplest possible choice and it is the first guess if nothing is known in advance. Choice b) is based on the assumption that the strength of the temperature fluctuations is proportional to the static power density in the core, and thus the variance has the form of the static flux squared. Choice c) is based

on experimental evidence from a few measurements, in which it was found, contrary to the expectations on which assumption b) is based, that the core exit temperature fluctuations were significantly larger close to the core boundary than in the central regions[1]. Thus one purpose of the present conceptual study was to investigate the influence of two different types of non-constant noise source variance with opposite characteristics. In cases b) and c), only the short correlation length versions of $f(|x - x'|)$ were physically relevant, i.e. $l = a/10$ and $l = a/100$, for reasons mentioned earlier.

The results will be shown below in a number of Figures, for the cases listed above. In each Figure, results calculated for three different frequency values are shown. One far below the plateau region ($f = 10^{-3}$Hz), one within the plateau region ($f = 1$Hz) and one far above the plateau region ($f = 10^{3}$Hz). For practical purposes, it is the plateau frequency values that are the most important. The sub-plateau frequency case is expected to behave in a point-kinetic manner for the most cases, whereas the high-frequency case will show significant deviations from point kinetics in most cases. However, it has to be added that because of the large $\$_\infty$ of the system investigated, and the one-dimensional treatment instead of a 2-D one, the results belonging to the high-frequency case indicate what the plateau-frequency behaviour would be in a 2-D treatment.

3.1 THE CASE OF $\sigma(\hat{x}) = 1$

For the case $l = a$, quantitative results are shown in Figs 1a-1f. Fig. 1a shows the APSD values for the exact and for the point-kinetic solution together with the corresponding errors of the point-kinetic solution for the three frequencies mentioned for one half of the core. For the plateau frequency case, the point-kinetic approximation works very well. In the central part of the core, the deviations are within 0.5%,and somewhat larger deviations are only seen closer to the system boundary. Larger deviations can be seen at the high-frequency values, as predicted.

Fig. 1b shows two-dimensional plots of the absolute value of the cross-correlation function separately for the exact (termed “1-D approx.” on the figures) and the point-kinetic (termed as “0-D approx.”) solution, respectively. Fig. 1c shows the corresponding relative deviations between the two cases. The plots show the noise only for the quadrant $x, x' \in (0, a)$ for obvious reasons, and thus one actually sees the inner side of the surface shown. To expedite the comparison between the two solutions in graph form, Figs 1d-1f show the absolute value of the cross-spectra as functions of x' for various selected x values.

The conclusions for the validity of the point kinetic approximation are the same as in the case of the auto-spectra, namely that at plateau frequencies, there is no noticeable deviation from the point kinetic behaviour, whereas at high frequencies, there is a noticeable deviation.

Figures 2 and 3 show results corresponding to $l = a/10$ (15 cm) and $l = a/100$ (1.5 cm), respectively. The structure of the figures follows the same system as in Fig. 1. It can be seen that the deviations from point kinetic behaviour increase with decreasing correlation length monotonically, but at plateau frequencies it remains still quite moderate. For the case of shortest correlation length $l = 1.5$ cm (Fig. 3), the deviation from point kinetics in the central part of the core ($|x| \leq 0.5$) is still about 2%,and they increase to about 3% close to the boundary only. As a

contrast, at high frequencies the deviations are in the range of -30% at the core centre and -60% close to the boundary.

At this point it has to be mentioned that on one significant point, our analysis deviates from most other noise analysis work in the field which were published previously. In this analysis we use material constants that were extracted from two-group group-constants of a realistic PWR. This was achieved by using a core loading of the Ringhals 4 PWR and the Studsvik core master system code SIMULATE[23]. As is seen in Table I, with these data one obtains $\$_\infty \equiv \rho_\infty/\beta = 5.45$. In all earlier work, a power reactor was assumed as having $\$_\infty \approx 1$ [19, 20, 22] whereas a small compact core, in which point kinetics is nearly always valid, was associated with $\$_\infty \gg 1$. In reference 19 for instance a 1-D system with $\$_\infty = 2.127$ was classified as representing a small compact core. This has the significance that the system we investigate in this work belongs to the category that would have been classed as a small compact system with predominantly point kinetic behaviour according to earlier experience.

The significance of the value of $\$_\infty$ on the behaviour of the system can be seen from (14) by noticing that, since at plateau frequencies

$$G_0(\omega) \approx \frac{1}{\beta}, \tag{36}$$

thus one has

$$B^2(\omega) \approx B_0^2\left(1 - \frac{1}{\$_\infty}\right) \tag{37}$$

For $\$_\infty \gg 1$, $B^2(\omega) \approx B_0^2$ which explains the point kinetic response of the reactor. For $\$_\infty \leq 1$, significant deviations can be expected from point kinetics. This amounts for saying that if we had used an $\$_\infty$ value close to unity, much larger deviations from point kinetics would have occurred.

The difference between the $\$_\infty$ value used by us and that in the earlier works has several reasons, one important fact being that in the earlier works a modification of the 3-dimensional $\$_\infty$ was made to account for leakage in the neglected dimensions, which leads to a smaller value for the 1-D $\$_\infty$. Such an adjustment was not made in the present work. Thus in general the results shown here underestimate the deviations from point kinetics when comparing to a realistic 3-D case. In order to have a fair comparison with earlier results and with 2-D calculations, the high-frequency results need be considered also when judging the applicability of the point reactor approximation.

3.2 THE CASES B) AND C) FOR $\sigma(\hat{r})$

In this case only the versions $l = a/10 = 15$ cm and $l = a/100 = 1.5$ cm correspond to physically realistic perturbation. The case of $\sigma(\hat{x}) = \cos B_0\hat{x}$ for these two different correlation lengths is shown in Figures 4a-f and 5a-f. It is seen that the deviations from point kinetics are somewhat larger at plateau frequencies than for the previous case of $\sigma(\hat{x}) = const$. For case b) the deviations are approximately twice as large as in case a). Otherwise the tendencies are

relatively similar to the previous cases, in particular the fact that the point kinetic approximation underestimates the exact solution in the centre of the core and overestimates it close to the reactor boundary what regards the auto-spectrum.

The last case of

$$\sigma(\hat{x}) = \frac{1}{1-\left(\frac{x}{(a+\delta a)}\right)^2}$$

is shown for $l = 15$ cm and $l = 1.5$ cm in Figs 6 and 7, respectively. The tendencies are again similar to the previous two cases. The deviations from point kinetics are larger than for the case of $\sigma(\hat{x}) = const$ but smaller than for $\sigma(\hat{x}) = \cos B_0\hat{x}$. Again, point kinetics underestimates the exact solution at the core centre and overestimates it at the core periphery.

4. DISCUSSION AND CONCLUSIONS

From the above results it can be concluded that for noise source correlation lengths much shorter than system dimensions, noticeable deviations from point kinetics occur. On the other hand, the form of $\sigma(\hat{x})$ has a relatively weak influence on the validity of point kinetics. The deviations are moderate at plateau frequencies in the cases investigated in the present work. At any rate, they cannot explain the difference of a factor 2 to 5 between the true MTC value and the one that is determined by noise measurements. The reason for a difference of this magnitude lies mainly with other reasons, for instance the overestimation of the reactivity effect when calculated from a local measurement and assuming that the perturbation is homogeneous in the core, as mentioned earlier.

Nevertheless it has to be emphasised that due to the one dimensional treatment here, the deviations from point kinetics as it can be expected in a realistic 3-D case are definitely underestimated. As a rule, 2-D or 3-D models predict larger deviations from point kinetics than 1-D ones for the same type of perturbation and system sizes and material constants. Based on this it is safe to conclude that in a realistic 2-D model the deviations from point kinetics will be significant enough such that they must be accounted for in order to obtain a correct estimate of the MTC. This will be investigated in the continuation of this work. For the present study, the results of the 2-D calculations were estimated by considering high-frequency results also, in which case a considerable deviation from point kinetics was found.

Finally it is worth mentioning that in the cases investigated, in the auto-power spectra of the neutron noise, the deviations from point kinetics have a different sign at the core centre and at the core periphery. Thus somewhere in between, at around the core half-width $x \approx a/2$ the error is zero. This means that the errors regarding the assumption of point kinetics when evaluating the noise measurements can be minimised if the noise data in the measurements are taken at about the core half width. It will be interesting to investigate whether the same property is found in 2-D,

where the deviations from point kinetics are expected to be much larger. It will also have to be investigated how this property depends on the forms of the spatial correlation of the perturbation, e.g. how a possible space dependence of the correlation length and asymmetry of the correlations affect it.

5. ACKNOWLEDGEMENTS

This work was supported by a research grant from the Swedish Nuclear Power Inspectorate, grant No. 14.5-991060-99180.

6. REFERENCES

1. J. K-H. Karlsson, personal communication (2000).

2. E. Türkcan, *Prog. Nuc. Energy*, **9**, pp. 437 (1982).

3. G. Pór, E. Izsák, J. Valkó, "Some Results of Noise Measurements in a PWR NPP", *Prog. Nuc. Energy*, **15**, pp. 387-393 (1985).

4. J. D. Herr, J. R. Thomas Jr., "Noise Analysis for Monitoring the Moderator Temperature Coefficient of Pressurized Water Reactors: II. Experimental", *Nuc. Sci. Eng.*, **108**, pp. 241-246 (1991).

5. J. R. Thomas Jr., A. W. Clem, "PWR Moderator Coefficient via Noise Analysis: Time Series Methods", Proc. SMORN VI, Gatlinburg, Tennessee, USA, Vol. 1, pp. 34.01-34.12 (May 19-24, 1991).

6. R. Oguma, B-G. Bergdahl, B. Liao, J. Lorenzen, "Study of Noise Analysis Method for Estimation of Moderator Temperature Coefficient in a PWR", Proc. SMORN VII, Avignon, France, Vol. 2, pp. 32-40 (June 19-23, 1995).

7. R. Oguma, B-G. Bergdahl, B. Liao, J. Lorenzen, *Development of Moderator Temperature Coefficient Monitoring Technique Using Noise Analysis in PWRs, Result of noise analysis for measurement on 95-12-07*, EuroSim report ES-95-29, Nyköping, Sweden (1995).

8. B. R. Upadhyaya, D. J. Shieh, F. J. Sweeney, O. Glöcker, "Analysis of In-Core Dynamics in Pressurized Water Reactors with Application to Parameter Monitoring", *Prog. Nuc. Energy*, **21**, pp. 261-269 (1988).

9. L. J. Kostic, J. Runkel, D. Stegemann, "Thermohydraulics Surveillance of Pressurized

Water Reactors by Experimental and Theoretical Investigations of the Low Frequency Noise Field", *Prog. Nuc. Energy*, **21**, pp. 421-430 (1988).

10. D. J. Shieh, B. R. Upadhyaya, F. J. Sweeney, "Application of Noise Analysis Technique for Monitoring the Moderator Temperature Coefficient of Reactivity in Pressurized Water Reactors", *Nuc. Sci. Eng.*, **95**, pp. 14-21 (1987).

11. L. Kostic, A. Husemann, J. Runkel, D. Stegemann, P. Kahlstatt, "Estimation of PWR Moderator Temperature Coefficient as a Function of Neutron Noise Amplitude", Proc. SMORN VI, Gatlinburg, Tennessee, USA, Vol. 1, pp. 35.01-35.12 (May 19-24, 1991).

12. G. Pór, I. Jozsa, "Estimation of the Temperature Reactivity Coefficient in Operating Nuclear Power Plant", Proc. SMORN VII, Avignon, France, Vol. 2, pp. 41-47 (June 19-23, 1995).

13. E. Laggiard, J. Runkel, "Evaluation of the Moderator Temperature Coefficient of Reactivity in a PWR by Means of Noise Analysis", *Ann. Nucl. Energy*, **24**, pp. 411-417 (1997).

14. L. Kostic, "Monitoring of the Temperature Reactivity Coefficient at the PWR Nuclear Power Plant", *Ann. Nucl. Energy*, **24**, pp. 55-64 (1997).

15. E. Laggiard, J. Runkel, "Noise Analysis Estimation of the Moderator Temperature Coefficient for a PWR Fuel Cycle", *Ann. Nucl. Energy*, **26**, pp. 149-156 (1999).

16. Ch. Demazière, V. Arjanov, J. K-H. Karlsson, I. Pázsit, *Final Report on the Research Project Ringhals Diagnostics and Monitoring, Stage 4*, CTH-RF-145/RR-6 (1999).

17. I. Pázsit, "Two-Phase Flow Identification by Correlation Techniques", *Ann. Nucl. Energy* **13**, pp. 37-41 (1986).

18. I. Pázsit, "Density Correlations in Two-Phase Flow and Fusion Plasma Transport", *J. Phys.*, ***D*** **27**, pp. 2046-53 (1994).

19. G. Kosály, L. Meskó, I. Pázsit, "Investigations of the Possibility of Using Static Calculations (Adiabatic Approximation) in the Theory of Neutron Noise", *Ann. Nucl. Energy*, **4**, pp. 79-89 (1977).

20. I. Pázsit , G. Th. Analytis, "Theoretical Investigation of the Neutron Noise Diagnostics of Two-Dimensional Control Rod Vibrations in a PWR", *Ann. Nucl. Energy*, **7**, pp. 171-183 (1980).

21. I. Pázsit, O. Glöckler, "On the Neutron Noise Diagnostics of PWR Control Rod Vibrations I. Periodic Vibrations", *Nucl. Sci. Eng*., **85**, pp. 167-177 (1983).

22. N. S. Garis, I. Pázsit, D. C. Sahni, "Modelling of a Vibrating Reactor Boundary and

Calculation of the Induced Neutron Noise", *Ann. Nucl. Energy,* **23**, pp. 1197 - 1208 (1996).

23. J. A. Umbarger, A. S. DiGiovine, *SIMULATE-3 - Advanced Three-Dimensional Two-Group Reactor Analysis Code - User's Manual*, Studsvik Report, Studsvik of America (1992).

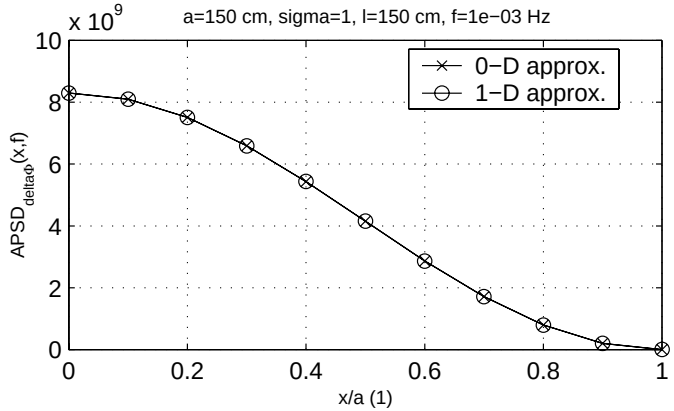
x 10^9
a=150 cm, sigma=1, l=150 cm, f=1e−03 Hz
0−D approx.
1−D approx.
APSD_deltaΦ(x,f)
x/a (1)

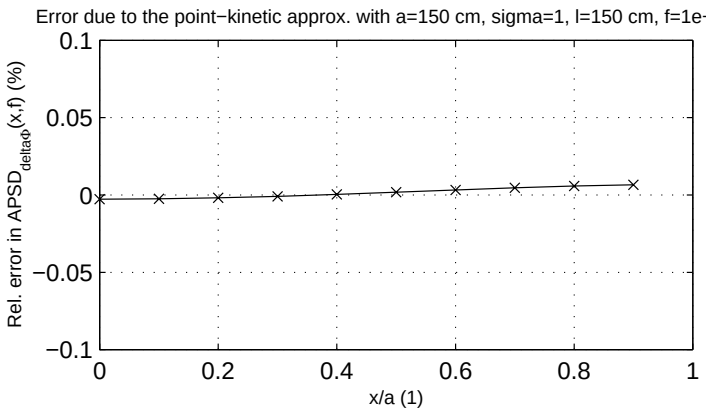
Error due to the point−kinetic approx. with a=150 cm, sigma=1, l=150 cm, f=1e−03 Hz
Rel. error in APSD_deltaΦ(x,f) (%)
x/a (1)

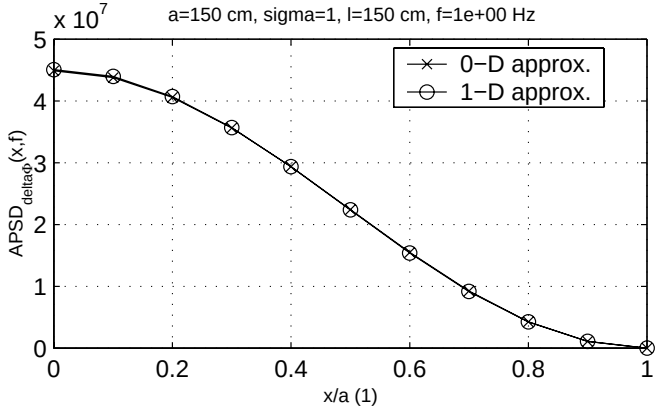
x 10^7
a=150 cm, sigma=1, l=150 cm, f=1e+00 Hz
0−D approx.
1−D approx.
APSD_deltaΦ(x,f)
x/a (1)

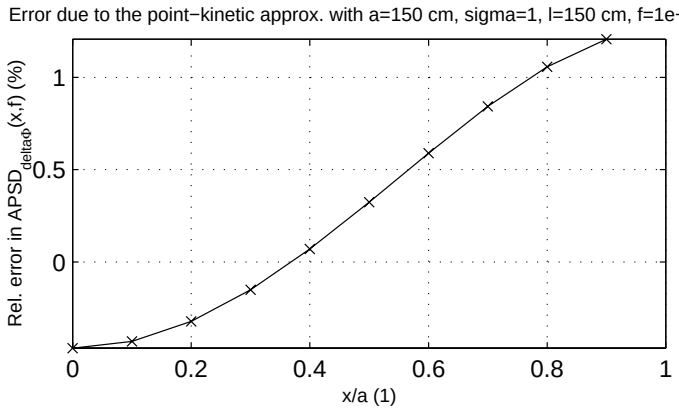
Error due to the point−kinetic approx. with a=150 cm, sigma=1, l=150 cm, f=1e+00 Hz
Rel. error in APSD_deltaΦ(x,f) (%)
x/a (1)

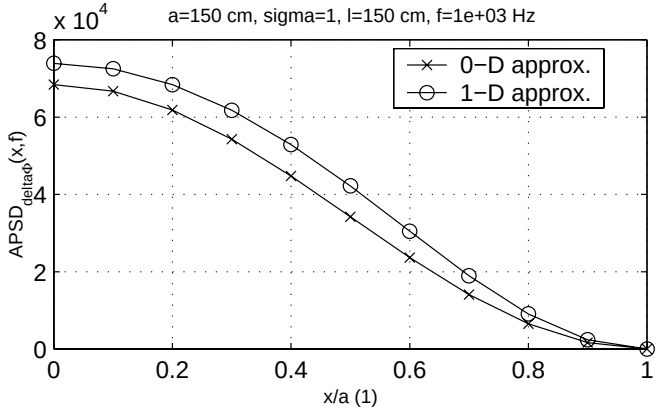
x 10^4
a=150 cm, sigma=1, l=150 cm, f=1e+03 Hz
0−D approx.
1−D approx.
APSD_deltaΦ(x,f)
x/a (1)

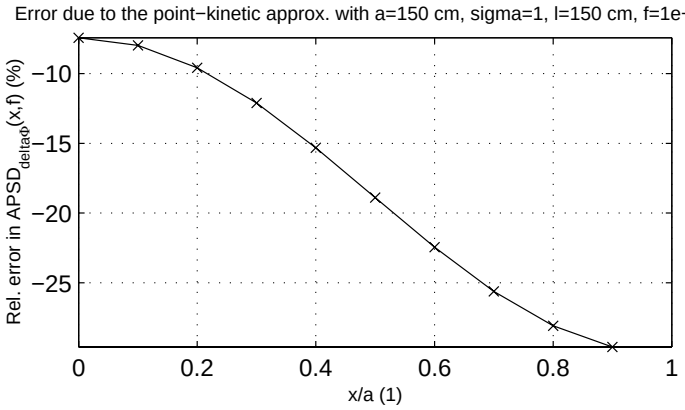
Error due to the point−kinetic approx. with a=150 cm, sigma=1, l=150 cm, f=1e+03 Hz
Rel. error in APSD_deltaΦ(x,f) (%)
x/a (1)

Fig. 1a

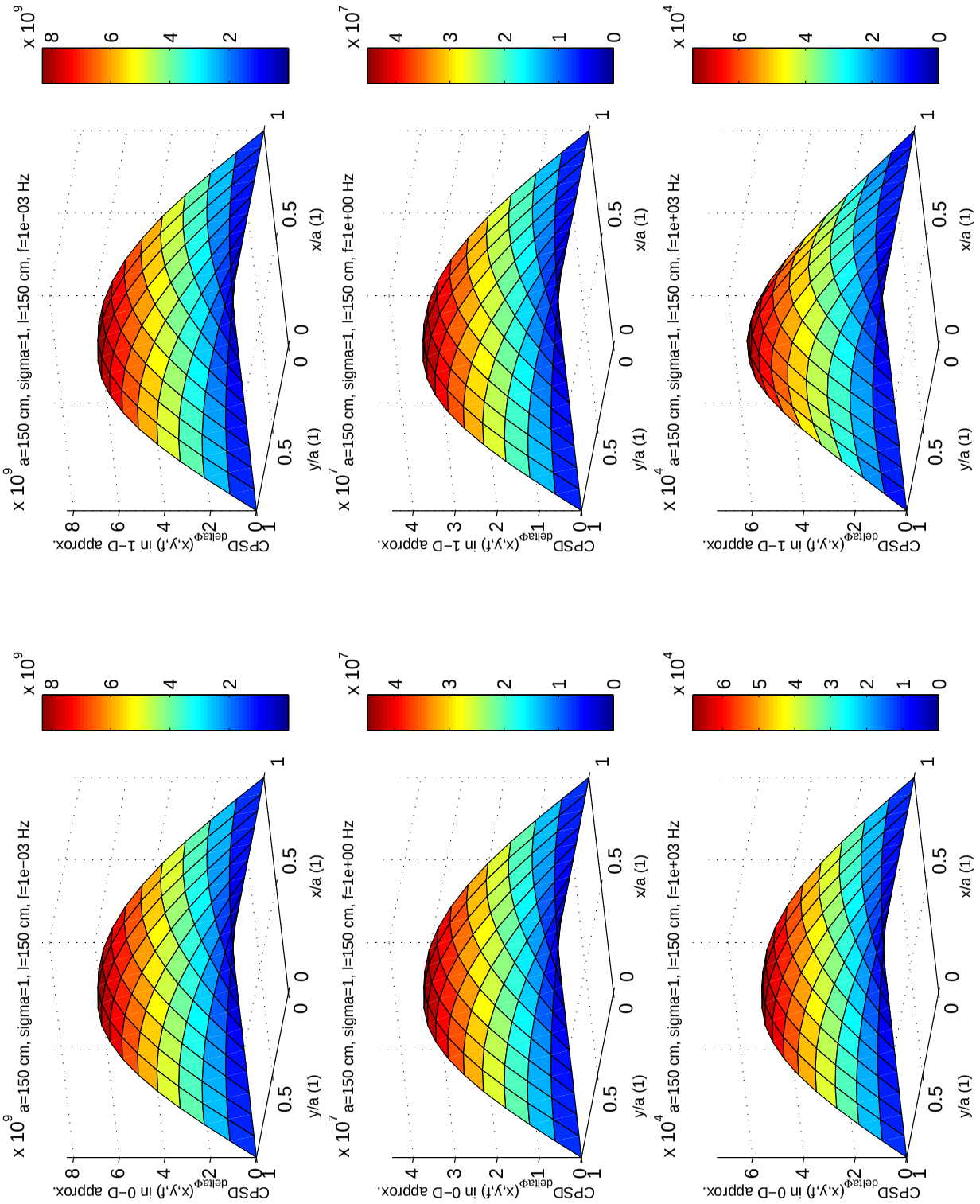
x 10^9 a=150 cm, sigma=1, l=150 cm, f=1e−03 Hz
CPSD_deltaΦ(x,y,f) in 0−D approx.
x 10^9 a=150 cm, sigma=1, l=150 cm, f=1e−03 Hz
CPSD_deltaΦ(x,y,f) in 1−D approx.
x 10^7 a=150 cm, sigma=1, l=150 cm, f=1e+00 Hz
CPSD_deltaΦ(x,y,f) in 0−D approx.
x 10^7 a=150 cm, sigma=1, l=150 cm, f=1e+00 Hz
CPSD_deltaΦ(x,y,f) in 1−D approx.
x 10^4 a=150 cm, sigma=1, l=150 cm, f=1e+03 Hz
CPSD_deltaΦ(x,y,f) in 0−D approx.
x 10^4 a=150 cm, sigma=1, l=150 cm, f=1e+03 Hz
CPSD_deltaΦ(x,y,f) in 1−D approx.
x/a (1)
y/a (1)

Fig. 1b

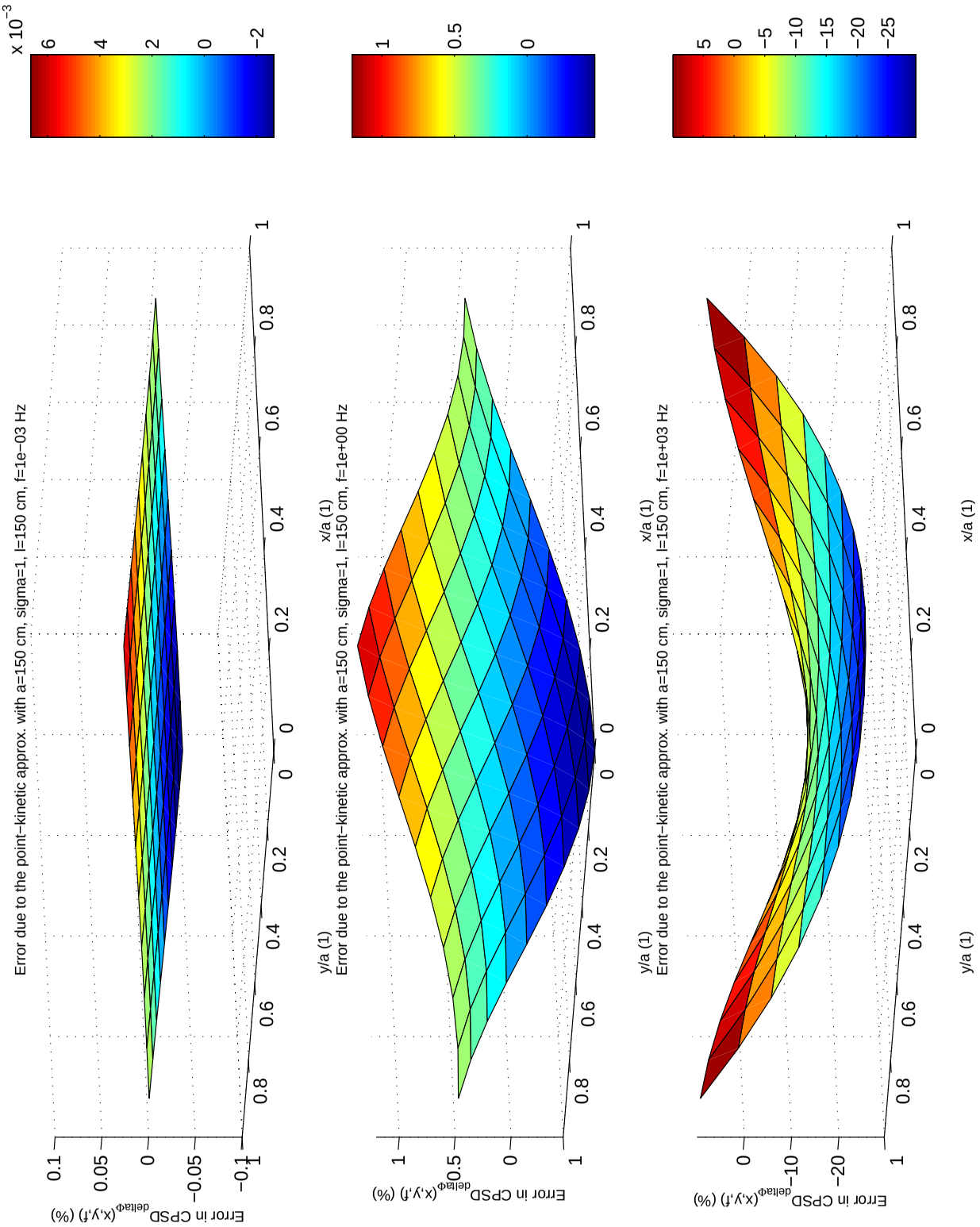
x 10^-3
6
4
2
0
−2
1
0.5
0
5
0
−5
−10
−15
−20
−25
Error due to the point−kinetic approx. with a=150 cm, sigma=1, l=150 cm, f=1e−03 Hz
Error in CPSD_deltaΦ(x,y,f) (%)
0.1
0.05
0
−0.05
−0.1
x/a (1)
y/a (1)
0
0.2
0.4
0.6
0.8
1
Error due to the point−kinetic approx. with a=150 cm, sigma=1, l=150 cm, f=1e+00 Hz
Error in CPSD_deltaΦ(x,y,f) (%)
1
0.5
0
Error due to the point−kinetic approx. with a=150 cm, sigma=1, l=150 cm, f=1e+03 Hz
Error in CPSD_deltaΦ(x,y,f) (%)
0
−10
−20

Fig. 1c

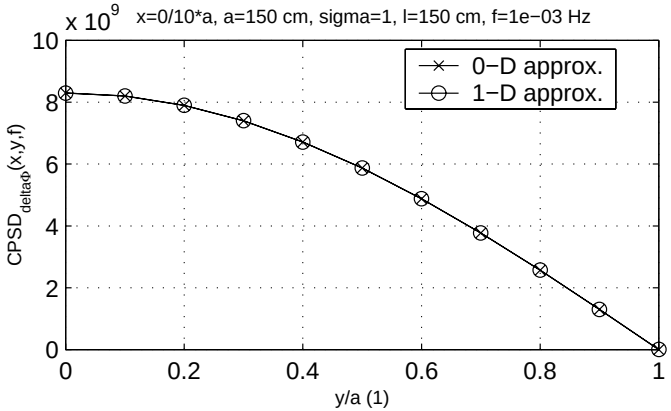
x 10^9 x=0/10*a, a=150 cm, sigma=1, l=150 cm, f=1e−03 Hz
0−D approx.
1−D approx.
CPSD_deltaΦ(x,y,f)
y/a (1)

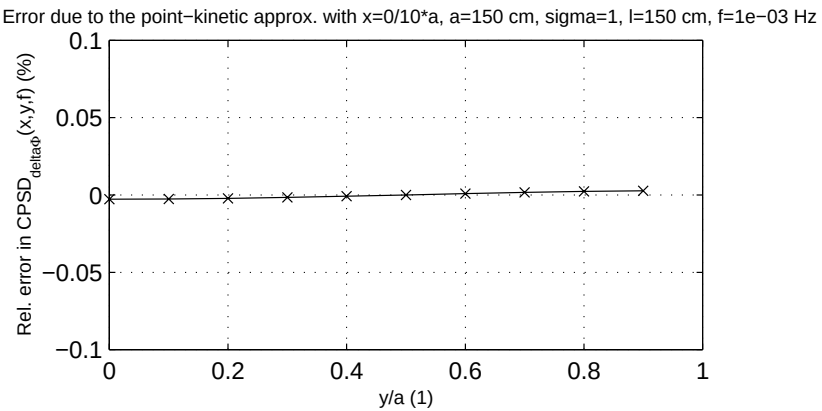
Error due to the point−kinetic approx. with x=0/10*a, a=150 cm, sigma=1, l=150 cm, f=1e−03 Hz
Rel. error in CPSD_deltaΦ(x,y,f) (%)
y/a (1)

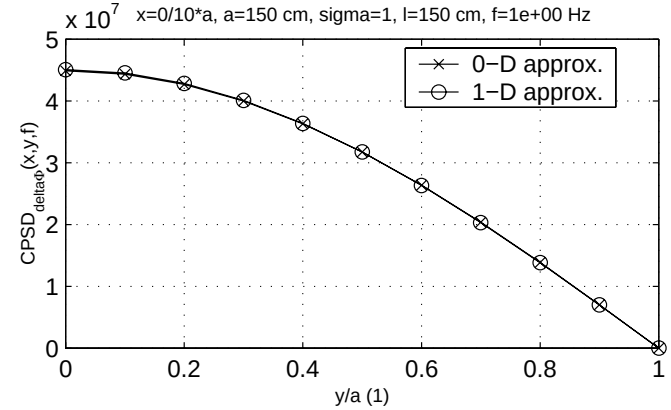
x 10^7 x=0/10*a, a=150 cm, sigma=1, l=150 cm, f=1e+00 Hz
0−D approx.
1−D approx.
CPSD_deltaΦ(x,y,f)
y/a (1)

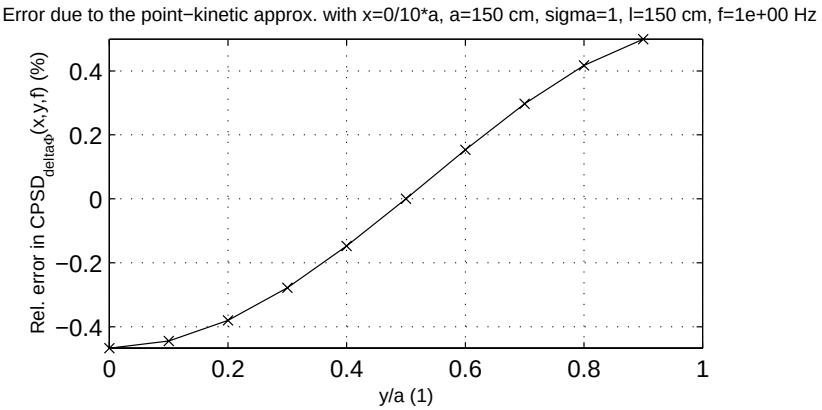
Error due to the point−kinetic approx. with x=0/10*a, a=150 cm, sigma=1, l=150 cm, f=1e+00 Hz
Rel. error in CPSD_deltaΦ(x,y,f) (%)
y/a (1)

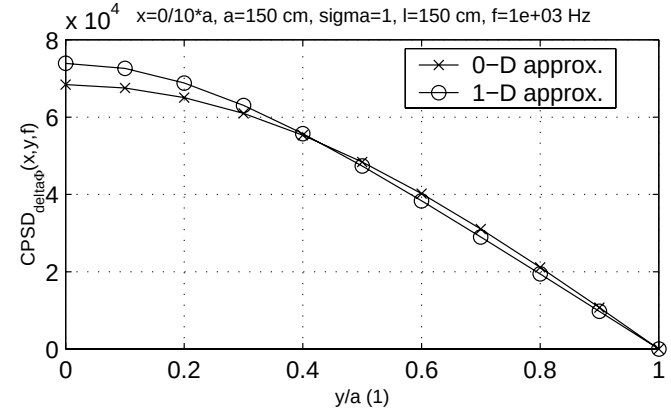
x 10^4 x=0/10*a, a=150 cm, sigma=1, l=150 cm, f=1e+03 Hz
0−D approx.
1−D approx.
CPSD_deltaΦ(x,y,f)
y/a (1)

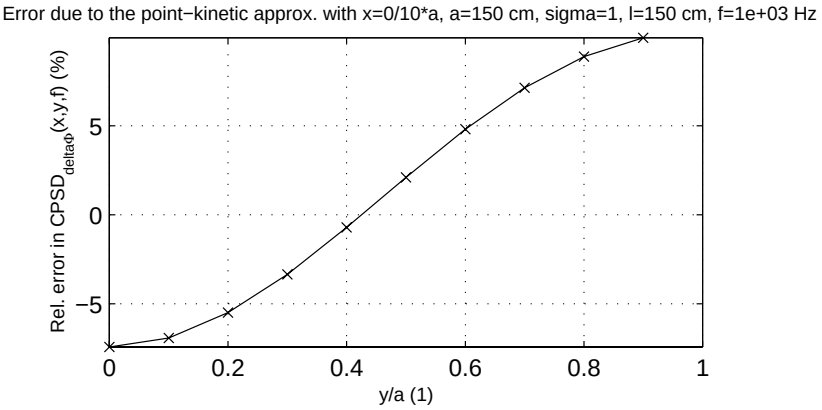
Error due to the point−kinetic approx. with x=0/10*a, a=150 cm, sigma=1, l=150 cm, f=1e+03 Hz
Rel. error in CPSD_deltaΦ(x,y,f) (%)
y/a (1)

Fig. 1d

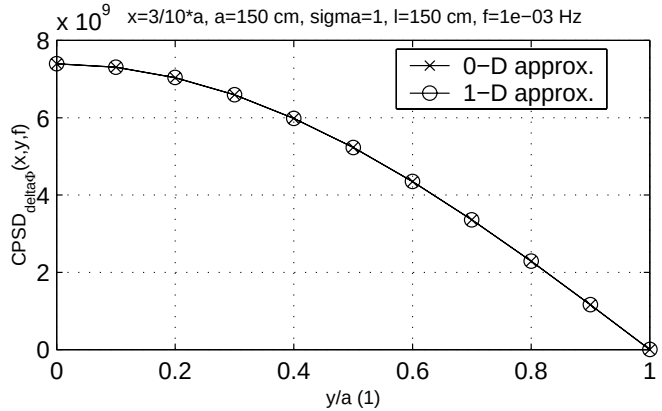
x 10^9
x=3/10*a, a=150 cm, sigma=1, l=150 cm, f=1e−03 Hz
0−D approx.
1−D approx.
CPSD_deltaΦ(x,y,f)
y/a (1)

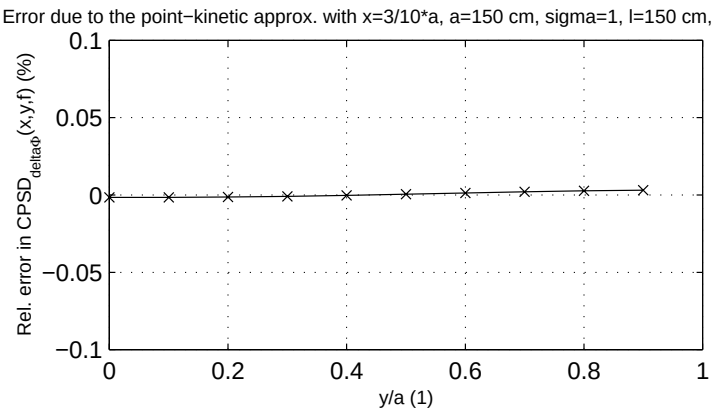
Error due to the point−kinetic approx. with x=3/10*a, a=150 cm, sigma=1, l=150 cm, f=1e−03 Hz
Rel. error in CPSD_deltaΦ(x,y,f) (%)
y/a (1)

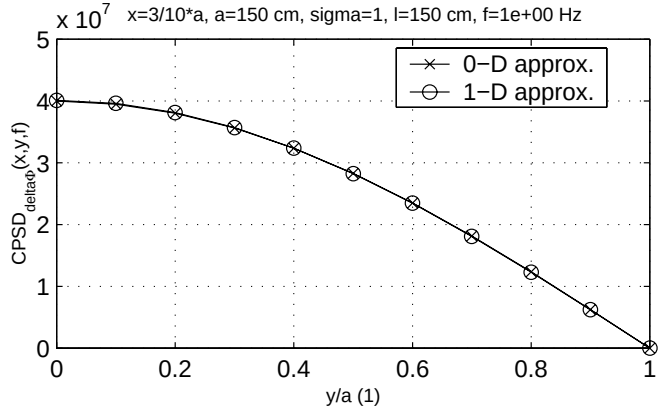
x 10^7
x=3/10*a, a=150 cm, sigma=1, l=150 cm, f=1e+00 Hz
0−D approx.
1−D approx.
CPSD_deltaΦ(x,y,f)
y/a (1)

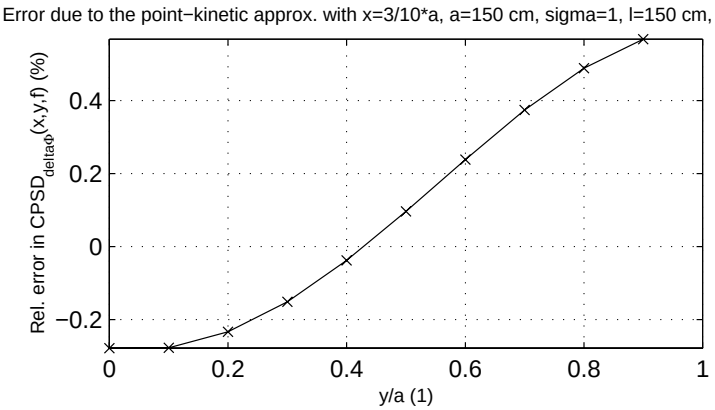
Error due to the point−kinetic approx. with x=3/10*a, a=150 cm, sigma=1, l=150 cm, f=1e+00 Hz
Rel. error in CPSD_deltaΦ(x,y,f) (%)
y/a (1)

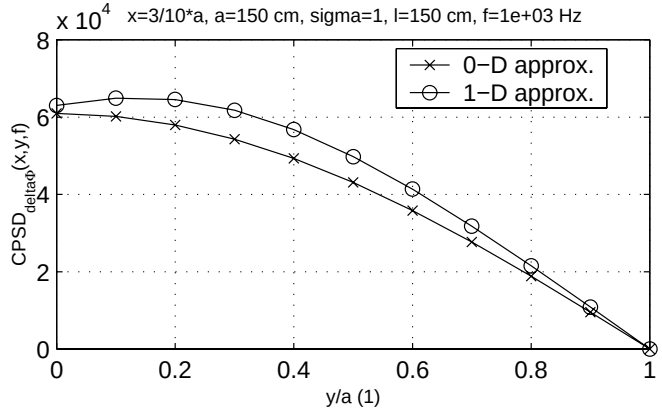
x 10^4
x=3/10*a, a=150 cm, sigma=1, l=150 cm, f=1e+03 Hz
0−D approx.
1−D approx.
CPSD_deltaΦ(x,y,f)
y/a (1)

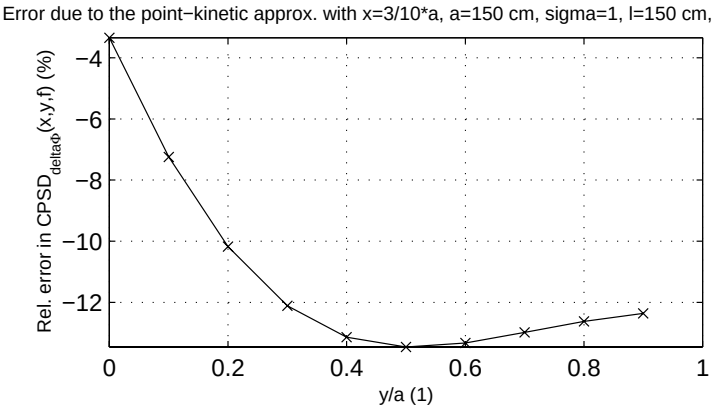
Error due to the point−kinetic approx. with x=3/10*a, a=150 cm, sigma=1, l=150 cm, f=1e+03 Hz
Rel. error in CPSD_deltaΦ(x,y,f) (%)
y/a (1)

Fig. 1e

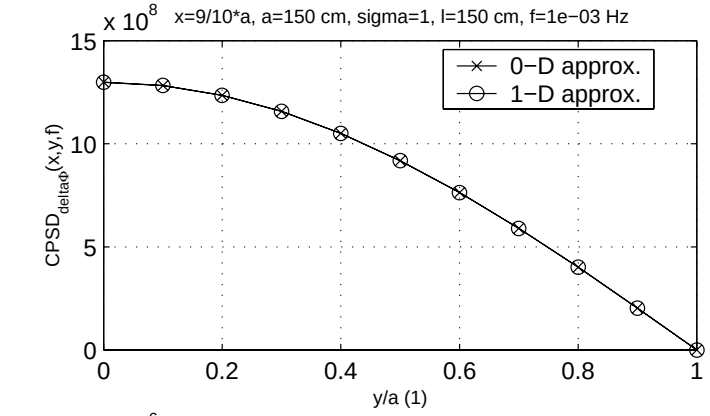
x 10^8 x=9/10*a, a=150 cm, sigma=1, l=150 cm, f=1e−03 Hz
0−D approx.
1−D approx.
CPSD_deltaΦ(x,y,f)
y/a (1)

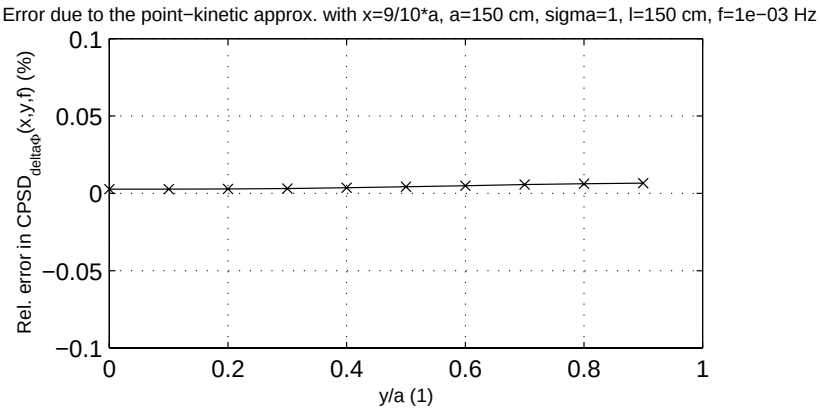
Error due to the point−kinetic approx. with x=9/10*a, a=150 cm, sigma=1, l=150 cm, f=1e−03 Hz
Rel. error in CPSD_deltaΦ(x,y,f) (%)
y/a (1)

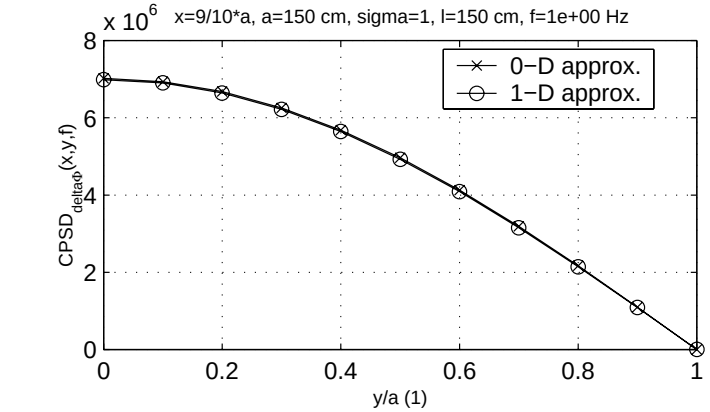
x 10^6 x=9/10*a, a=150 cm, sigma=1, l=150 cm, f=1e+00 Hz
0−D approx.
1−D approx.
CPSD_deltaΦ(x,y,f)
y/a (1)

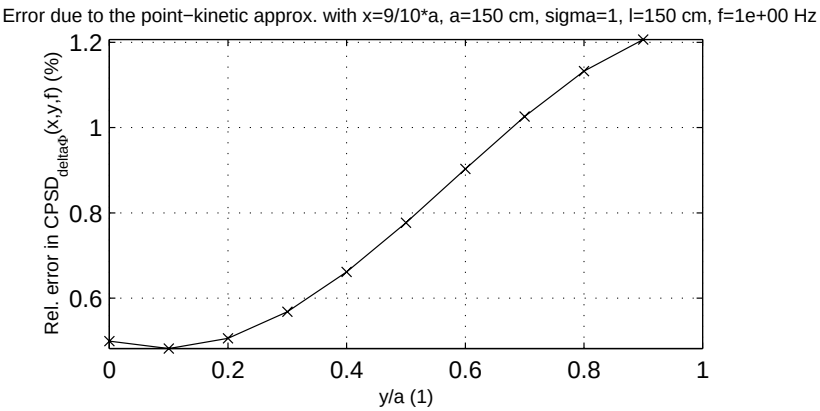
Error due to the point−kinetic approx. with x=9/10*a, a=150 cm, sigma=1, l=150 cm, f=1e+00 Hz
Rel. error in CPSD_deltaΦ(x,y,f) (%)
y/a (1)

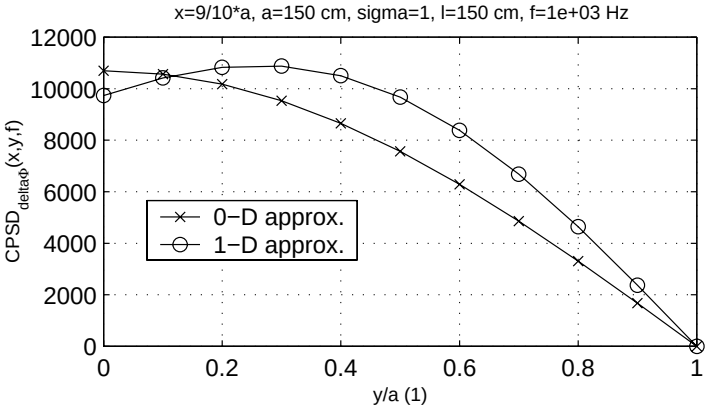
x=9/10*a, a=150 cm, sigma=1, l=150 cm, f=1e+03 Hz
0−D approx.
1−D approx.
CPSD_deltaΦ(x,y,f)
y/a (1)

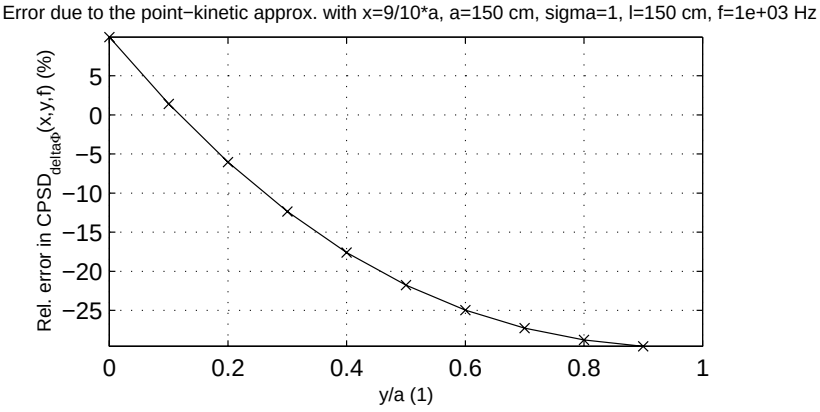
Error due to the point−kinetic approx. with x=9/10*a, a=150 cm, sigma=1, l=150 cm, f=1e+03 Hz
Rel. error in CPSD_deltaΦ(x,y,f) (%)
y/a (1)

Fig. 1f

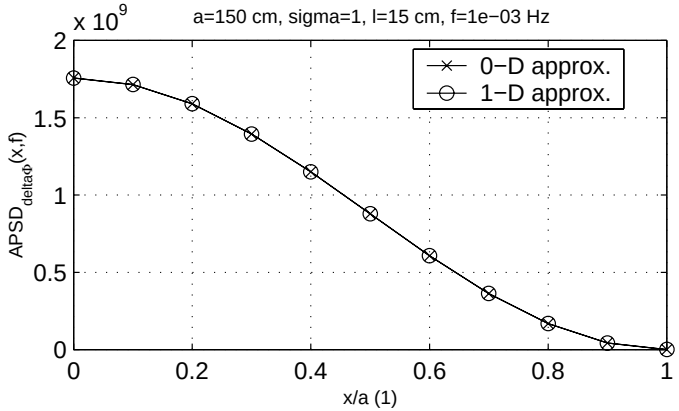
x 10^9
a=150 cm, sigma=1, l=15 cm, f=1e−03 Hz
0−D approx.
1−D approx.
APSD_deltaΦ(x,f)
x/a (1)

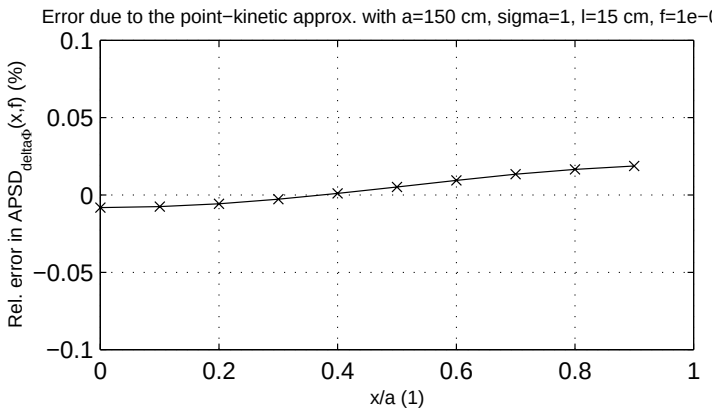
Error due to the point−kinetic approx. with a=150 cm, sigma=1, l=15 cm, f=1e−03 Hz
Rel. error in APSD_deltaΦ(x,f) (%)
x/a (1)

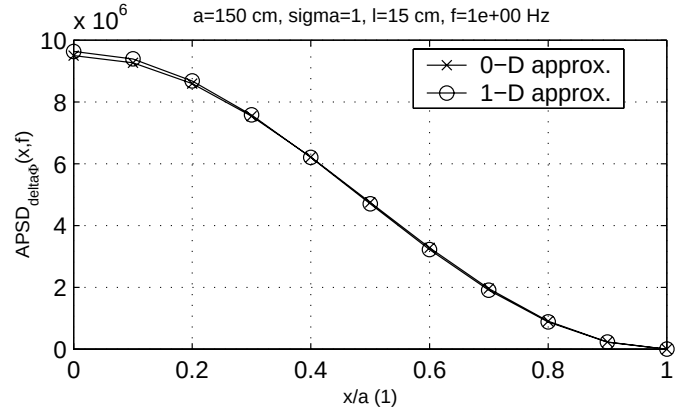
x 10^6
a=150 cm, sigma=1, l=15 cm, f=1e+00 Hz
0−D approx.
1−D approx.
APSD_deltaΦ(x,f)
x/a (1)

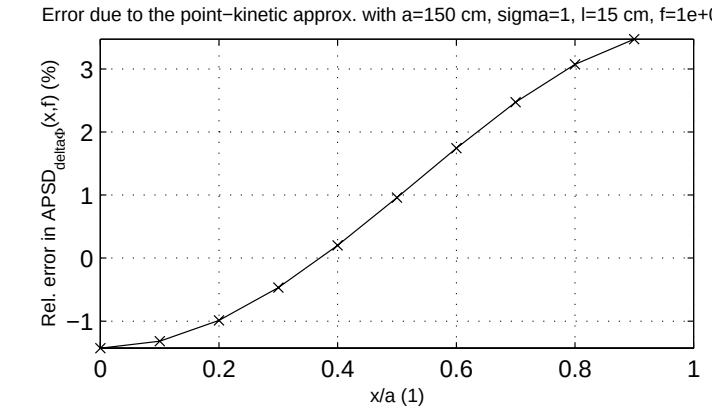
Error due to the point−kinetic approx. with a=150 cm, sigma=1, l=15 cm, f=1e+00 Hz
Rel. error in APSD_deltaΦ(x,f) (%)
x/a (1)

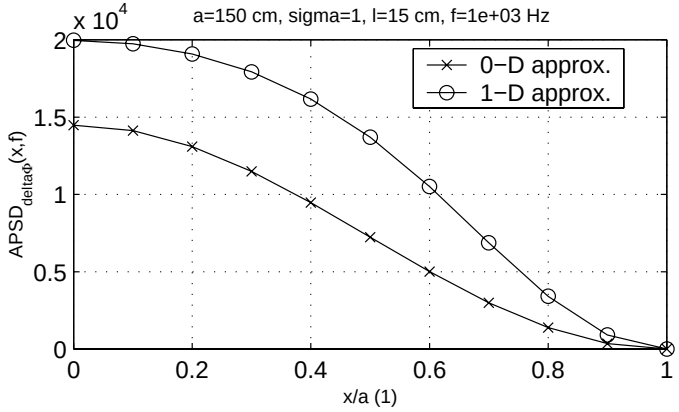
x 10^4
a=150 cm, sigma=1, l=15 cm, f=1e+03 Hz
0−D approx.
1−D approx.
APSD_deltaΦ(x,f)
x/a (1)

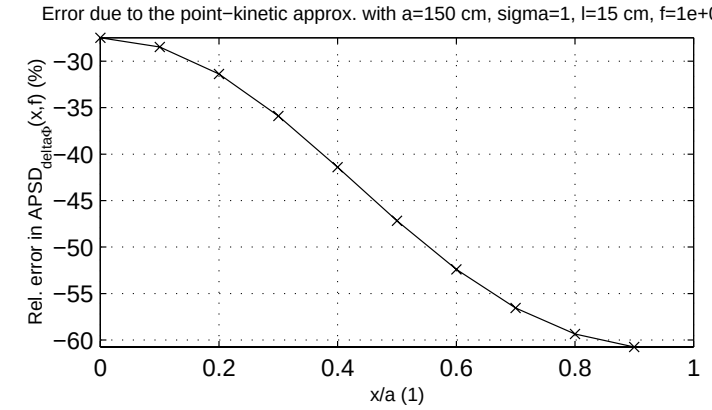
Error due to the point−kinetic approx. with a=150 cm, sigma=1, l=15 cm, f=1e+03 Hz
Rel. error in APSD_deltaΦ(x,f) (%)
x/a (1)

Fig. 2a

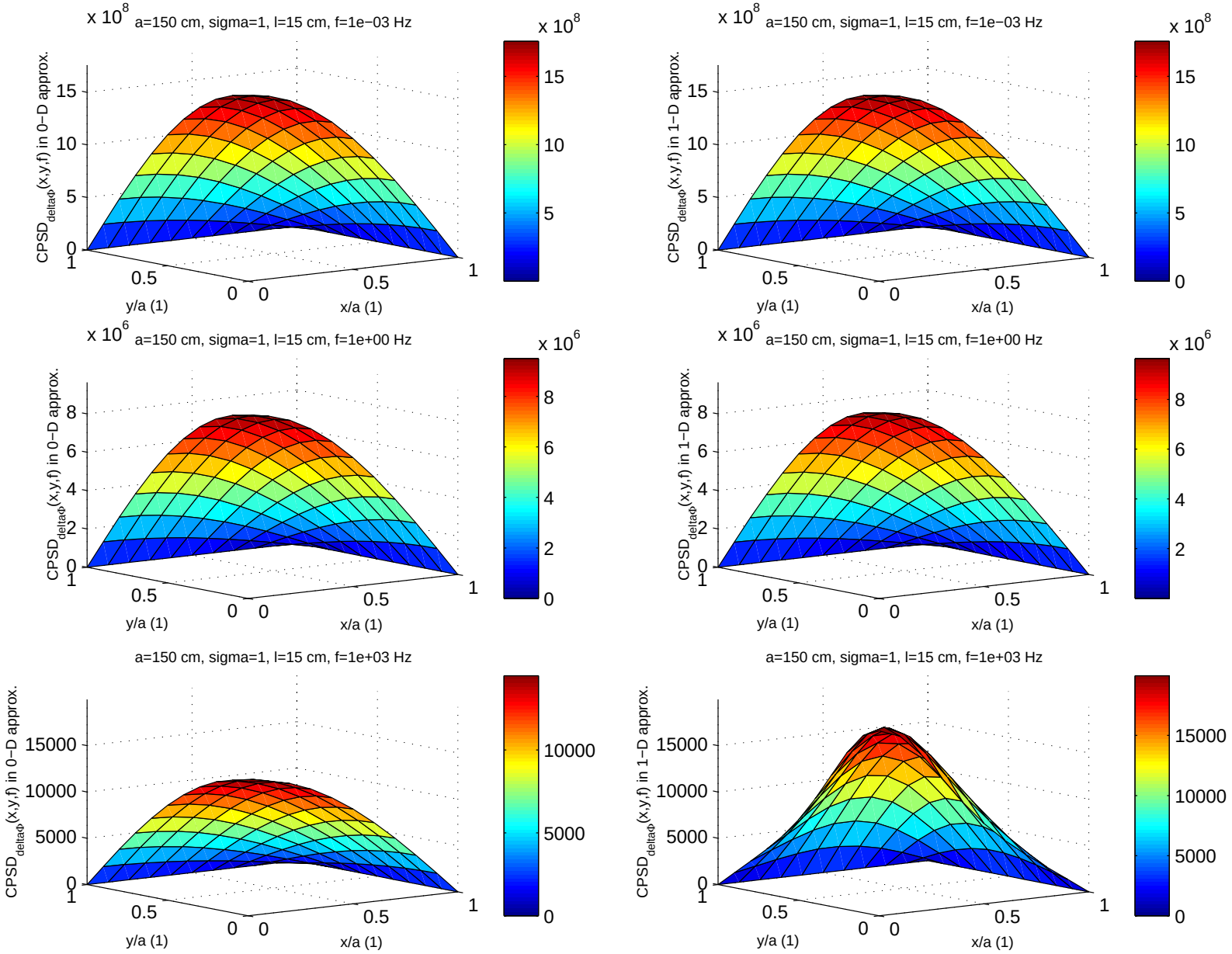
x 10^8 a=150 cm, sigma=1, l=15 cm, f=1e−03 Hz
CPSD_deltaΦ(x,y,f) in 0−D approx.
CPSD_deltaΦ(x,y,f) in 1−D approx.
y/a (1)
x/a (1)
x 10^6 a=150 cm, sigma=1, l=15 cm, f=1e+00 Hz
a=150 cm, sigma=1, l=15 cm, f=1e+03 Hz

Fig. 2b

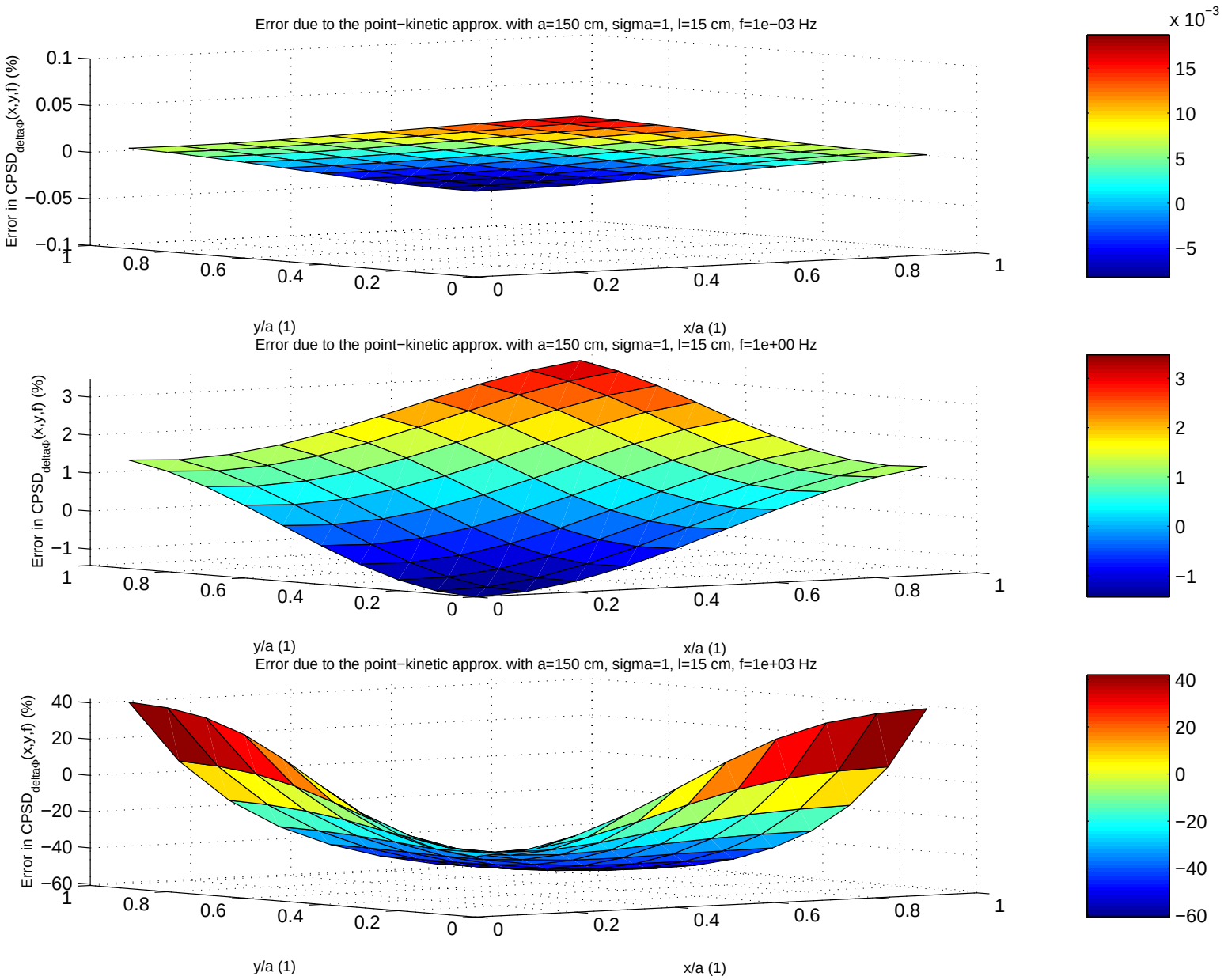
Error due to the point−kinetic approx. with a=150 cm, sigma=1, l=15 cm, f=1e−03 Hz
Error in CPSD_deltaΦ(x,y,f) (%)
0.1
0.05
0
−0.05
−0.1
x 10^−3
15
10
5
0
−5
y/a (1)
x/a (1)
Error due to the point−kinetic approx. with a=150 cm, sigma=1, l=15 cm, f=1e+00 Hz
Error in CPSD_deltaΦ(x,y,f) (%)
3
2
1
0
−1
y/a (1)
x/a (1)
Error due to the point−kinetic approx. with a=150 cm, sigma=1, l=15 cm, f=1e+03 Hz
Error in CPSD_deltaΦ(x,y,f) (%)
40
20
0
−20
−40
−60
y/a (1)
x/a (1)

Fig. 2c

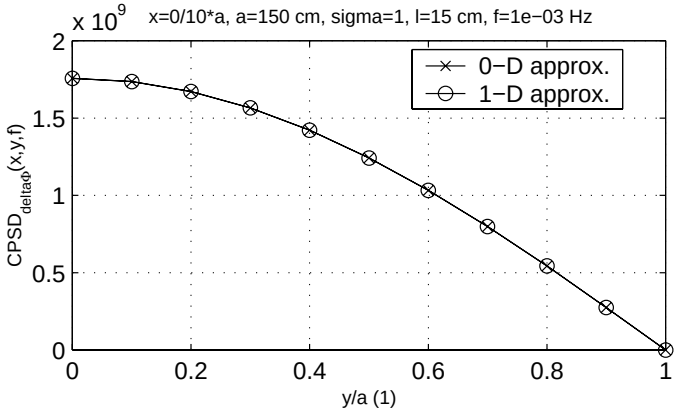
x 10^9
x=0/10*a, a=150 cm, sigma=1, l=15 cm, f=1e−03 Hz
0−D approx.
1−D approx.
CPSD_deltaΦ(x,y,f)
y/a (1)

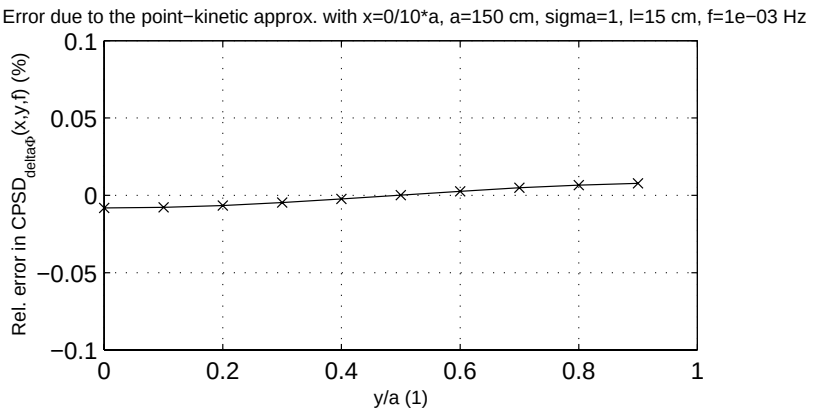
Error due to the point−kinetic approx. with x=0/10*a, a=150 cm, sigma=1, l=15 cm, f=1e−03 Hz
Rel. error in CPSD_deltaΦ(x,y,f) (%)
y/a (1)

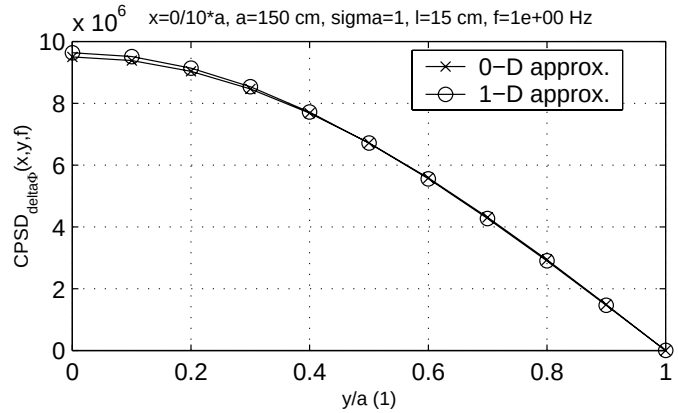
x 10^6
x=0/10*a, a=150 cm, sigma=1, l=15 cm, f=1e+00 Hz
0−D approx.
1−D approx.
CPSD_deltaΦ(x,y,f)
y/a (1)

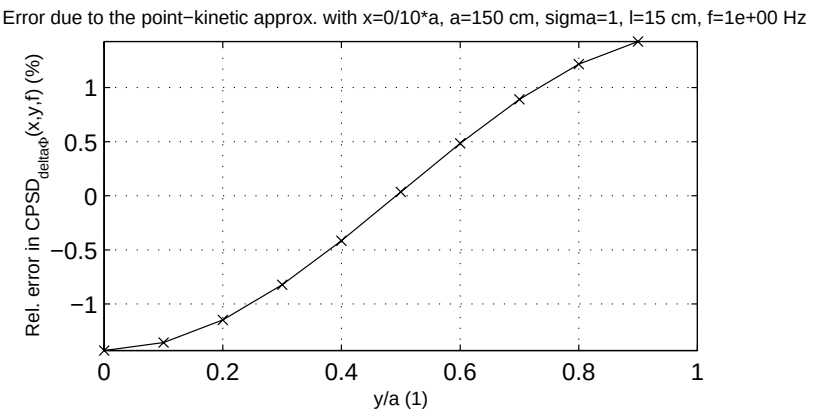
Error due to the point−kinetic approx. with x=0/10*a, a=150 cm, sigma=1, l=15 cm, f=1e+00 Hz
Rel. error in CPSD_deltaΦ(x,y,f) (%)
y/a (1)

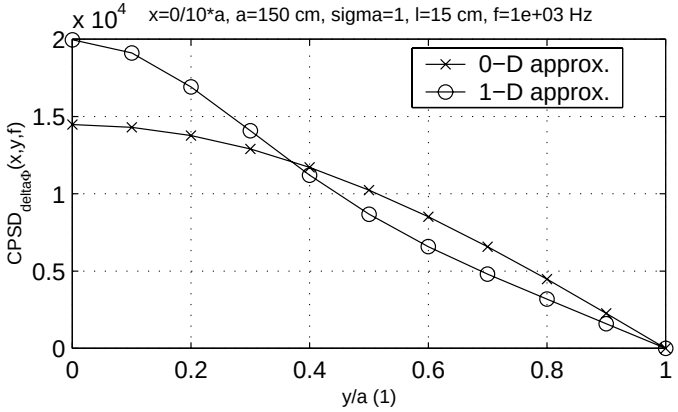
x 10^4
x=0/10*a, a=150 cm, sigma=1, l=15 cm, f=1e+03 Hz
0−D approx.
1−D approx.
CPSD_deltaΦ(x,y,f)
y/a (1)

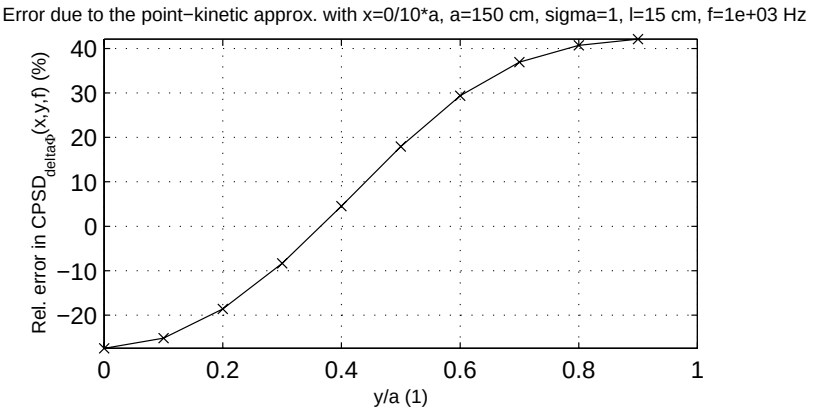
Error due to the point−kinetic approx. with x=0/10*a, a=150 cm, sigma=1, l=15 cm, f=1e+03 Hz
Rel. error in CPSD_deltaΦ(x,y,f) (%)
y/a (1)

Fig. 2d

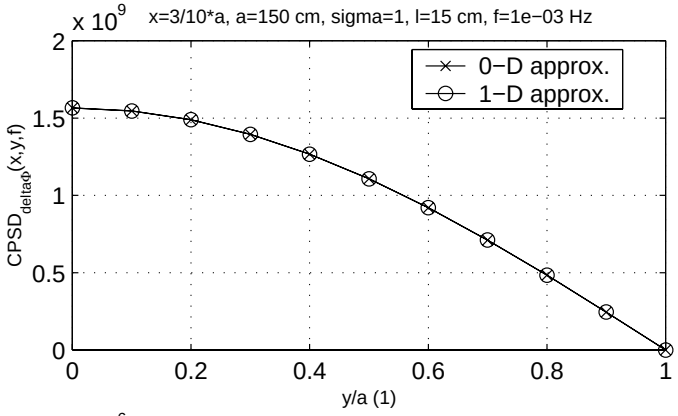
x 10^9
x=3/10*a, a=150 cm, sigma=1, l=15 cm, f=1e−03 Hz
0−D approx.
1−D approx.
CPSD_deltaΦ(x,y,f)
y/a (1)

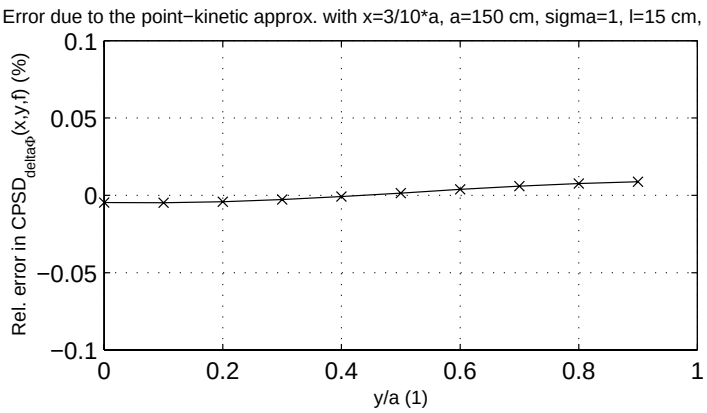
Error due to the point−kinetic approx. with x=3/10*a, a=150 cm, sigma=1, l=15 cm, f=1e−03 Hz
Rel. error in CPSD_deltaΦ(x,y,f) (%)
y/a (1)

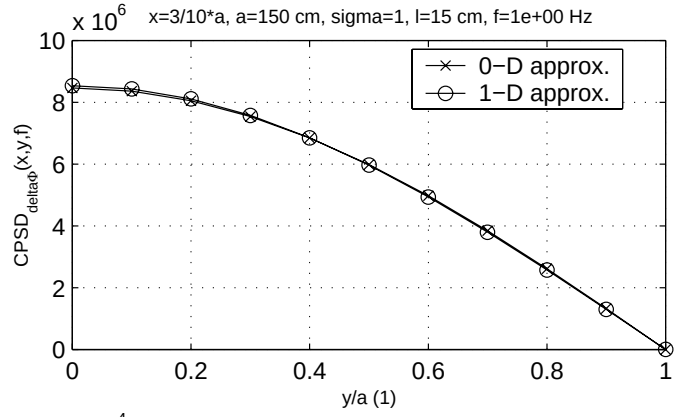
x 10^6
x=3/10*a, a=150 cm, sigma=1, l=15 cm, f=1e+00 Hz
0−D approx.
1−D approx.
CPSD_deltaΦ(x,y,f)
y/a (1)

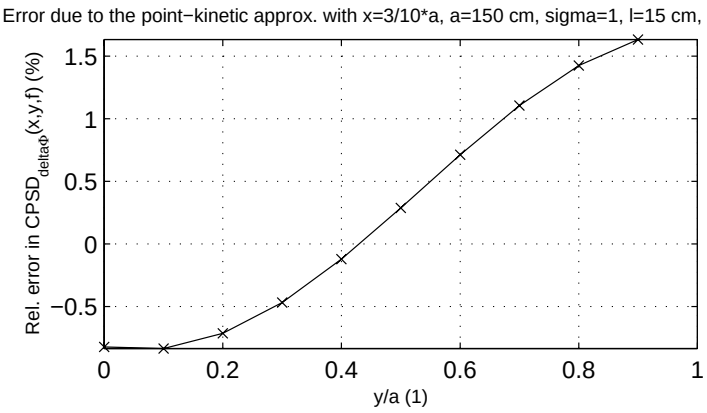
Error due to the point−kinetic approx. with x=3/10*a, a=150 cm, sigma=1, l=15 cm, f=1e+00 Hz
Rel. error in CPSD_deltaΦ(x,y,f) (%)
y/a (1)

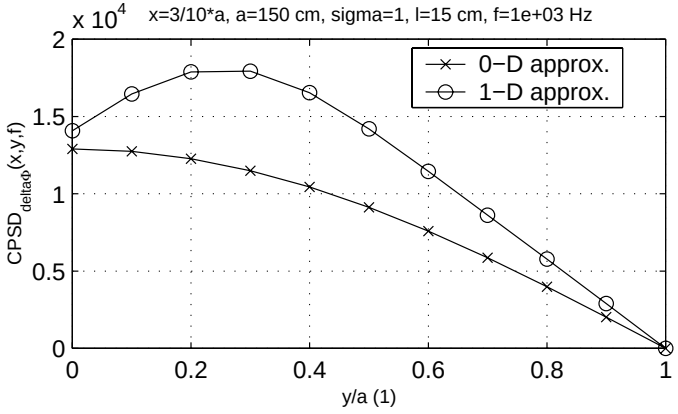
x 10^4
x=3/10*a, a=150 cm, sigma=1, l=15 cm, f=1e+03 Hz
0−D approx.
1−D approx.
CPSD_deltaΦ(x,y,f)
y/a (1)

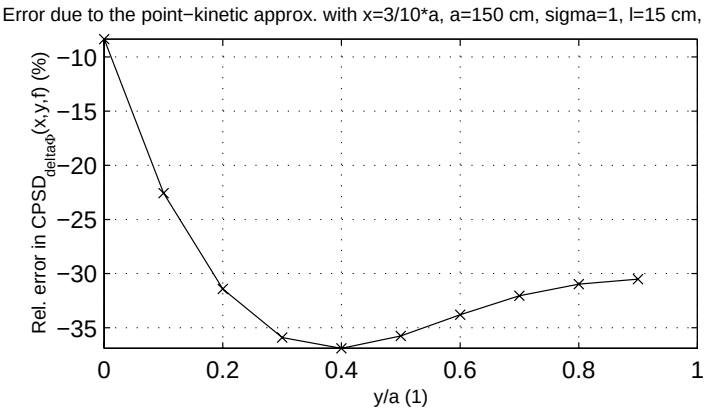
Error due to the point−kinetic approx. with x=3/10*a, a=150 cm, sigma=1, l=15 cm, f=1e+03 Hz
Rel. error in CPSD_deltaΦ(x,y,f) (%)
y/a (1)

Fig. 2e

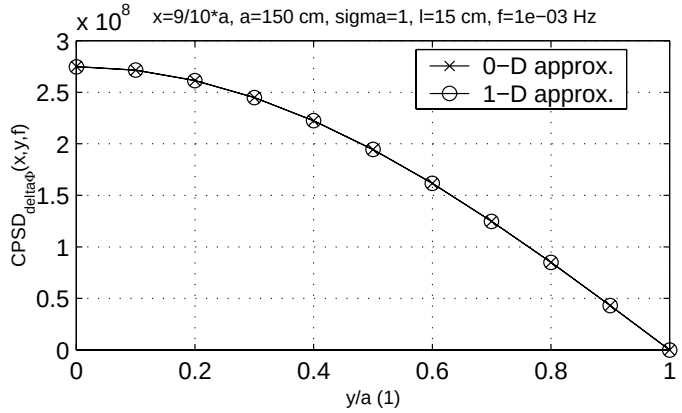
x 10^8
x=9/10*a, a=150 cm, sigma=1, l=15 cm, f=1e−03 Hz
0−D approx.
1−D approx.
CPSD_deltaΦ(x,y,f)
y/a (1)

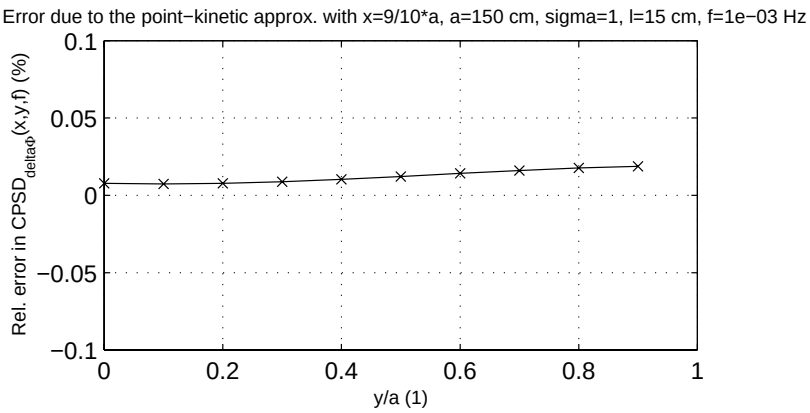
Error due to the point−kinetic approx. with x=9/10*a, a=150 cm, sigma=1, l=15 cm, f=1e−03 Hz
Rel. error in CPSD_deltaΦ(x,y,f) (%)
y/a (1)

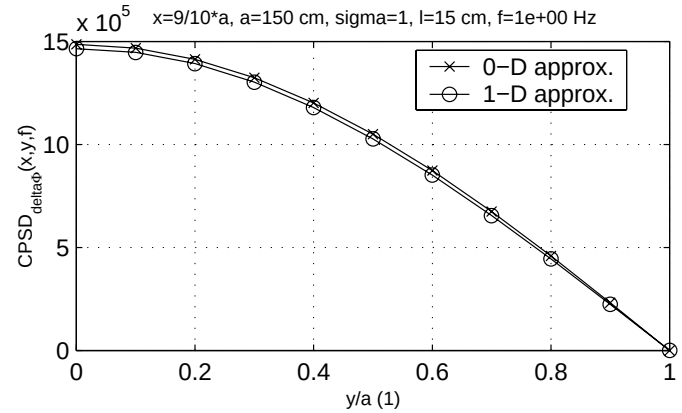
x 10^5
x=9/10*a, a=150 cm, sigma=1, l=15 cm, f=1e+00 Hz
0−D approx.
1−D approx.
CPSD_deltaΦ(x,y,f)
y/a (1)

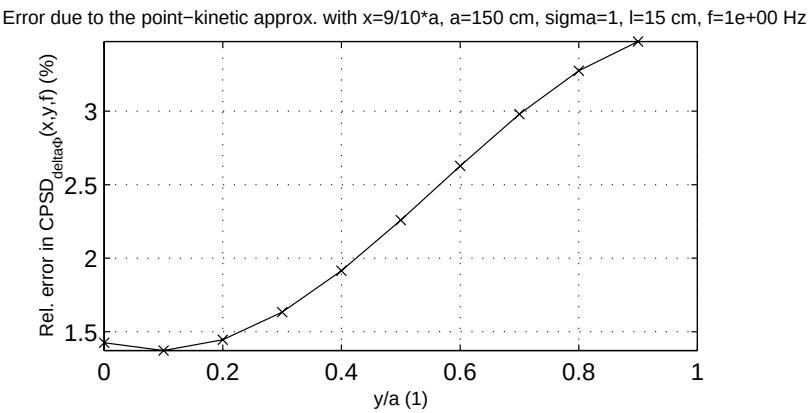
Error due to the point−kinetic approx. with x=9/10*a, a=150 cm, sigma=1, l=15 cm, f=1e+00 Hz
Rel. error in CPSD_deltaΦ(x,y,f) (%)
y/a (1)

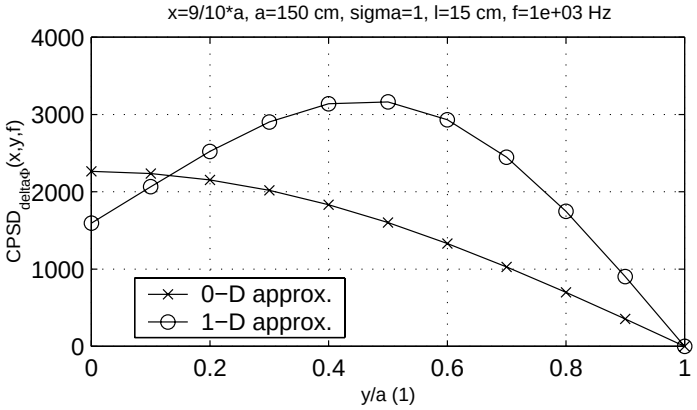
x=9/10*a, a=150 cm, sigma=1, l=15 cm, f=1e+03 Hz
0−D approx.
1−D approx.
CPSD_deltaΦ(x,y,f)
y/a (1)

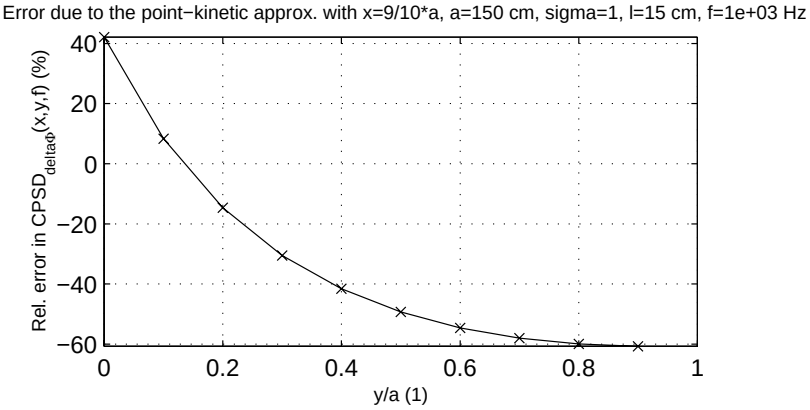
Error due to the point−kinetic approx. with x=9/10*a, a=150 cm, sigma=1, l=15 cm, f=1e+03 Hz
Rel. error in CPSD_deltaΦ(x,y,f) (%)
y/a (1)

Fig. 2f

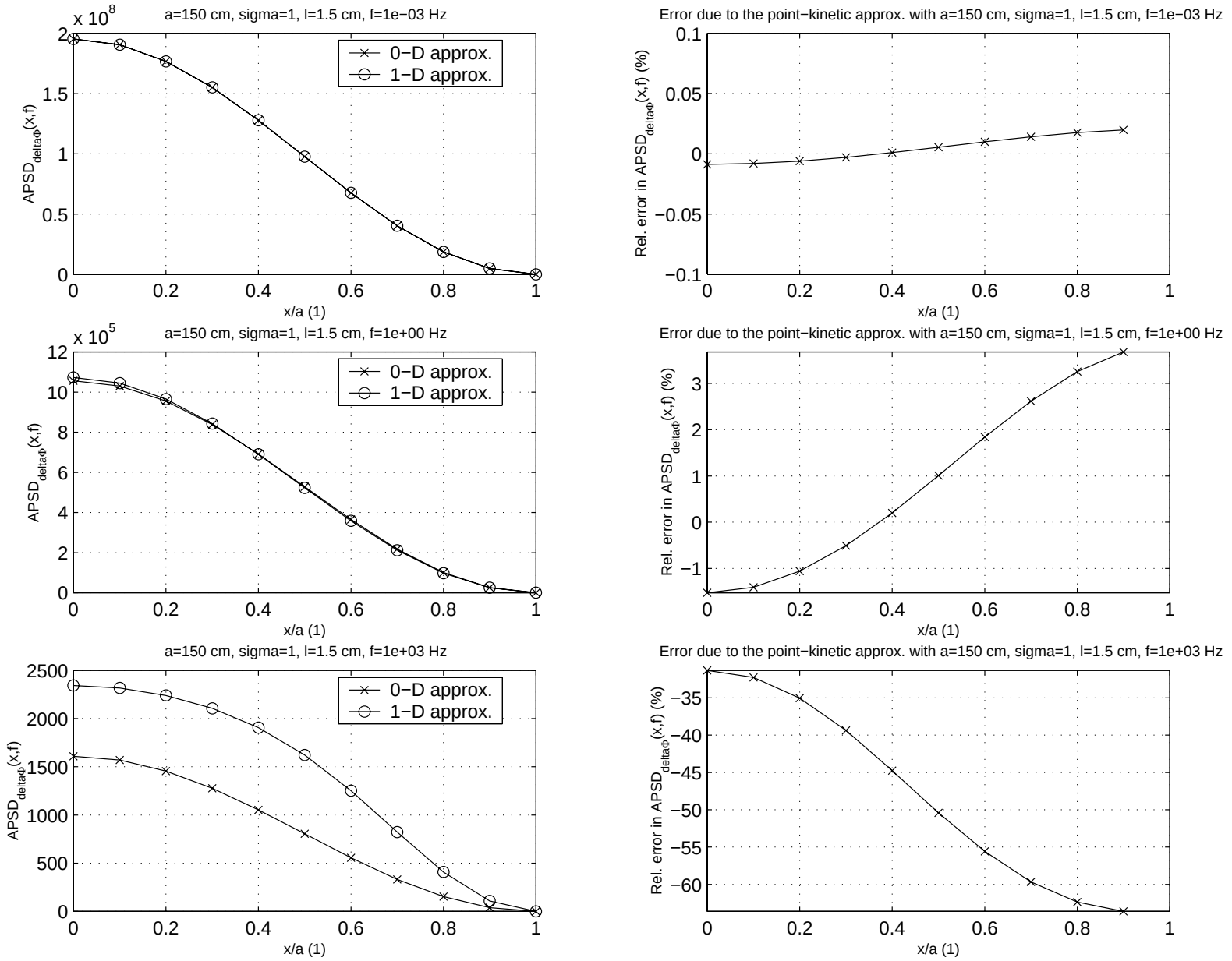
a=150 cm, sigma=1, l=1.5 cm, f=1e−03 Hz
x 10^8
0−D approx.
1−D approx.
APSD_deltaΦ(x,f)
x/a (1)
Error due to the point−kinetic approx. with a=150 cm, sigma=1, l=1.5 cm, f=1e−03 Hz
Rel. error in APSD_deltaΦ(x,f) (%)
x/a (1)
a=150 cm, sigma=1, l=1.5 cm, f=1e+00 Hz
x 10^5
0−D approx.
1−D approx.
APSD_deltaΦ(x,f)
x/a (1)
Error due to the point−kinetic approx. with a=150 cm, sigma=1, l=1.5 cm, f=1e+00 Hz
Rel. error in APSD_deltaΦ(x,f) (%)
x/a (1)
a=150 cm, sigma=1, l=1.5 cm, f=1e+03 Hz
0−D approx.
1−D approx.
APSD_deltaΦ(x,f)
x/a (1)
Error due to the point−kinetic approx. with a=150 cm, sigma=1, l=1.5 cm, f=1e+03 Hz
Rel. error in APSD_deltaΦ(x,f) (%)
x/a (1)

Fig. 3a

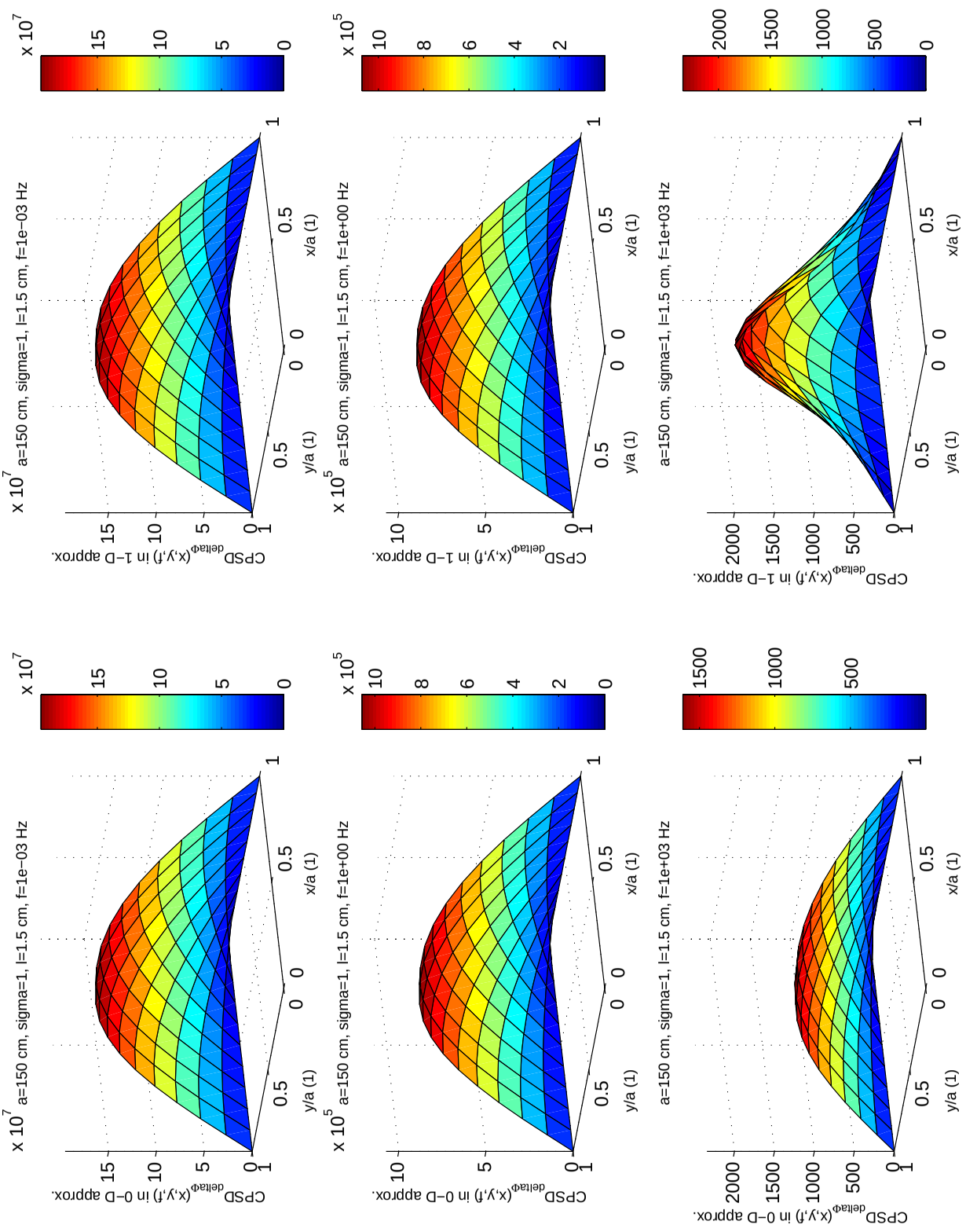
x 10^7
a=150 cm, sigma=1, l=1.5 cm, f=1e−03 Hz
CPSD_deltaφ(x,y,f) in 0−D approx.
y/a (1)
x/a (1)
x 10^5
a=150 cm, sigma=1, l=1.5 cm, f=1e+00 Hz
CPSD_deltaφ(x,y,f) in 0−D approx.
y/a (1)
x/a (1)
a=150 cm, sigma=1, l=1.5 cm, f=1e+03 Hz
CPSD_deltaφ(x,y,f) in 0−D approx.
y/a (1)
x/a (1)
x 10^7
a=150 cm, sigma=1, l=1.5 cm, f=1e−03 Hz
CPSD_deltaφ(x,y,f) in 1−D approx.
y/a (1)
x/a (1)
x 10^5
a=150 cm, sigma=1, l=1.5 cm, f=1e+00 Hz
CPSD_deltaφ(x,y,f) in 1−D approx.
y/a (1)
x/a (1)
a=150 cm, sigma=1, l=1.5 cm, f=1e+03 Hz
CPSD_deltaφ(x,y,f) in 1−D approx.
y/a (1)
x/a (1)

Fig. 3b

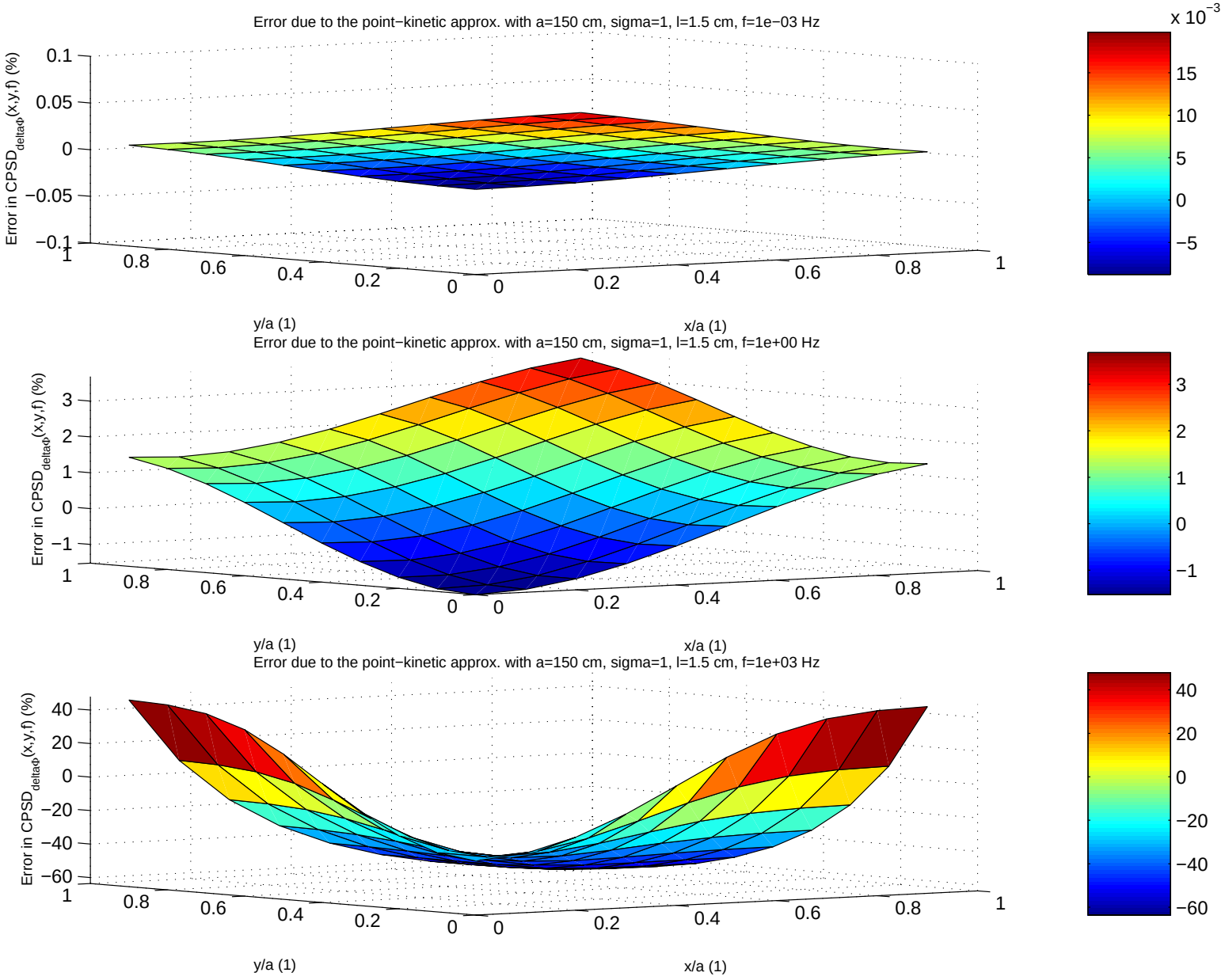
Error due to the point−kinetic approx. with a=150 cm, sigma=1, l=1.5 cm, f=1e−03 Hz
Error in CPSD_deltaΦ(x,y,f) (%)
0.1
0.05
0
−0.05
−0.1
x 10^−3
15
10
5
0
−5
y/a (1)
x/a (1)
Error due to the point−kinetic approx. with a=150 cm, sigma=1, l=1.5 cm, f=1e+00 Hz
Error in CPSD_deltaΦ(x,y,f) (%)
3
2
1
0
−1
y/a (1)
x/a (1)
Error due to the point−kinetic approx. with a=150 cm, sigma=1, l=1.5 cm, f=1e+03 Hz
Error in CPSD_deltaΦ(x,y,f) (%)
40
20
0
−20
−40
−60
y/a (1)
x/a (1)

Fig. 3c

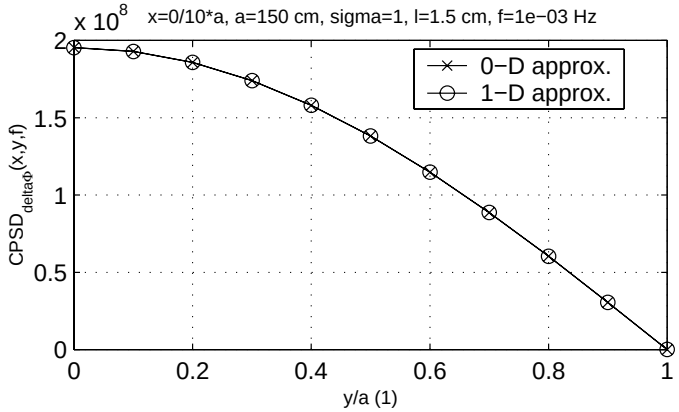
x 10^8
x=0/10*a, a=150 cm, sigma=1, l=1.5 cm, f=1e−03 Hz
0−D approx.
1−D approx.
CPSD_deltaΦ(x,y,f)
y/a (1)

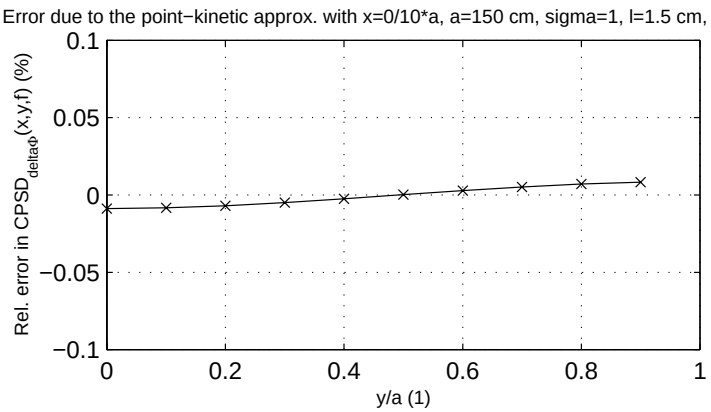
Error due to the point−kinetic approx. with x=0/10*a, a=150 cm, sigma=1, l=1.5 cm, f=1e−03 Hz
Rel. error in CPSD_deltaΦ(x,y,f) (%)
y/a (1)

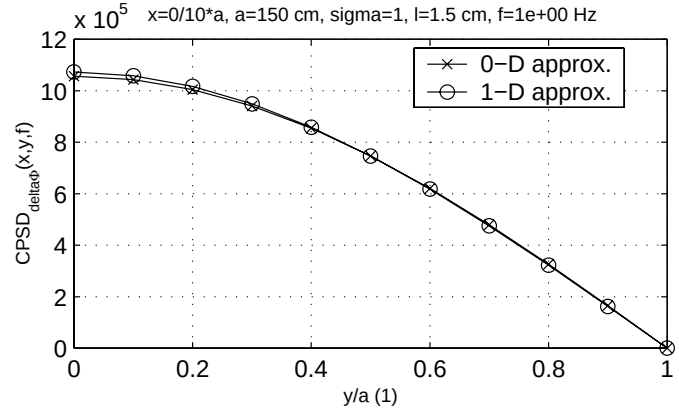
x 10^5
x=0/10*a, a=150 cm, sigma=1, l=1.5 cm, f=1e+00 Hz
0−D approx.
1−D approx.
CPSD_deltaΦ(x,y,f)
y/a (1)

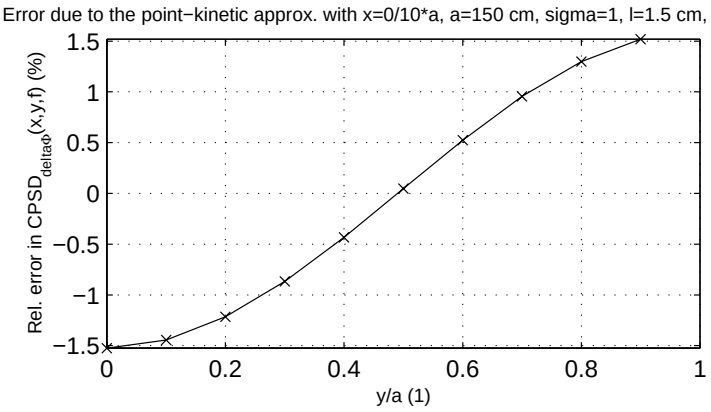
Error due to the point−kinetic approx. with x=0/10*a, a=150 cm, sigma=1, l=1.5 cm, f=1e+00 Hz
Rel. error in CPSD_deltaΦ(x,y,f) (%)
y/a (1)

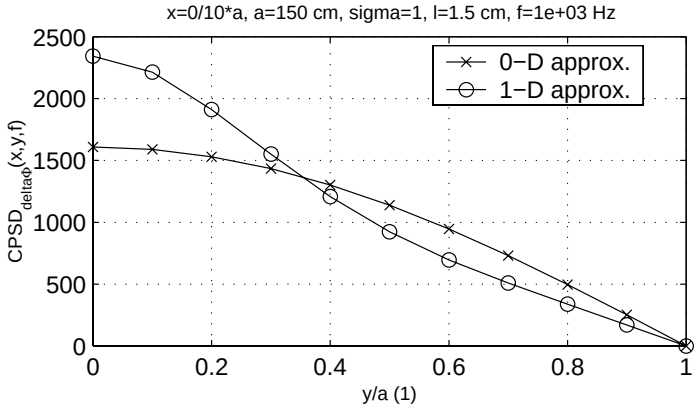
x=0/10*a, a=150 cm, sigma=1, l=1.5 cm, f=1e+03 Hz
0−D approx.
1−D approx.
CPSD_deltaΦ(x,y,f)
y/a (1)

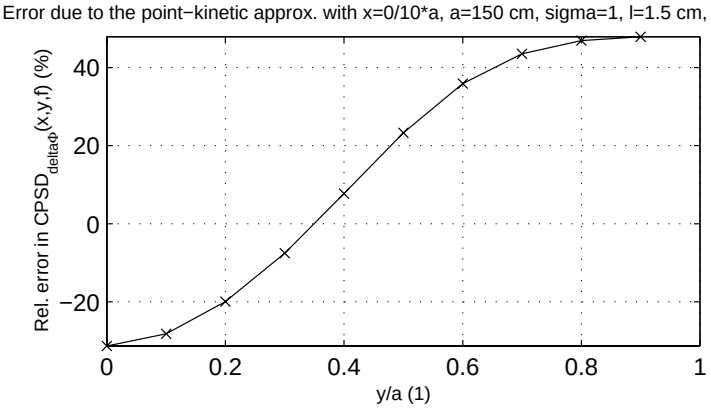
Error due to the point−kinetic approx. with x=0/10*a, a=150 cm, sigma=1, l=1.5 cm, f=1e+03 Hz
Rel. error in CPSD_deltaΦ(x,y,f) (%)
y/a (1)

Fig. 3d

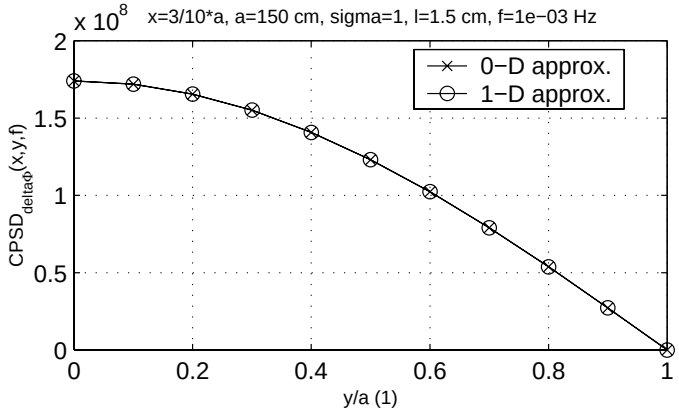
x 10^8
x=3/10*a, a=150 cm, sigma=1, l=1.5 cm, f=1e−03 Hz
0−D approx.
1−D approx.
CPSD_deltaΦ(x,y,f)
y/a (1)

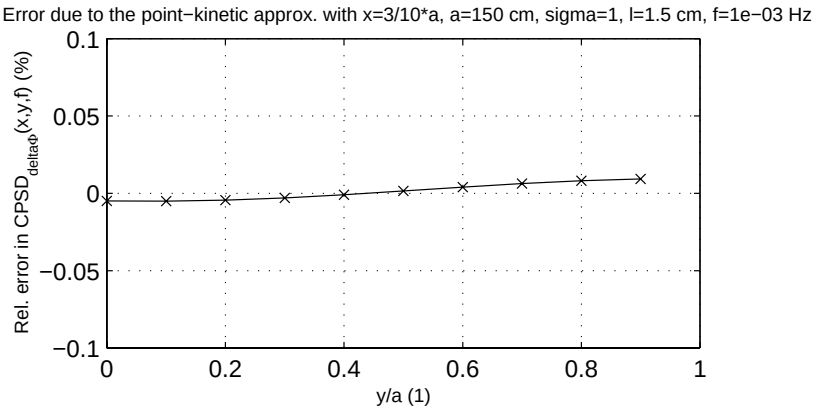
Error due to the point−kinetic approx. with x=3/10*a, a=150 cm, sigma=1, l=1.5 cm, f=1e−03 Hz
Rel. error in CPSD_deltaΦ(x,y,f) (%)
y/a (1)

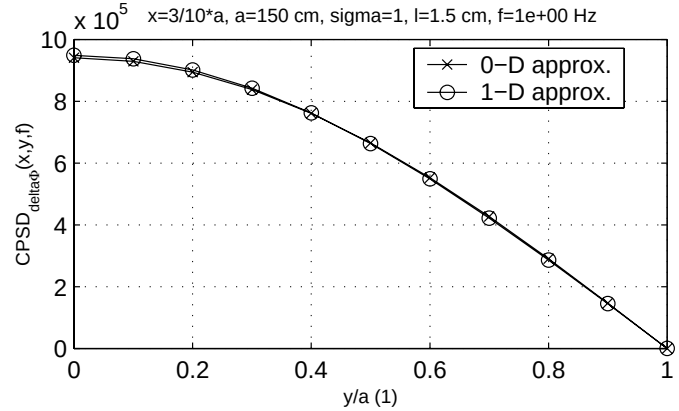
x 10^5
x=3/10*a, a=150 cm, sigma=1, l=1.5 cm, f=1e+00 Hz
0−D approx.
1−D approx.
CPSD_deltaΦ(x,y,f)
y/a (1)

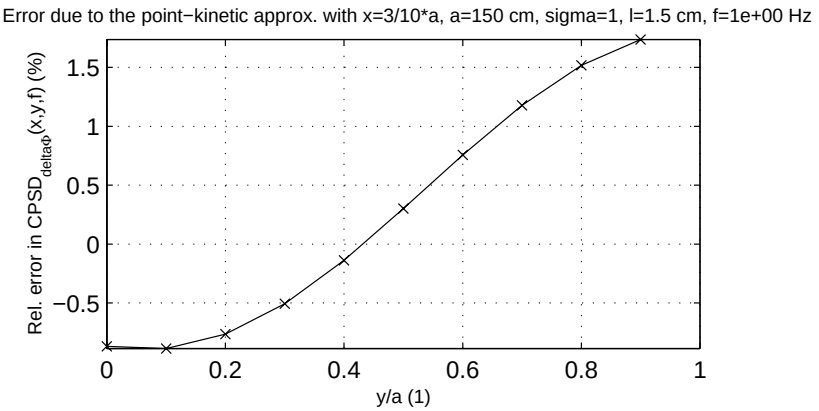
Error due to the point−kinetic approx. with x=3/10*a, a=150 cm, sigma=1, l=1.5 cm, f=1e+00 Hz
Rel. error in CPSD_deltaΦ(x,y,f) (%)
y/a (1)

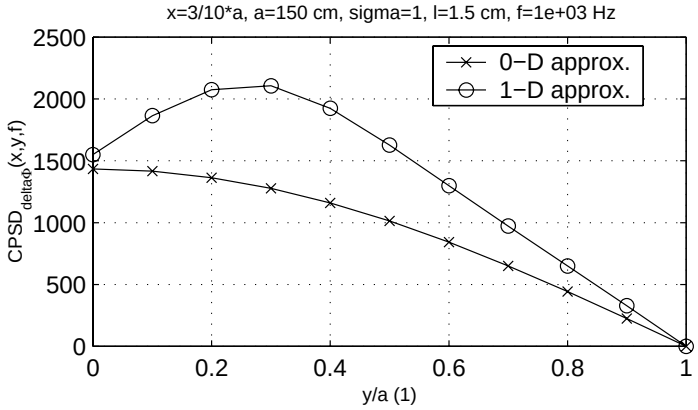
x=3/10*a, a=150 cm, sigma=1, l=1.5 cm, f=1e+03 Hz
0−D approx.
1−D approx.
CPSD_deltaΦ(x,y,f)
y/a (1)

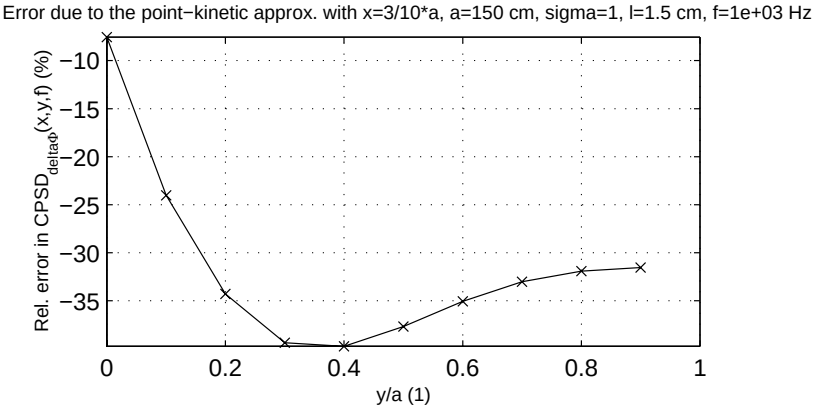
Error due to the point−kinetic approx. with x=3/10*a, a=150 cm, sigma=1, l=1.5 cm, f=1e+03 Hz
Rel. error in CPSD_deltaΦ(x,y,f) (%)
y/a (1)

Fig. 3e

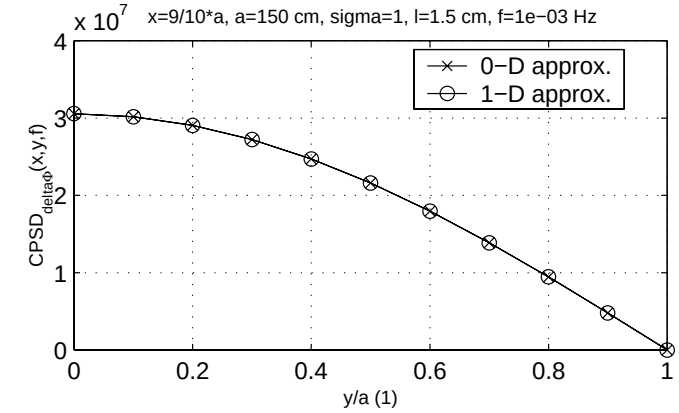
x 10^7
x=9/10*a, a=150 cm, sigma=1, l=1.5 cm, f=1e−03 Hz
0−D approx.
1−D approx.
CPSD_deltaΦ(x,y,f)
y/a (1)

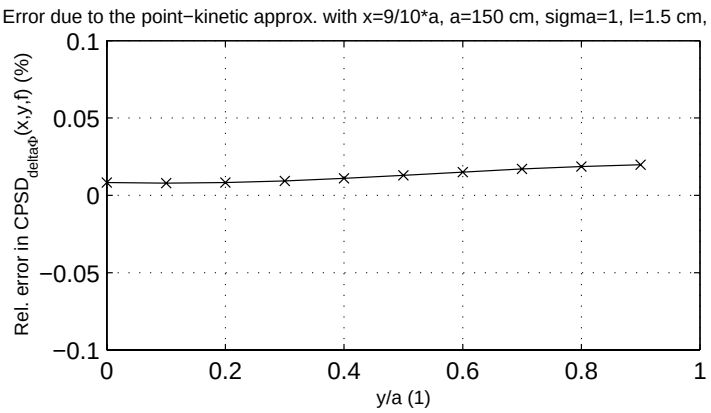
Error due to the point−kinetic approx. with x=9/10*a, a=150 cm, sigma=1, l=1.5 cm, f=1e−03 Hz
Rel. error in CPSD_deltaΦ(x,y,f) (%)
y/a (1)

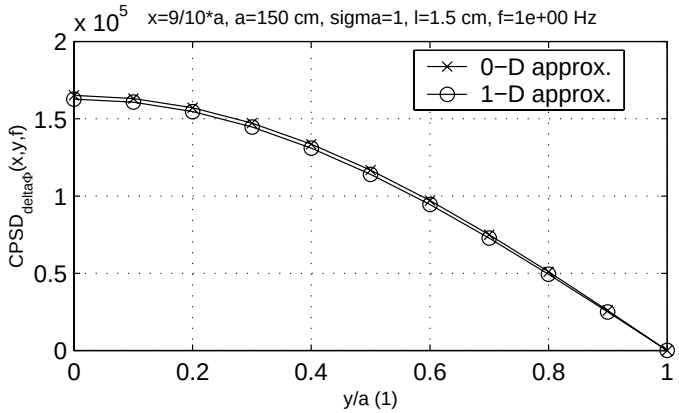
x 10^5
x=9/10*a, a=150 cm, sigma=1, l=1.5 cm, f=1e+00 Hz
0−D approx.
1−D approx.
CPSD_deltaΦ(x,y,f)
y/a (1)

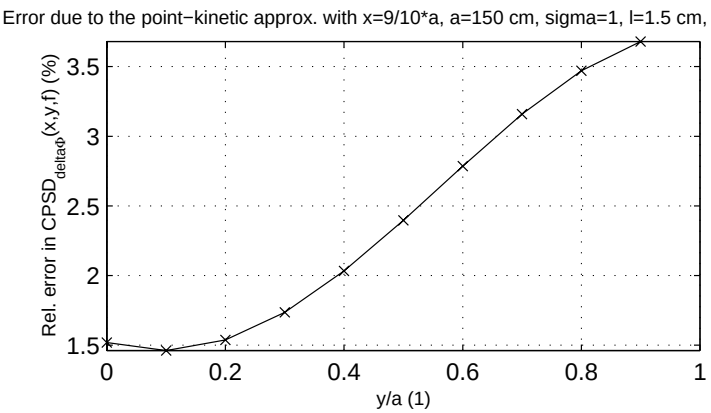
Error due to the point−kinetic approx. with x=9/10*a, a=150 cm, sigma=1, l=1.5 cm, f=1e+00 Hz
Rel. error in CPSD_deltaΦ(x,y,f) (%)
y/a (1)

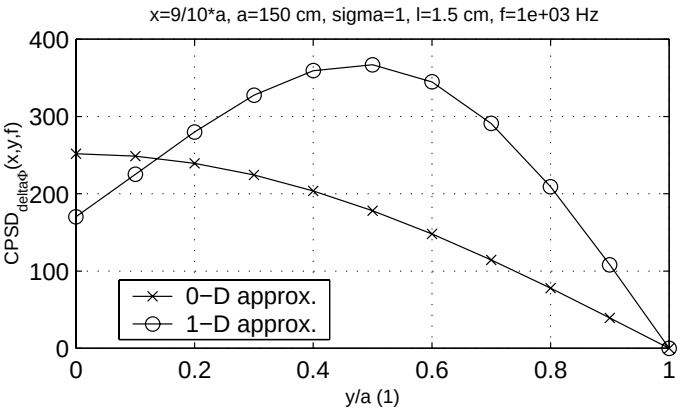
x=9/10*a, a=150 cm, sigma=1, l=1.5 cm, f=1e+03 Hz
0−D approx.
1−D approx.
CPSD_deltaΦ(x,y,f)
y/a (1)

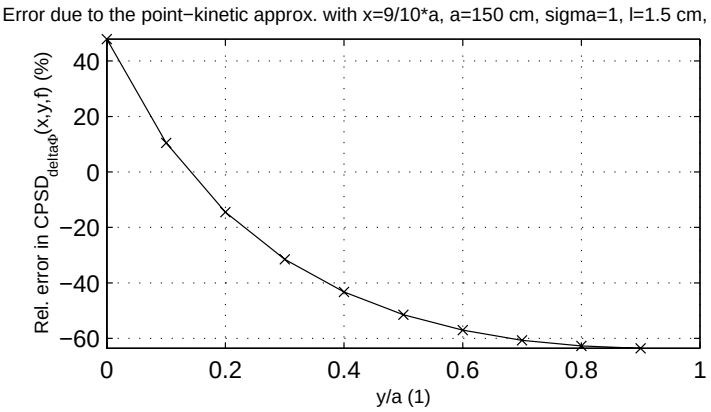
Error due to the point−kinetic approx. with x=9/10*a, a=150 cm, sigma=1, l=1.5 cm, f=1e+03 Hz
Rel. error in CPSD_deltaΦ(x,y,f) (%)
y/a (1)

Fig. 3f

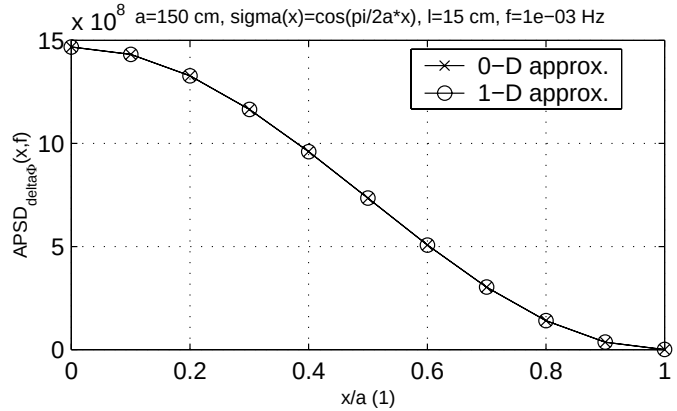
x 10^8 a=150 cm, sigma(x)=cos(pi/2a*x), l=15 cm, f=1e−03 Hz
0−D approx.
1−D approx.
APSD_deltaΦ(x,f)
x/a (1)

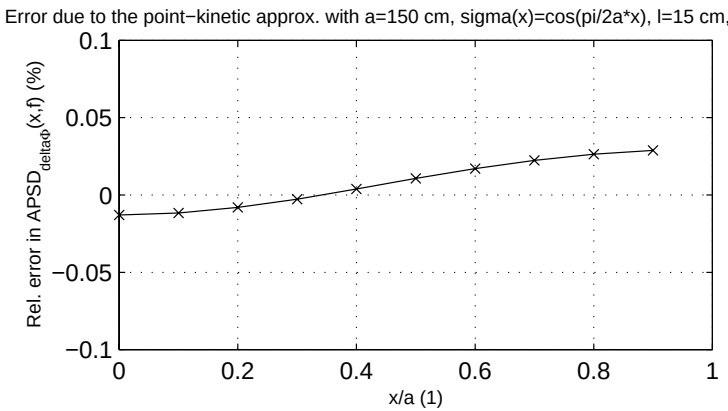
Error due to the point−kinetic approx. with a=150 cm, sigma(x)=cos(pi/2a*x), l=15 cm, f=1e−03 Hz
Rel. error in APSD_deltaΦ(x,f) (%)
x/a (1)

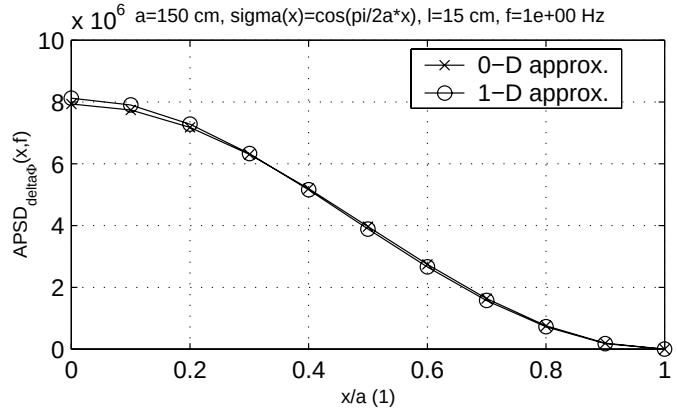
x 10^6 a=150 cm, sigma(x)=cos(pi/2a*x), l=15 cm, f=1e+00 Hz
0−D approx.
1−D approx.
APSD_deltaΦ(x,f)
x/a (1)

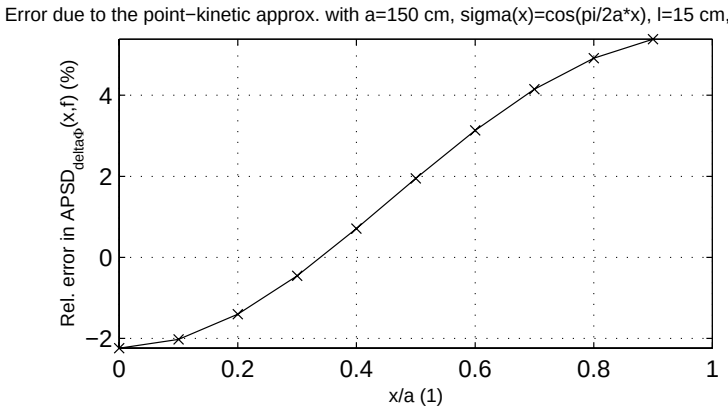
Error due to the point−kinetic approx. with a=150 cm, sigma(x)=cos(pi/2a*x), l=15 cm, f=1e+00 Hz
Rel. error in APSD_deltaΦ(x,f) (%)
x/a (1)

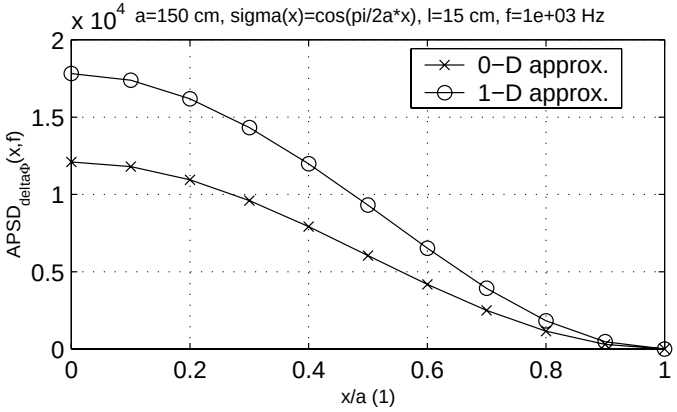
x 10^4 a=150 cm, sigma(x)=cos(pi/2a*x), l=15 cm, f=1e+03 Hz
0−D approx.
1−D approx.
APSD_deltaΦ(x,f)
x/a (1)

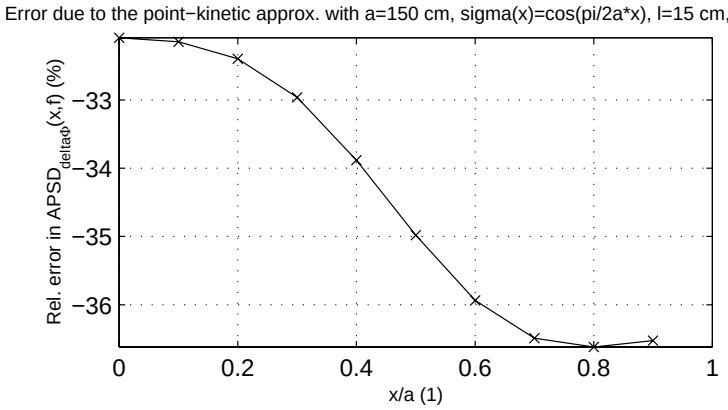
Error due to the point−kinetic approx. with a=150 cm, sigma(x)=cos(pi/2a*x), l=15 cm, f=1e+03 Hz
Rel. error in APSD_deltaΦ(x,f) (%)
x/a (1)

Fig. 4a

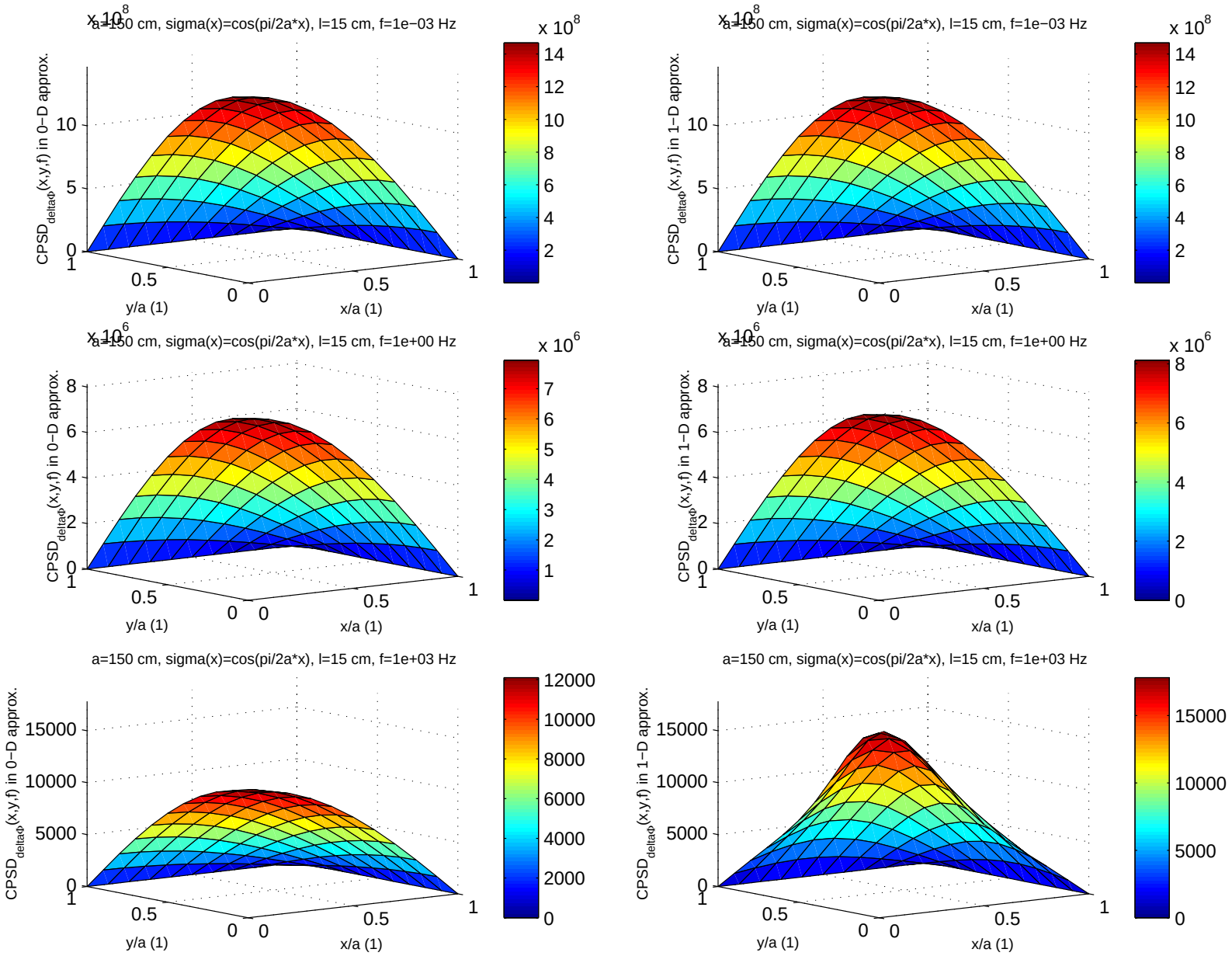
a=150 cm, sigma(x)=cos(pi/2a*x), l=15 cm, f=1e−03 Hz
x 10^8
CPSD_deltaΦ(x,y,f) in 0−D approx.
CPSD_deltaΦ(x,y,f) in 1−D approx.
y/a (1)
x/a (1)
a=150 cm, sigma(x)=cos(pi/2a*x), l=15 cm, f=1e+00 Hz
x 10^6
a=150 cm, sigma(x)=cos(pi/2a*x), l=15 cm, f=1e+03 Hz

Fig. 4b

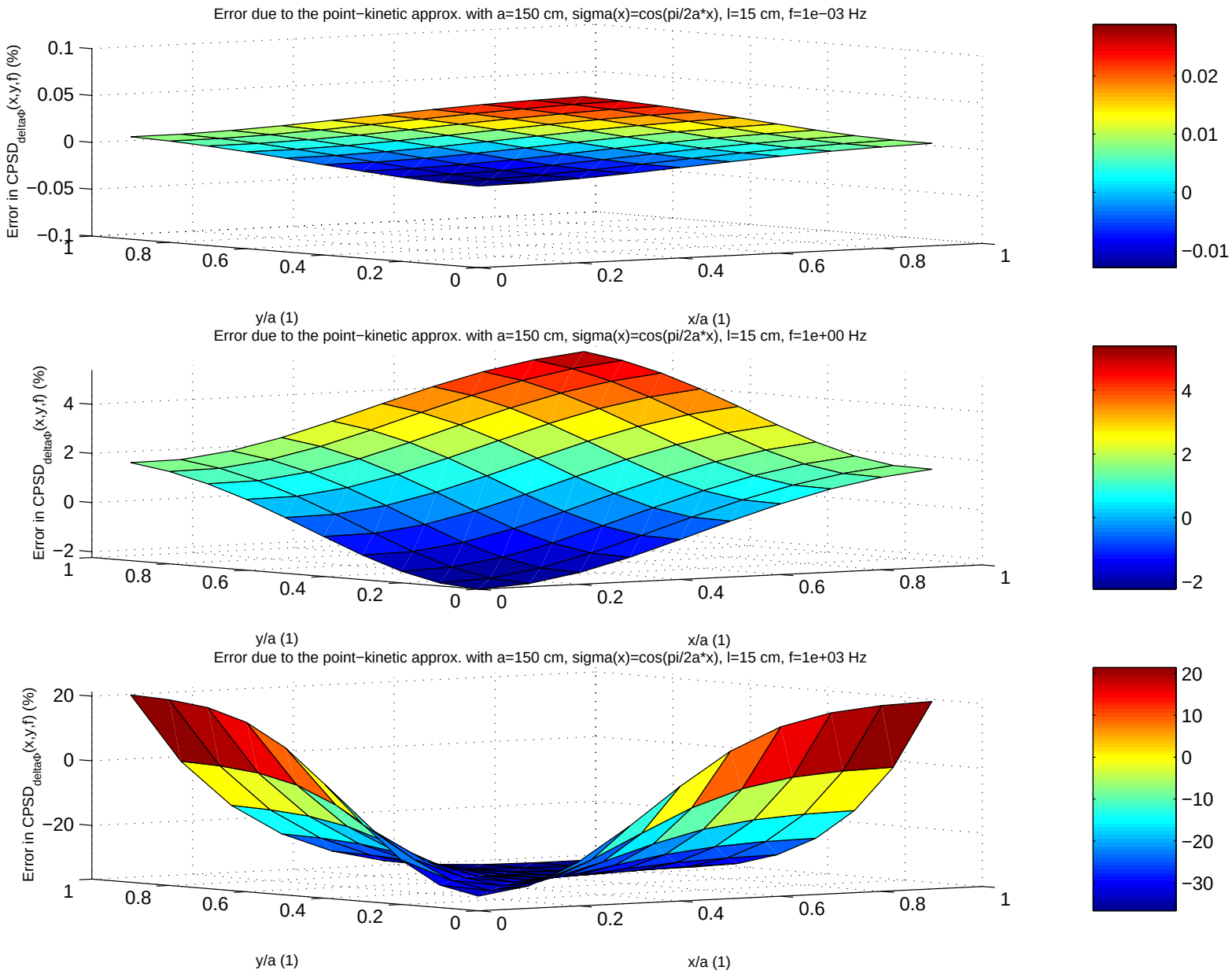
Error due to the point−kinetic approx. with a=150 cm, sigma(x)=cos(pi/2a*x), l=15 cm, f=1e−03 Hz
Error in CPSD_deltaΦ(x,y,f) (%)
0.1
0.05
0
−0.05
−0.1
1
0.8
0.6
0.4
0.2
0
y/a (1)
0
0.2
0.4
0.6
0.8
1
x/a (1)
0.02
0.01
0
−0.01
Error due to the point−kinetic approx. with a=150 cm, sigma(x)=cos(pi/2a*x), l=15 cm, f=1e+00 Hz
Error in CPSD_deltaΦ(x,y,f) (%)
4
2
0
−2
y/a (1)
x/a (1)
Error due to the point−kinetic approx. with a=150 cm, sigma(x)=cos(pi/2a*x), l=15 cm, f=1e+03 Hz
Error in CPSD_deltaΦ(x,y,f) (%)
20
0
−20
y/a (1)
x/a (1)
10
−10
−30

Fig. 4c

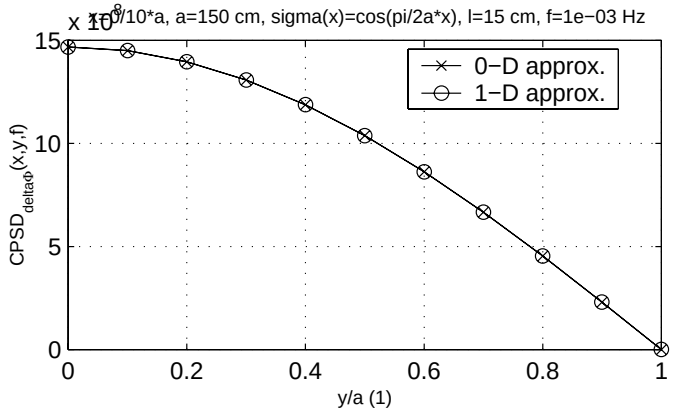
x=0/10*a, a=150 cm, sigma(x)=cos(pi/2a*x), l=15 cm, f=1e−03 Hz
x 10^8
0−D approx.
1−D approx.
CPSD_deltaΦ(x,y,f)
y/a (1)

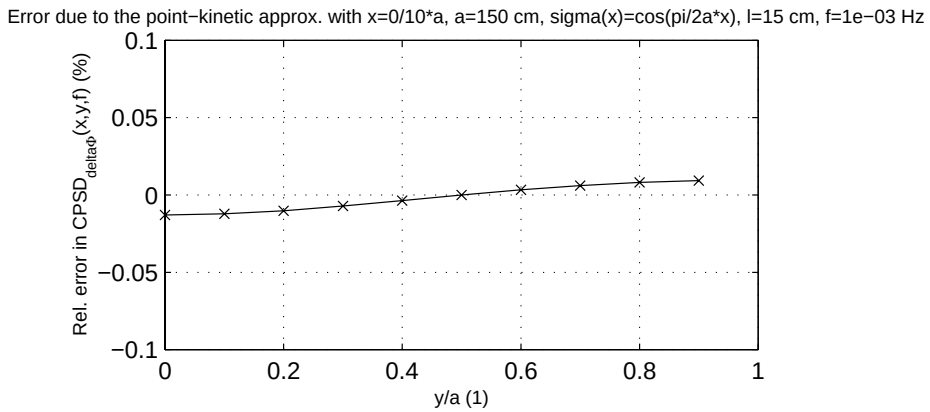
Error due to the point−kinetic approx. with x=0/10*a, a=150 cm, sigma(x)=cos(pi/2a*x), l=15 cm, f=1e−03 Hz
Rel. error in CPSD_deltaΦ(x,y,f) (%)
y/a (1)

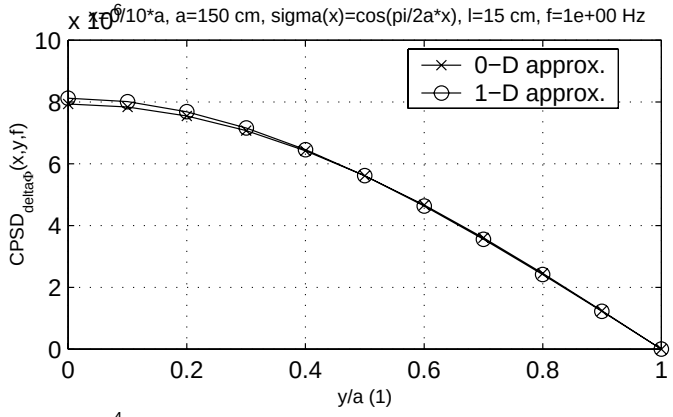
x=0/10*a, a=150 cm, sigma(x)=cos(pi/2a*x), l=15 cm, f=1e+00 Hz
x 10^6
0−D approx.
1−D approx.
CPSD_deltaΦ(x,y,f)
y/a (1)

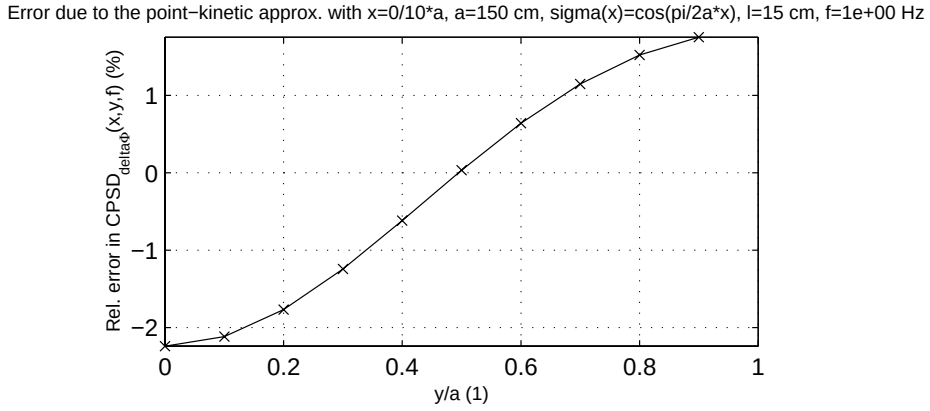
Error due to the point−kinetic approx. with x=0/10*a, a=150 cm, sigma(x)=cos(pi/2a*x), l=15 cm, f=1e+00 Hz
Rel. error in CPSD_deltaΦ(x,y,f) (%)
y/a (1)

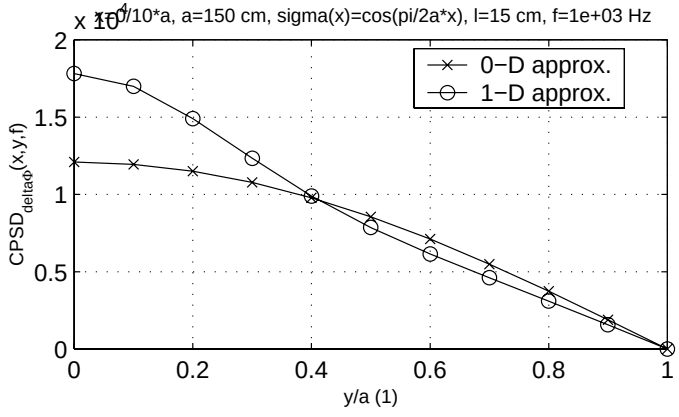
x=0/10*a, a=150 cm, sigma(x)=cos(pi/2a*x), l=15 cm, f=1e+03 Hz
x 10^4
0−D approx.
1−D approx.
CPSD_deltaΦ(x,y,f)
y/a (1)

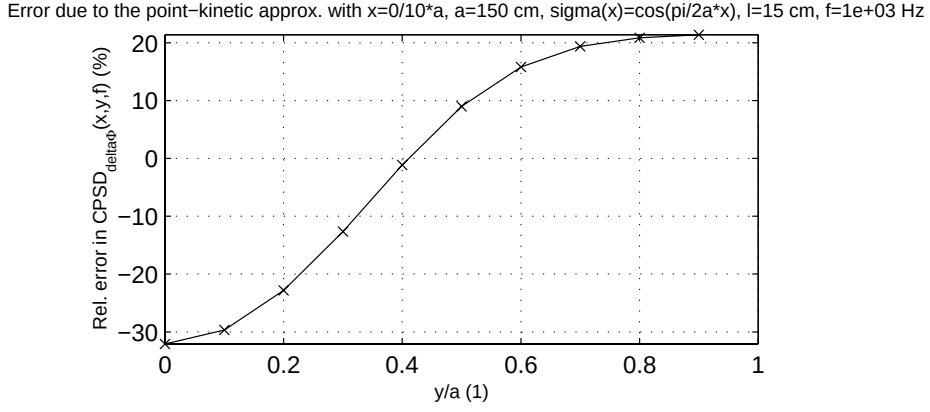
Error due to the point−kinetic approx. with x=0/10*a, a=150 cm, sigma(x)=cos(pi/2a*x), l=15 cm, f=1e+03 Hz
Rel. error in CPSD_deltaΦ(x,y,f) (%)
y/a (1)

Fig. 4d

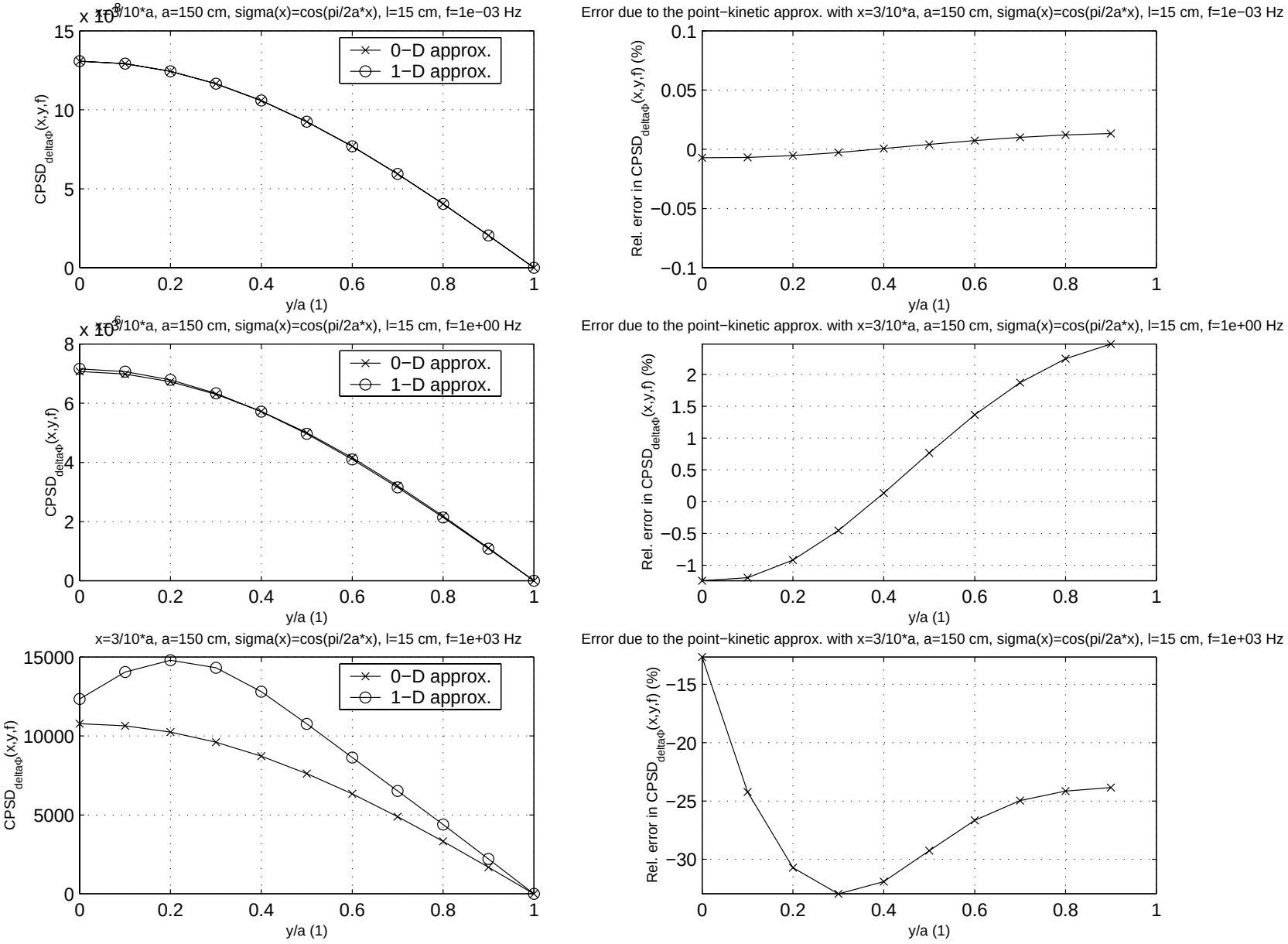
x=3/10*a, a=150 cm, sigma(x)=cos(pi/2a*x), l=15 cm, f=1e−03 Hz
x 10^8
CPSD_deltaΦ(x,y,f)
y/a (1)
0−D approx.
1−D approx.
Error due to the point−kinetic approx. with x=3/10*a, a=150 cm, sigma(x)=cos(pi/2a*x), l=15 cm, f=1e−03 Hz
Rel. error in CPSD_deltaΦ(x,y,f) (%)
y/a (1)
x=3/10*a, a=150 cm, sigma(x)=cos(pi/2a*x), l=15 cm, f=1e+00 Hz
x 10^6
CPSD_deltaΦ(x,y,f)
y/a (1)
0−D approx.
1−D approx.
Error due to the point−kinetic approx. with x=3/10*a, a=150 cm, sigma(x)=cos(pi/2a*x), l=15 cm, f=1e+00 Hz
Rel. error in CPSD_deltaΦ(x,y,f) (%)
y/a (1)
x=3/10*a, a=150 cm, sigma(x)=cos(pi/2a*x), l=15 cm, f=1e+03 Hz
CPSD_deltaΦ(x,y,f)
y/a (1)
0−D approx.
1−D approx.
Error due to the point−kinetic approx. with x=3/10*a, a=150 cm, sigma(x)=cos(pi/2a*x), l=15 cm, f=1e+03 Hz
Rel. error in CPSD_deltaΦ(x,y,f) (%)
y/a (1)

Fig. 4e

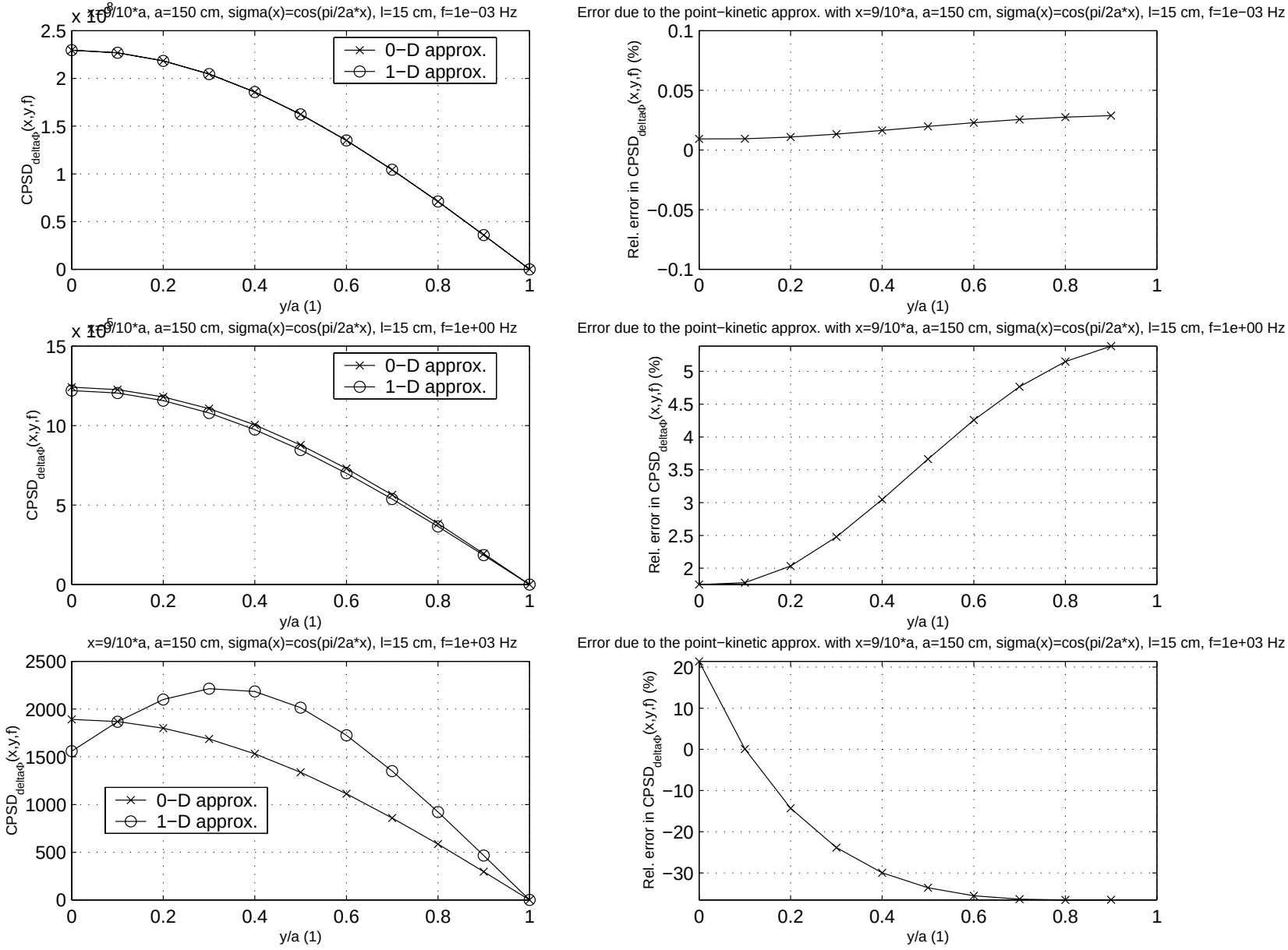
x=9/10*a, a=150 cm, sigma(x)=cos(pi/2a*x), l=15 cm, f=1e−03 Hz
x 10^8
0−D approx.
1−D approx.
CPSD_deltaΦ(x,y,f)
y/a (1)
Error due to the point−kinetic approx. with x=9/10*a, a=150 cm, sigma(x)=cos(pi/2a*x), l=15 cm, f=1e−03 Hz
Rel. error in CPSD_deltaΦ(x,y,f) (%)
y/a (1)
x=9/10*a, a=150 cm, sigma(x)=cos(pi/2a*x), l=15 cm, f=1e+00 Hz
x 10^5
0−D approx.
1−D approx.
CPSD_deltaΦ(x,y,f)
y/a (1)
Error due to the point−kinetic approx. with x=9/10*a, a=150 cm, sigma(x)=cos(pi/2a*x), l=15 cm, f=1e+00 Hz
Rel. error in CPSD_deltaΦ(x,y,f) (%)
y/a (1)
x=9/10*a, a=150 cm, sigma(x)=cos(pi/2a*x), l=15 cm, f=1e+03 Hz
0−D approx.
1−D approx.
CPSD_deltaΦ(x,y,f)
y/a (1)
Error due to the point−kinetic approx. with x=9/10*a, a=150 cm, sigma(x)=cos(pi/2a*x), l=15 cm, f=1e+03 Hz
Rel. error in CPSD_deltaΦ(x,y,f) (%)
y/a (1)

Fig. 4f

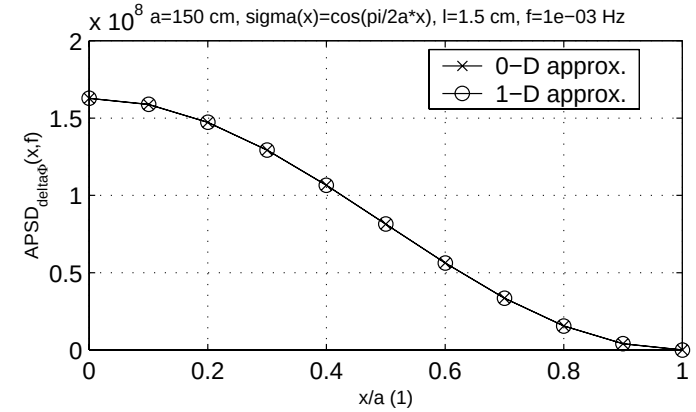
x 10^8 a=150 cm, sigma(x)=cos(pi/2a*x), l=1.5 cm, f=1e−03 Hz
0−D approx.
1−D approx.
APSD_deltaΦ(x,f)
x/a (1)

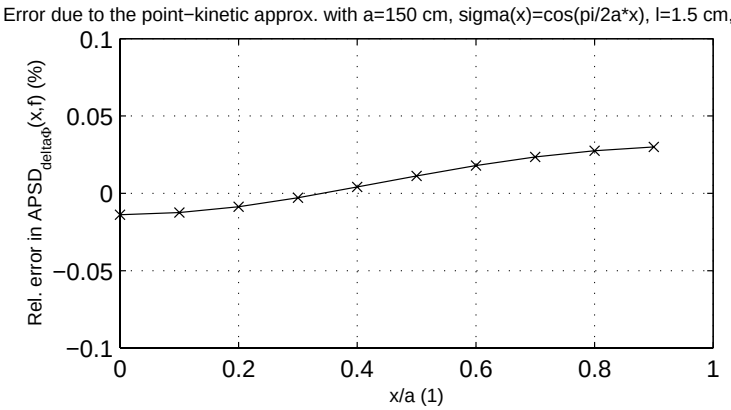
Error due to the point−kinetic approx. with a=150 cm, sigma(x)=cos(pi/2a*x), l=1.5 cm, f=1e−03 Hz
Rel. error in APSD_deltaΦ(x,f) (%)
x/a (1)

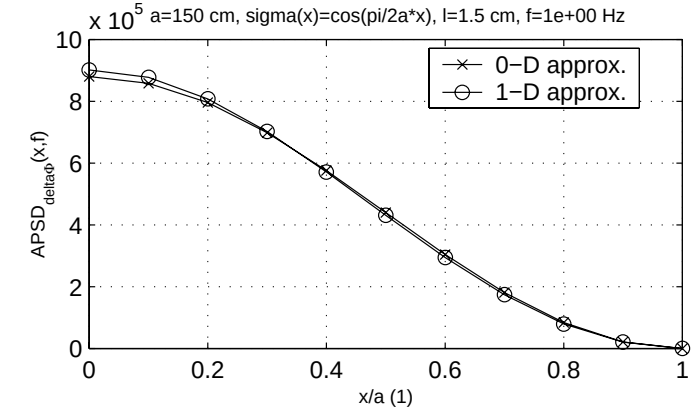
x 10^5 a=150 cm, sigma(x)=cos(pi/2a*x), l=1.5 cm, f=1e+00 Hz
0−D approx.
1−D approx.
APSD_deltaΦ(x,f)
x/a (1)

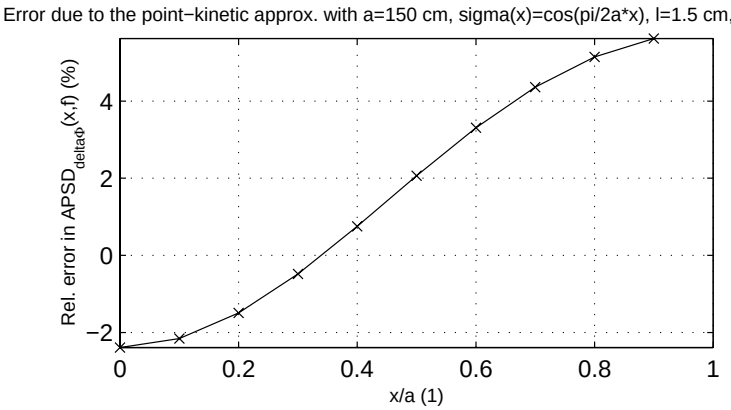
Error due to the point−kinetic approx. with a=150 cm, sigma(x)=cos(pi/2a*x), l=1.5 cm, f=1e+00 Hz
Rel. error in APSD_deltaΦ(x,f) (%)
x/a (1)

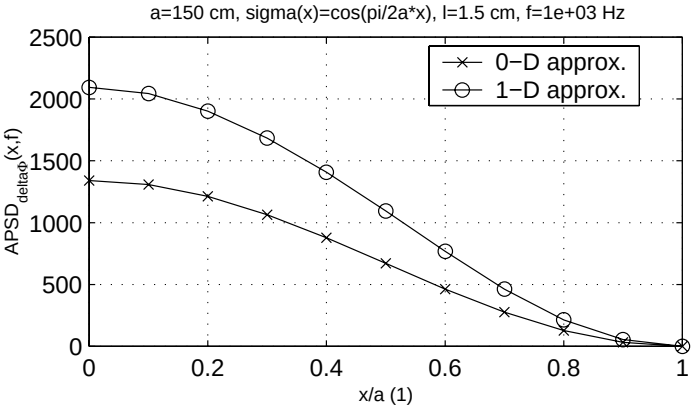
a=150 cm, sigma(x)=cos(pi/2a*x), l=1.5 cm, f=1e+03 Hz
0−D approx.
1−D approx.
APSD_deltaΦ(x,f)
x/a (1)

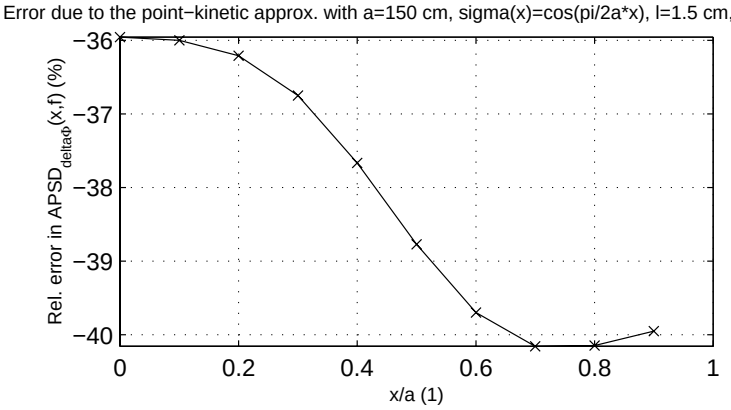
Error due to the point−kinetic approx. with a=150 cm, sigma(x)=cos(pi/2a*x), l=1.5 cm, f=1e+03 Hz
Rel. error in APSD_deltaΦ(x,f) (%)
x/a (1)

Fig. 5a

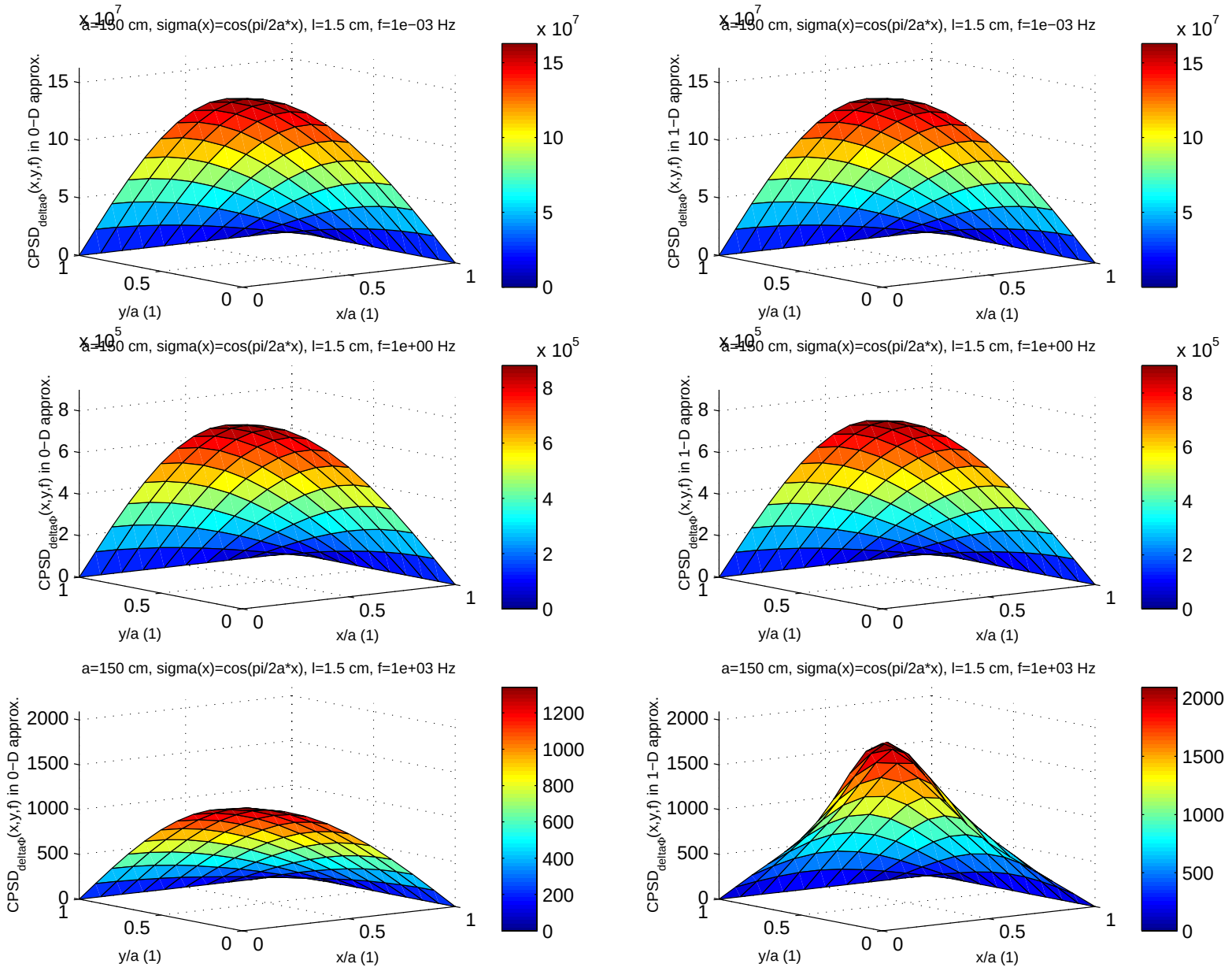
a=150 cm, sigma(x)=cos(pi/2a*x), l=1.5 cm, f=1e−03 Hz
x 10^7
CPSD_deltaΦ(x,y,f) in 0−D approx.
CPSD_deltaΦ(x,y,f) in 1−D approx.
y/a (1)
x/a (1)
a=150 cm, sigma(x)=cos(pi/2a*x), l=1.5 cm, f=1e+00 Hz
x 10^5
a=150 cm, sigma(x)=cos(pi/2a*x), l=1.5 cm, f=1e+03 Hz

Fig. 5b

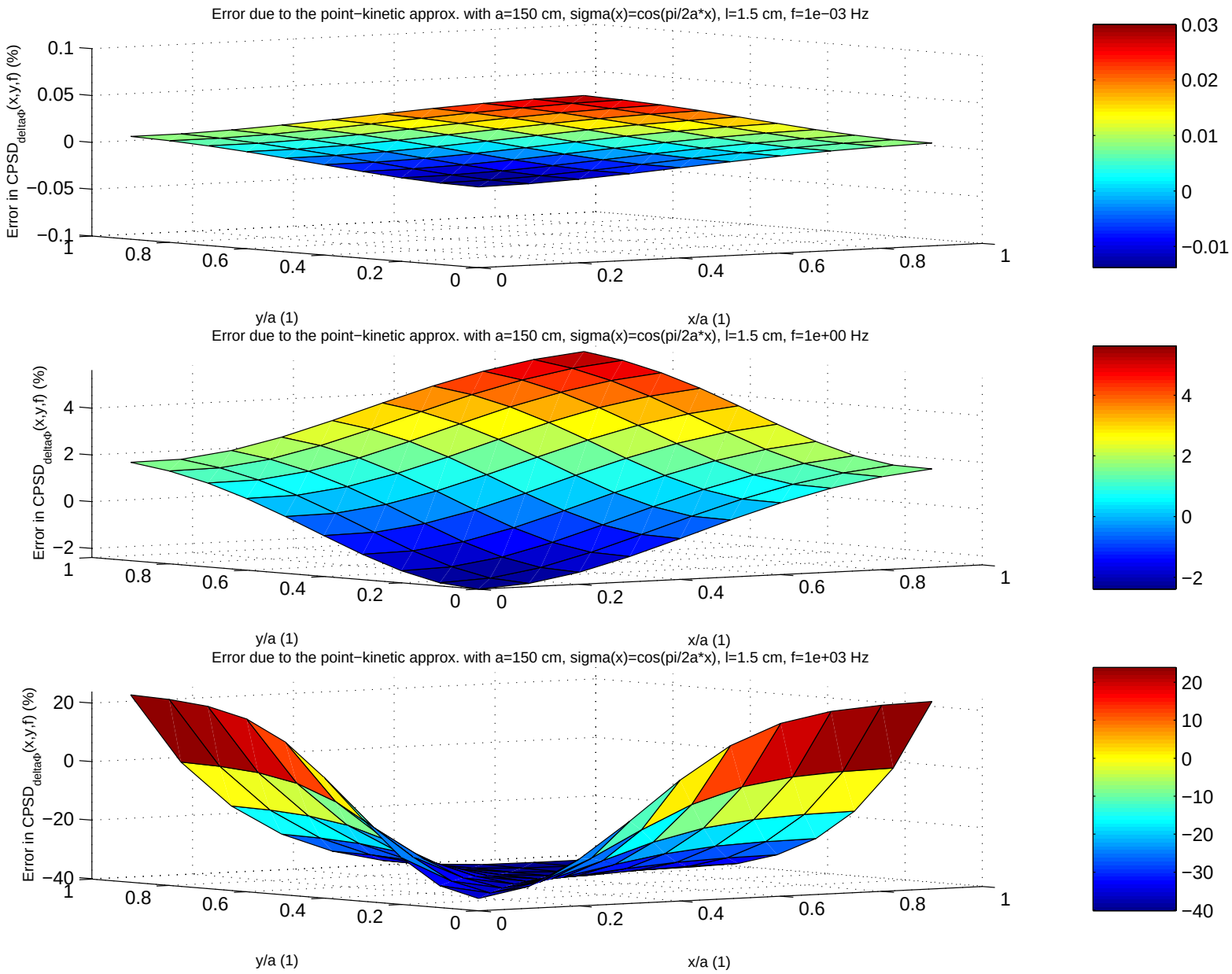
Error due to the point−kinetic approx. with a=150 cm, sigma(x)=cos(pi/2a*x), l=1.5 cm, f=1e−03 Hz
Error in CPSD_deltaΦ(x,y,f) (%)
0.1
0.05
0
−0.05
−0.1
1
0.8
0.6
0.4
0.2
0
y/a (1)
0
0.2
0.4
0.6
0.8
1
x/a (1)
0.03
0.02
0.01
0
−0.01
Error due to the point−kinetic approx. with a=150 cm, sigma(x)=cos(pi/2a*x), l=1.5 cm, f=1e+00 Hz
Error in CPSD_deltaΦ(x,y,f) (%)
4
2
0
−2
y/a (1)
x/a (1)
Error due to the point−kinetic approx. with a=150 cm, sigma(x)=cos(pi/2a*x), l=1.5 cm, f=1e+03 Hz
Error in CPSD_deltaΦ(x,y,f) (%)
20
0
−20
−40
y/a (1)
x/a (1)
20
10
0
−10
−20
−30
−40

Fig. 5c

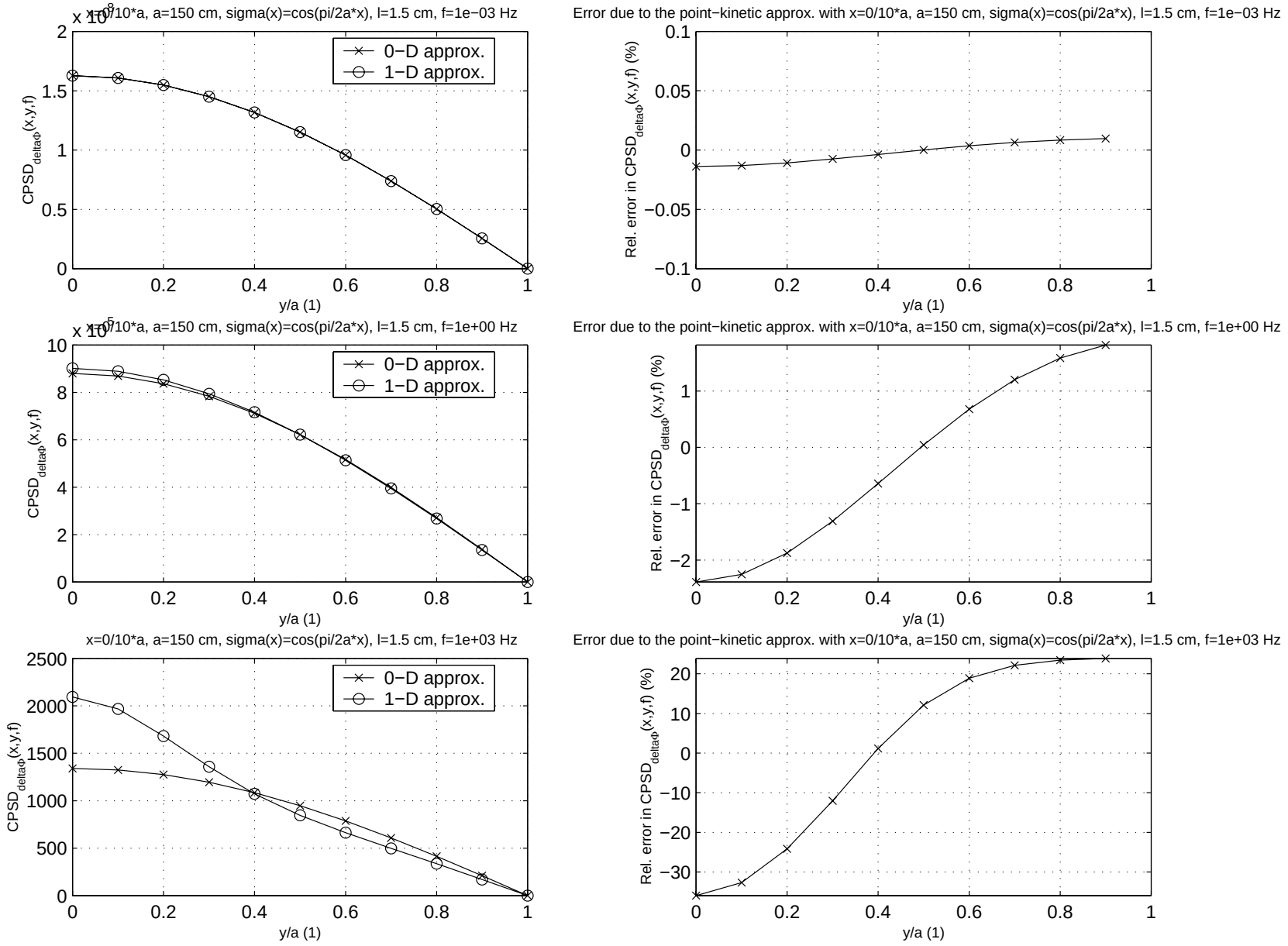
x=0/10*a, a=150 cm, sigma(x)=cos(pi/2a*x), l=1.5 cm, f=1e−03 Hz
x 10^−9
0−D approx.
1−D approx.
CPSD_deltaΦ(x,y,f)
y/a (1)
Error due to the point−kinetic approx. with x=0/10*a, a=150 cm, sigma(x)=cos(pi/2a*x), l=1.5 cm, f=1e−03 Hz
Rel. error in CPSD_deltaΦ(x,y,f) (%)
y/a (1)
x=0/10*a, a=150 cm, sigma(x)=cos(pi/2a*x), l=1.5 cm, f=1e+00 Hz
x 10^−5
0−D approx.
1−D approx.
CPSD_deltaΦ(x,y,f)
y/a (1)
Error due to the point−kinetic approx. with x=0/10*a, a=150 cm, sigma(x)=cos(pi/2a*x), l=1.5 cm, f=1e+00 Hz
Rel. error in CPSD_deltaΦ(x,y,f) (%)
y/a (1)
x=0/10*a, a=150 cm, sigma(x)=cos(pi/2a*x), l=1.5 cm, f=1e+03 Hz
0−D approx.
1−D approx.
CPSD_deltaΦ(x,y,f)
y/a (1)
Error due to the point−kinetic approx. with x=0/10*a, a=150 cm, sigma(x)=cos(pi/2a*x), l=1.5 cm, f=1e+03 Hz
Rel. error in CPSD_deltaΦ(x,y,f) (%)
y/a (1)

Fig. 5d

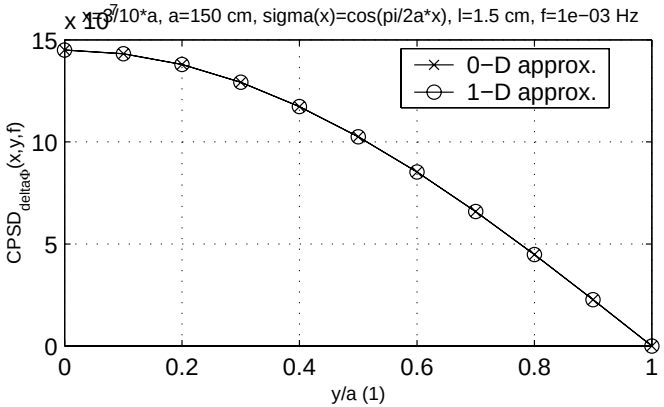
x=3/10*a, a=150 cm, sigma(x)=cos(pi/2a*x), l=1.5 cm, f=1e−03 Hz
x 10^7
0−D approx.
1−D approx.
CPSD_deltaΦ(x,y,f)
y/a (1)

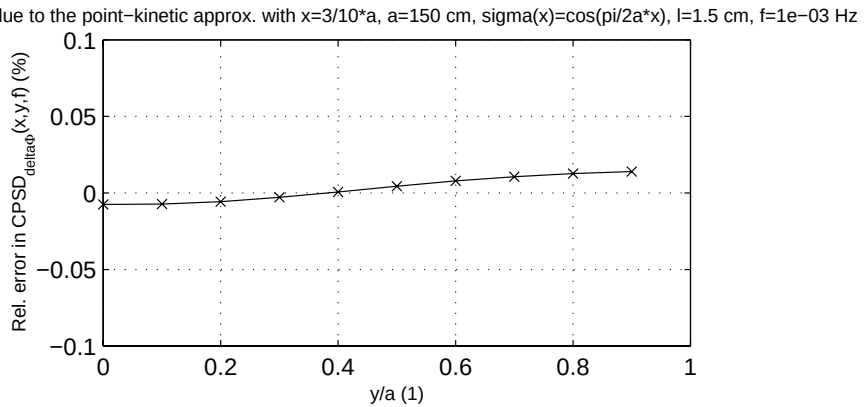
Error due to the point−kinetic approx. with x=3/10*a, a=150 cm, sigma(x)=cos(pi/2a*x), l=1.5 cm, f=1e−03 Hz
Rel. error in CPSD_deltaΦ(x,y,f) (%)
y/a (1)

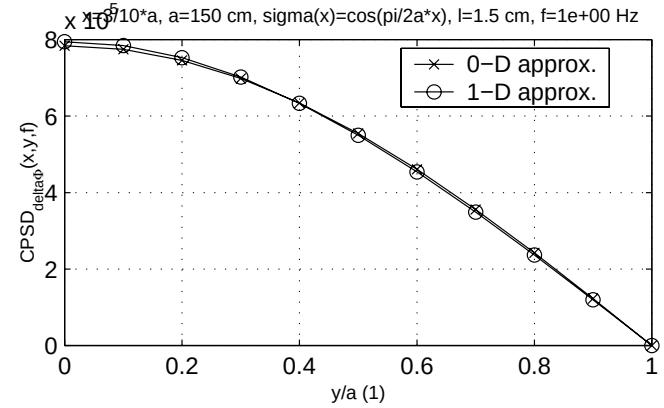
x=3/10*a, a=150 cm, sigma(x)=cos(pi/2a*x), l=1.5 cm, f=1e+00 Hz
x 10^5
0−D approx.
1−D approx.
CPSD_deltaΦ(x,y,f)
y/a (1)

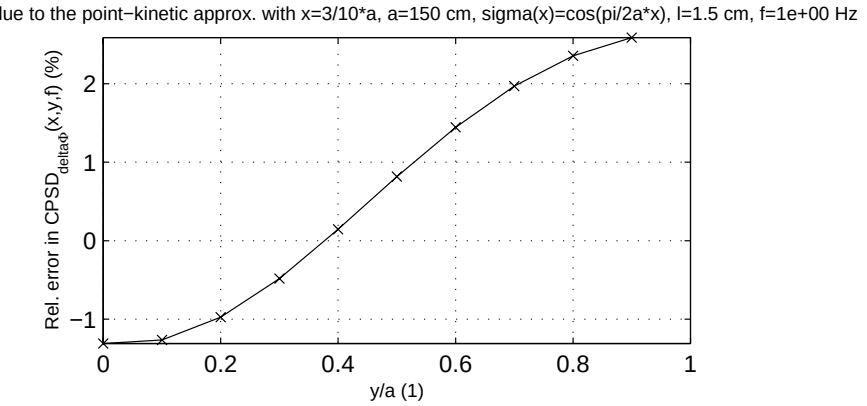
Error due to the point−kinetic approx. with x=3/10*a, a=150 cm, sigma(x)=cos(pi/2a*x), l=1.5 cm, f=1e+00 Hz
Rel. error in CPSD_deltaΦ(x,y,f) (%)
y/a (1)

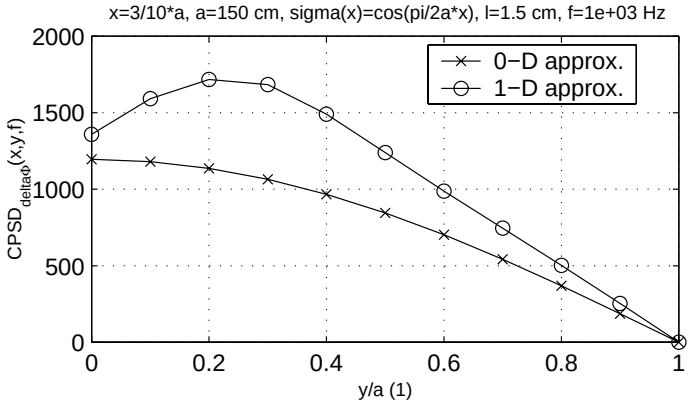
x=3/10*a, a=150 cm, sigma(x)=cos(pi/2a*x), l=1.5 cm, f=1e+03 Hz
0−D approx.
1−D approx.
CPSD_deltaΦ(x,y,f)
y/a (1)

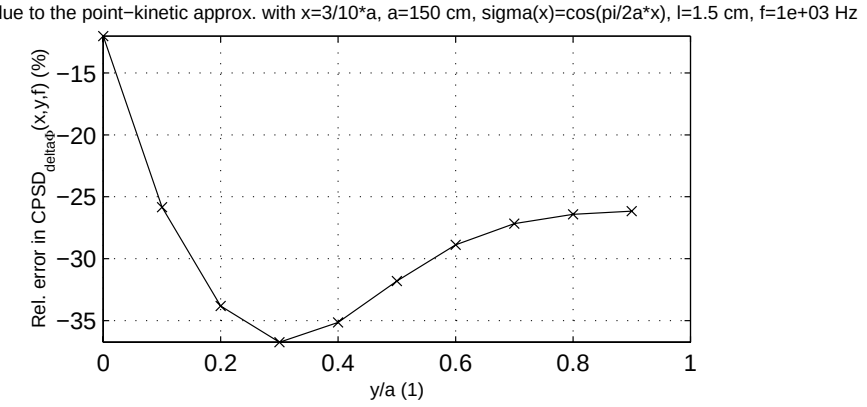
Error due to the point−kinetic approx. with x=3/10*a, a=150 cm, sigma(x)=cos(pi/2a*x), l=1.5 cm, f=1e+03 Hz
Rel. error in CPSD_deltaΦ(x,y,f) (%)
y/a (1)

Fig. 5e

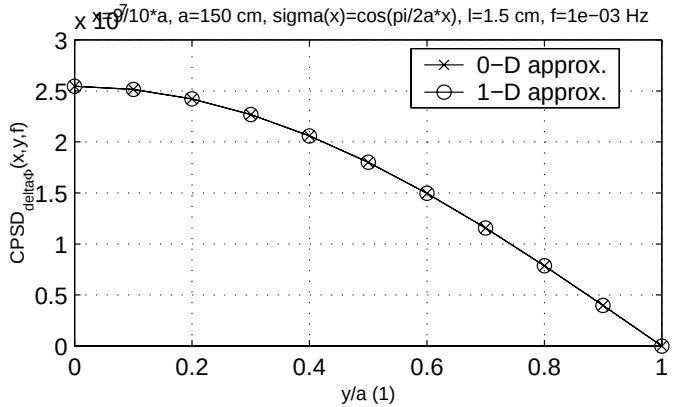
x=9/10*a, a=150 cm, sigma(x)=cos(pi/2a*x), l=1.5 cm, f=1e−03 Hz
x 10^7
CPSD_deltaΦ(x,y,f)
y/a (1)
0−D approx.
1−D approx.

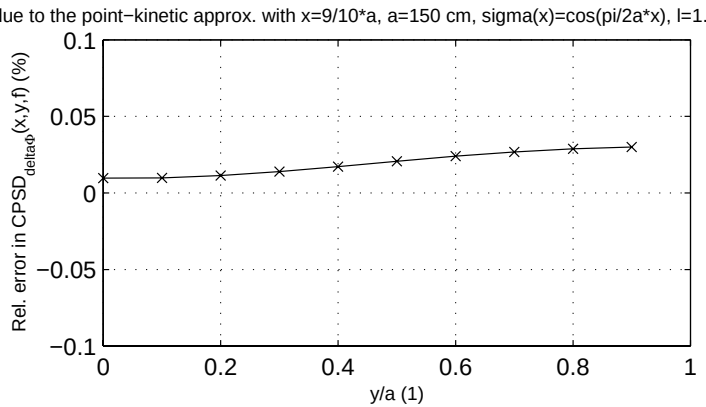
Error due to the point−kinetic approx. with x=9/10*a, a=150 cm, sigma(x)=cos(pi/2a*x), l=1.5 cm, f=1e−03 Hz
Rel. error in CPSD_deltaΦ(x,y,f) (%)
y/a (1)

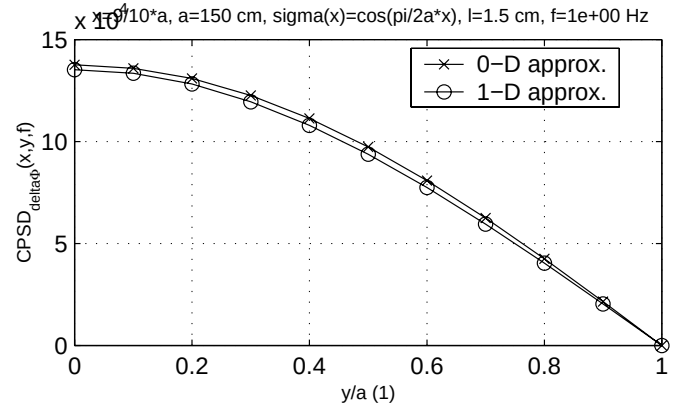
x=9/10*a, a=150 cm, sigma(x)=cos(pi/2a*x), l=1.5 cm, f=1e+00 Hz
x 10^4
CPSD_deltaΦ(x,y,f)
y/a (1)
0−D approx.
1−D approx.

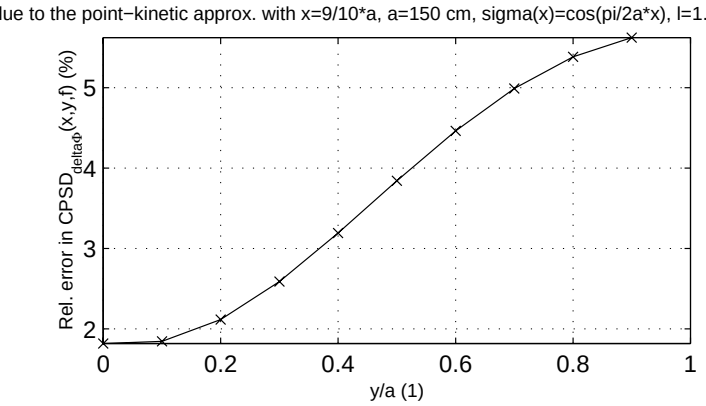
Error due to the point−kinetic approx. with x=9/10*a, a=150 cm, sigma(x)=cos(pi/2a*x), l=1.5 cm, f=1e+00 Hz
Rel. error in CPSD_deltaΦ(x,y,f) (%)
y/a (1)

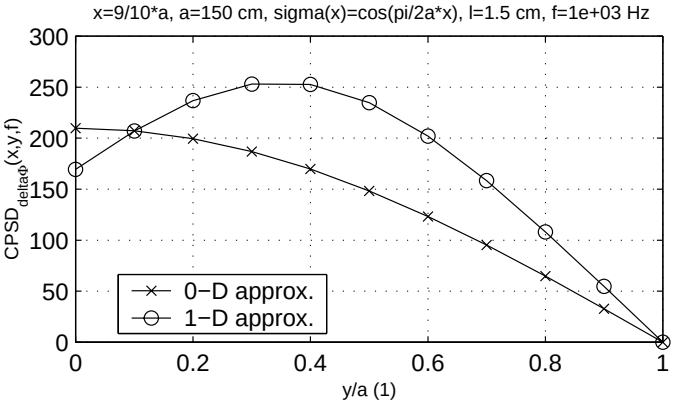
x=9/10*a, a=150 cm, sigma(x)=cos(pi/2a*x), l=1.5 cm, f=1e+03 Hz
CPSD_deltaΦ(x,y,f)
y/a (1)
0−D approx.
1−D approx.

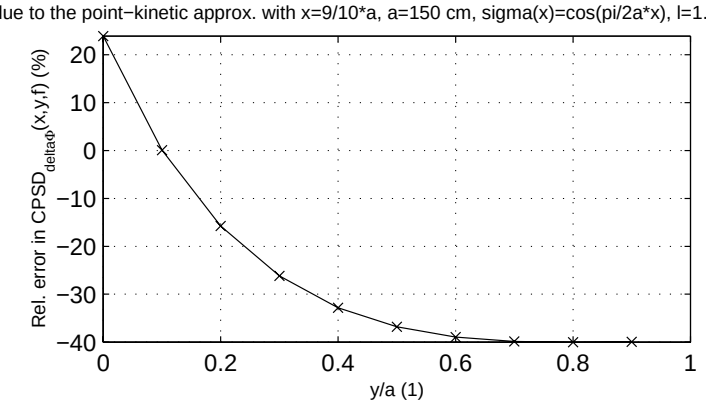
Error due to the point−kinetic approx. with x=9/10*a, a=150 cm, sigma(x)=cos(pi/2a*x), l=1.5 cm, f=1e+03 Hz
Rel. error in CPSD_deltaΦ(x,y,f) (%)
y/a (1)

Fig. 5f

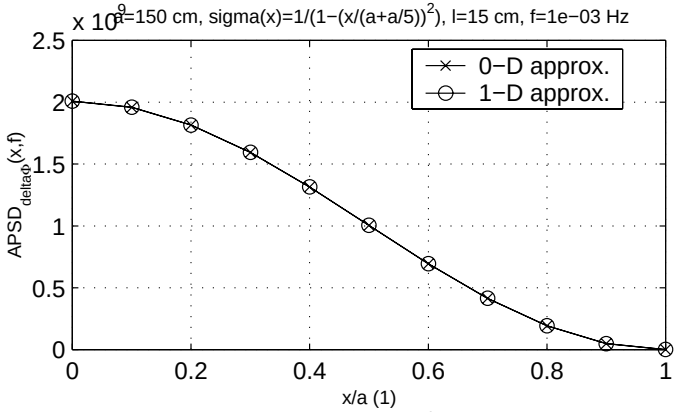
x 10^9
a=150 cm, sigma(x)=1/(1−(x/(a+a/5))^2), l=15 cm, f=1e−03 Hz
0−D approx.
1−D approx.
APSD_deltaΦ(x,f)
x/a (1)

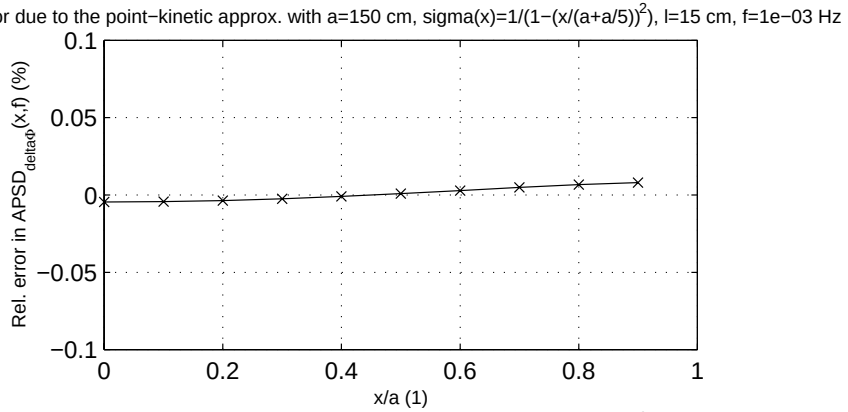
Error due to the point−kinetic approx. with a=150 cm, sigma(x)=1/(1−(x/(a+a/5))^2), l=15 cm, f=1e−03 Hz
Rel. error in APSD_deltaΦ(x,f) (%)
x/a (1)

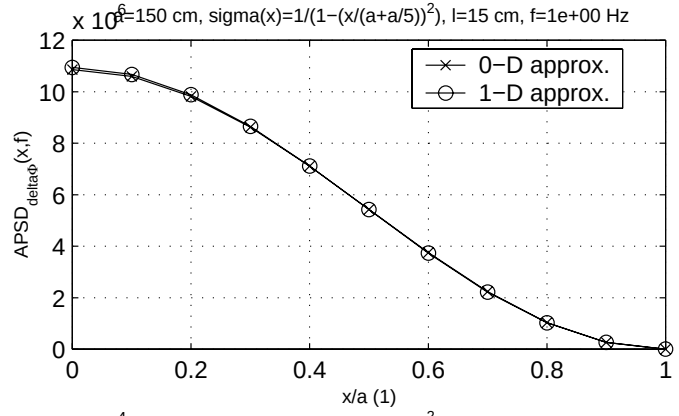
x 10^6
a=150 cm, sigma(x)=1/(1−(x/(a+a/5))^2), l=15 cm, f=1e+00 Hz
0−D approx.
1−D approx.
APSD_deltaΦ(x,f)
x/a (1)

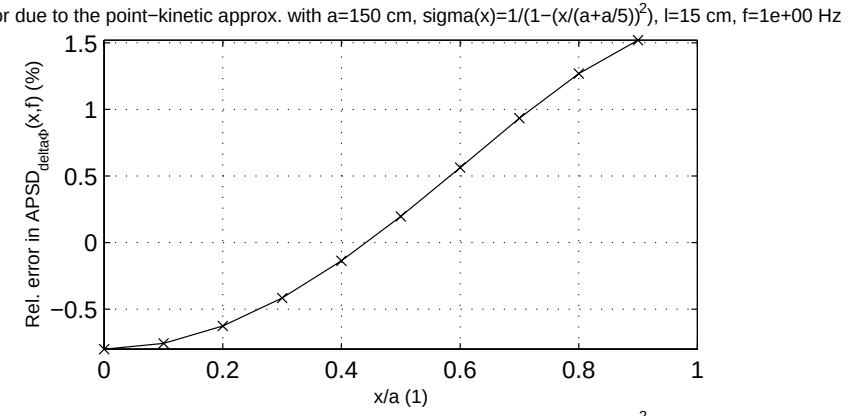
Error due to the point−kinetic approx. with a=150 cm, sigma(x)=1/(1−(x/(a+a/5))^2), l=15 cm, f=1e+00 Hz
Rel. error in APSD_deltaΦ(x,f) (%)
x/a (1)

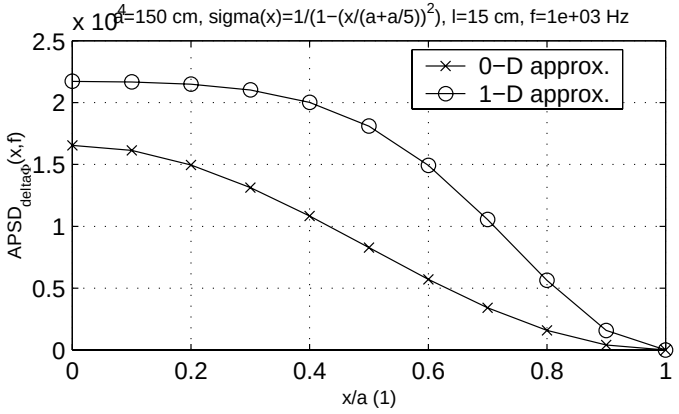
x 10^4
a=150 cm, sigma(x)=1/(1−(x/(a+a/5))^2), l=15 cm, f=1e+03 Hz
0−D approx.
1−D approx.
APSD_deltaΦ(x,f)
x/a (1)

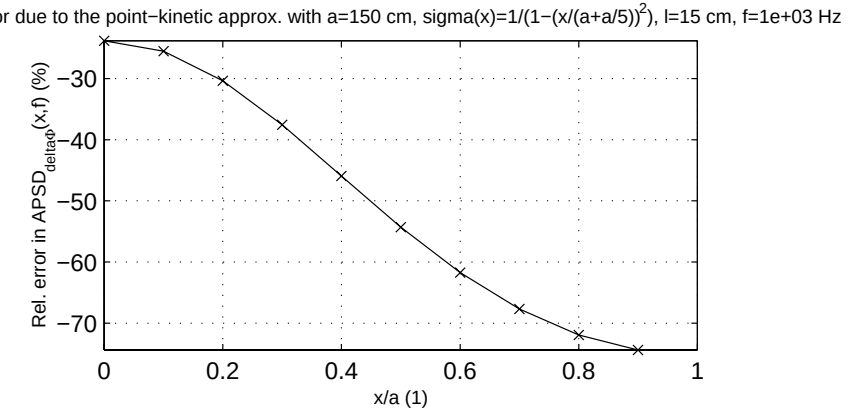
Error due to the point−kinetic approx. with a=150 cm, sigma(x)=1/(1−(x/(a+a/5))^2), l=15 cm, f=1e+03 Hz
Rel. error in APSD_deltaΦ(x,f) (%)
x/a (1)

Fig. 6a

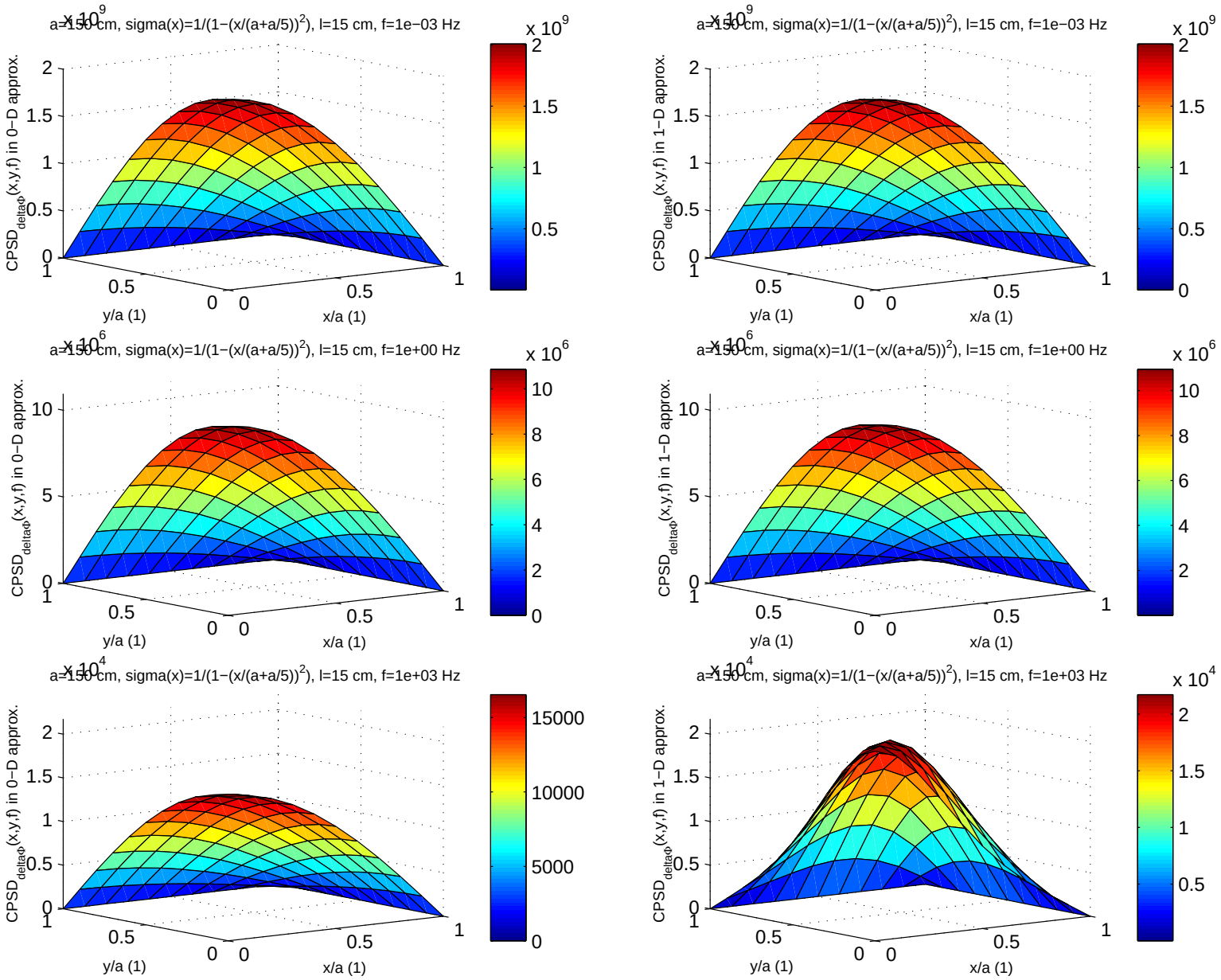
x 10^9
a=150 cm, sigma(x)=1/(1−(x/(a+a/5))^2), l=15 cm, f=1e−03 Hz
CPSD_deltaΦ(x,y,f) in 0−D approx.
y/a (1)
x/a (1)
x 10^9
a=150 cm, sigma(x)=1/(1−(x/(a+a/5))^2), l=15 cm, f=1e−03 Hz
CPSD_deltaΦ(x,y,f) in 1−D approx.
y/a (1)
x/a (1)
x 10^6
a=150 cm, sigma(x)=1/(1−(x/(a+a/5))^2), l=15 cm, f=1e+00 Hz
CPSD_deltaΦ(x,y,f) in 0−D approx.
y/a (1)
x/a (1)
x 10^6
a=150 cm, sigma(x)=1/(1−(x/(a+a/5))^2), l=15 cm, f=1e+00 Hz
CPSD_deltaΦ(x,y,f) in 1−D approx.
y/a (1)
x/a (1)
x 10^4
a=150 cm, sigma(x)=1/(1−(x/(a+a/5))^2), l=15 cm, f=1e+03 Hz
CPSD_deltaΦ(x,y,f) in 0−D approx.
y/a (1)
x/a (1)
x 10^4
a=150 cm, sigma(x)=1/(1−(x/(a+a/5))^2), l=15 cm, f=1e+03 Hz
CPSD_deltaΦ(x,y,f) in 1−D approx.
y/a (1)
x/a (1)

Fig. 6b

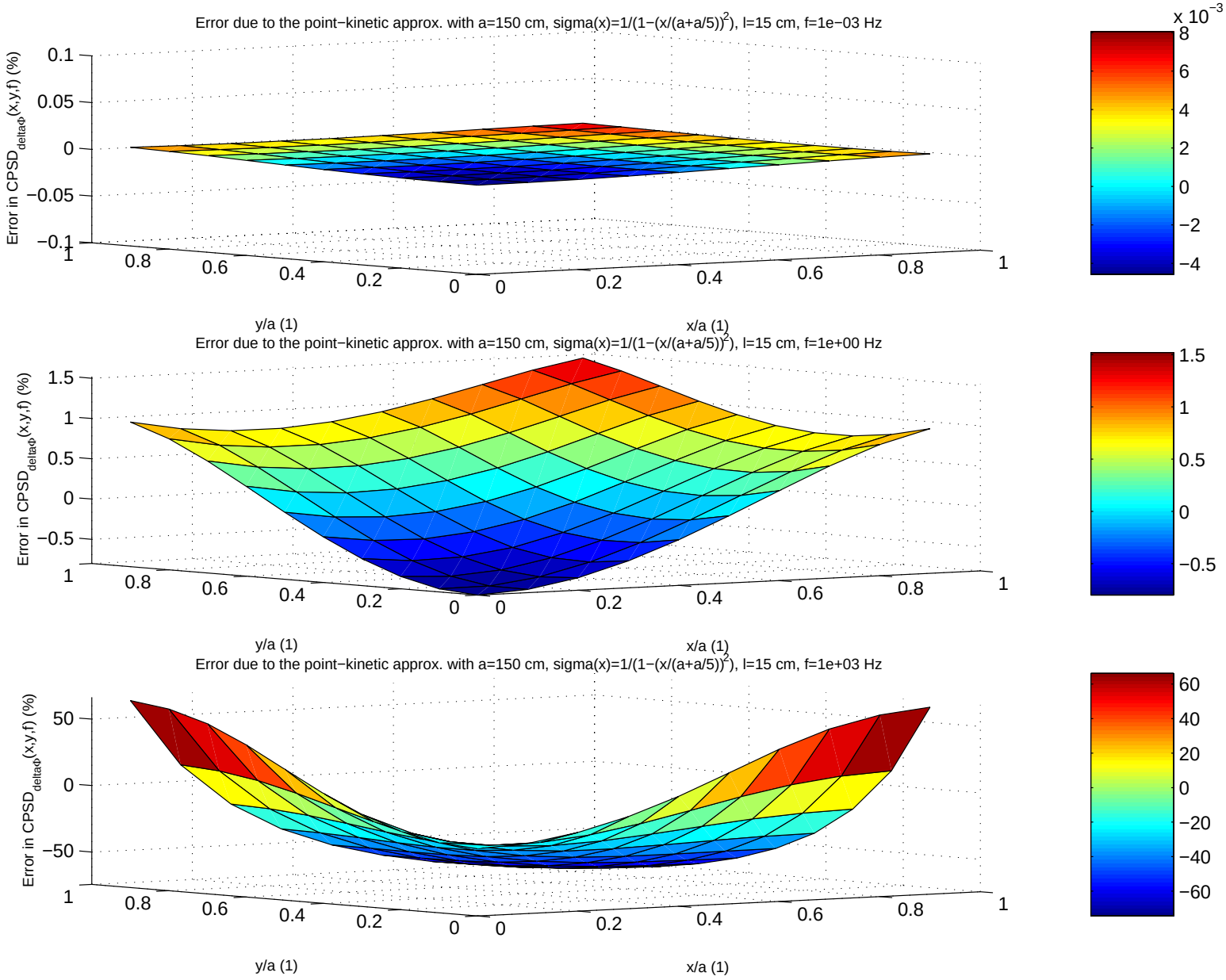
Error due to the point−kinetic approx. with a=150 cm, sigma(x)=1/(1−(x/(a+a/5))^2), l=15 cm, f=1e−03 Hz
Error in CPSD_deltaΦ(x,y,f) (%)
0.1
0.05
0
−0.05
−0.1
y/a (1)
x/a (1)
x 10^−3
8
6
4
2
0
−2
−4
Error due to the point−kinetic approx. with a=150 cm, sigma(x)=1/(1−(x/(a+a/5))^2), l=15 cm, f=1e+00 Hz
Error in CPSD_deltaΦ(x,y,f) (%)
1.5
1
0.5
0
−0.5
y/a (1)
x/a (1)
1.5
1
0.5
0
−0.5
Error due to the point−kinetic approx. with a=150 cm, sigma(x)=1/(1−(x/(a+a/5))^2), l=15 cm, f=1e+03 Hz
Error in CPSD_deltaΦ(x,y,f) (%)
50
0
−50
y/a (1)
x/a (1)
60
40
20
0
−20
−40
−60

Fig. 6c

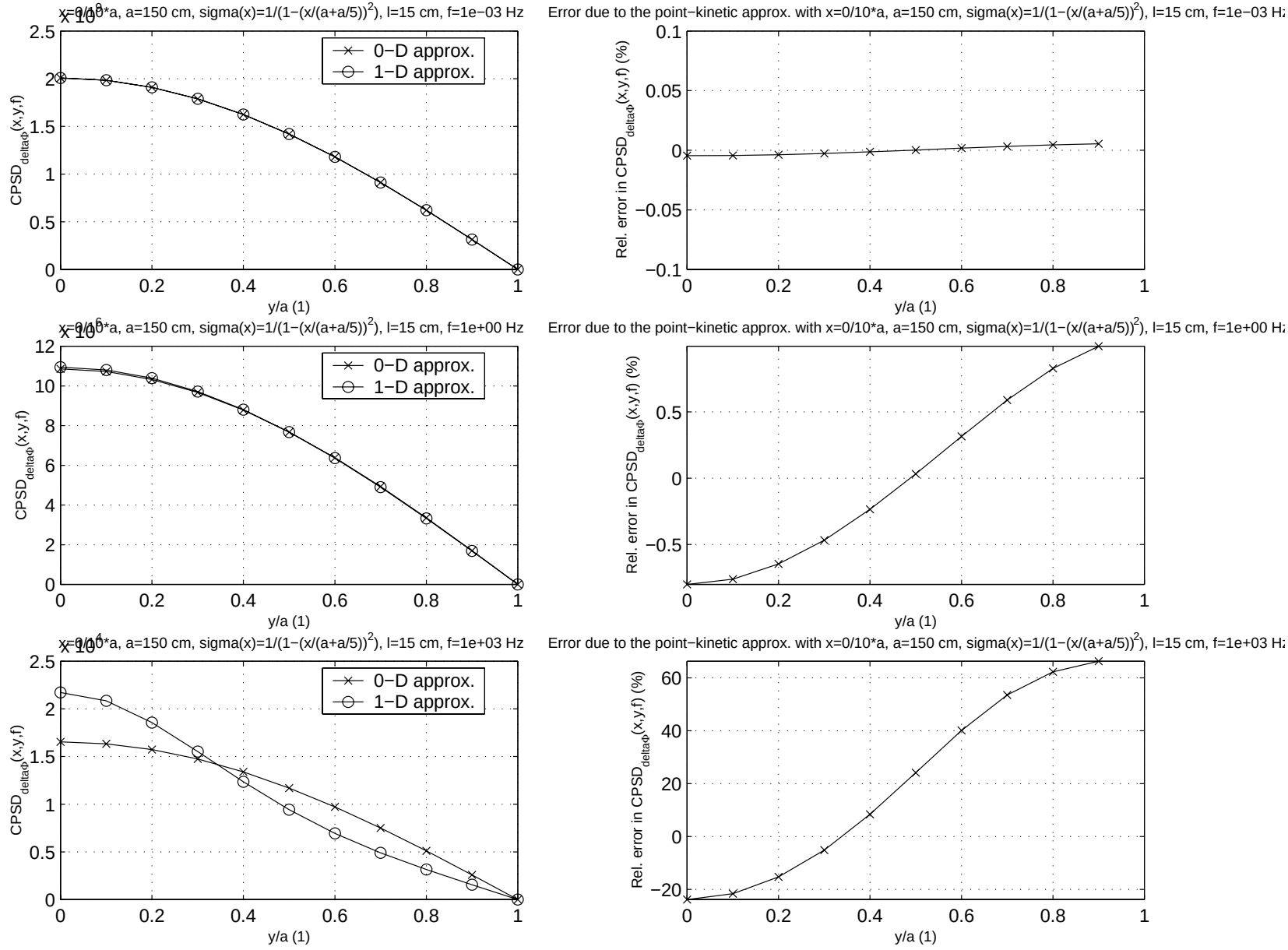
x=0/10*a, a=150 cm, sigma(x)=1/(1−(x/(a+a/5))^2), l=15 cm, f=1e−03 Hz
x 10^8
0−D approx.
1−D approx.
CPSD_deltaΦ(x,y,f)
y/a (1)
Error due to the point−kinetic approx. with x=0/10*a, a=150 cm, sigma(x)=1/(1−(x/(a+a/5))^2), l=15 cm, f=1e−03 Hz
Rel. error in CPSD_deltaΦ(x,y,f) (%)
y/a (1)
x=0/10*a, a=150 cm, sigma(x)=1/(1−(x/(a+a/5))^2), l=15 cm, f=1e+00 Hz
x 10^6
0−D approx.
1−D approx.
CPSD_deltaΦ(x,y,f)
y/a (1)
Error due to the point−kinetic approx. with x=0/10*a, a=150 cm, sigma(x)=1/(1−(x/(a+a/5))^2), l=15 cm, f=1e+00 Hz
Rel. error in CPSD_deltaΦ(x,y,f) (%)
y/a (1)
x=0/10*a, a=150 cm, sigma(x)=1/(1−(x/(a+a/5))^2), l=15 cm, f=1e+03 Hz
x 10^4
0−D approx.
1−D approx.
CPSD_deltaΦ(x,y,f)
y/a (1)
Error due to the point−kinetic approx. with x=0/10*a, a=150 cm, sigma(x)=1/(1−(x/(a+a/5))^2), l=15 cm, f=1e+03 Hz
Rel. error in CPSD_deltaΦ(x,y,f) (%)
y/a (1)

Fig. 6d

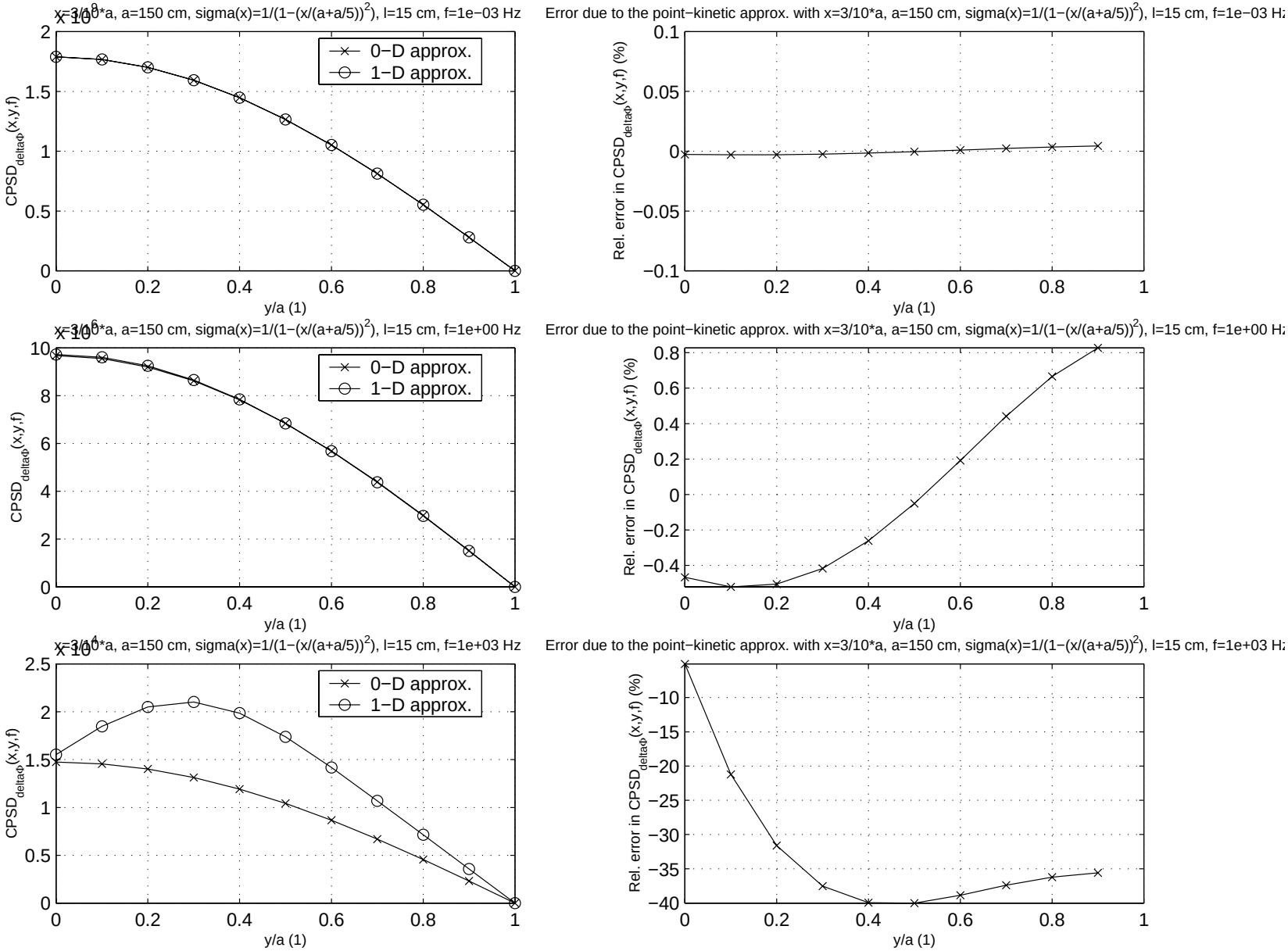
x=3/10*a, a=150 cm, sigma(x)=1/(1−(x/(a+a/5))^2), l=15 cm, f=1e−03 Hz
x 10^8
0−D approx.
1−D approx.
CPSD_deltaΦ(x,y,f)
y/a (1)
Error due to the point−kinetic approx. with x=3/10*a, a=150 cm, sigma(x)=1/(1−(x/(a+a/5))^2), l=15 cm, f=1e−03 Hz
Rel. error in CPSD_deltaΦ(x,y,f) (%)
y/a (1)
x=3/10*a, a=150 cm, sigma(x)=1/(1−(x/(a+a/5))^2), l=15 cm, f=1e+00 Hz
x 10^6
0−D approx.
1−D approx.
CPSD_deltaΦ(x,y,f)
y/a (1)
Error due to the point−kinetic approx. with x=3/10*a, a=150 cm, sigma(x)=1/(1−(x/(a+a/5))^2), l=15 cm, f=1e+00 Hz
Rel. error in CPSD_deltaΦ(x,y,f) (%)
y/a (1)
x=3/10*a, a=150 cm, sigma(x)=1/(1−(x/(a+a/5))^2), l=15 cm, f=1e+03 Hz
x 10^4
0−D approx.
1−D approx.
CPSD_deltaΦ(x,y,f)
y/a (1)
Error due to the point−kinetic approx. with x=3/10*a, a=150 cm, sigma(x)=1/(1−(x/(a+a/5))^2), l=15 cm, f=1e+03 Hz
Rel. error in CPSD_deltaΦ(x,y,f) (%)
y/a (1)

Fig. 6e

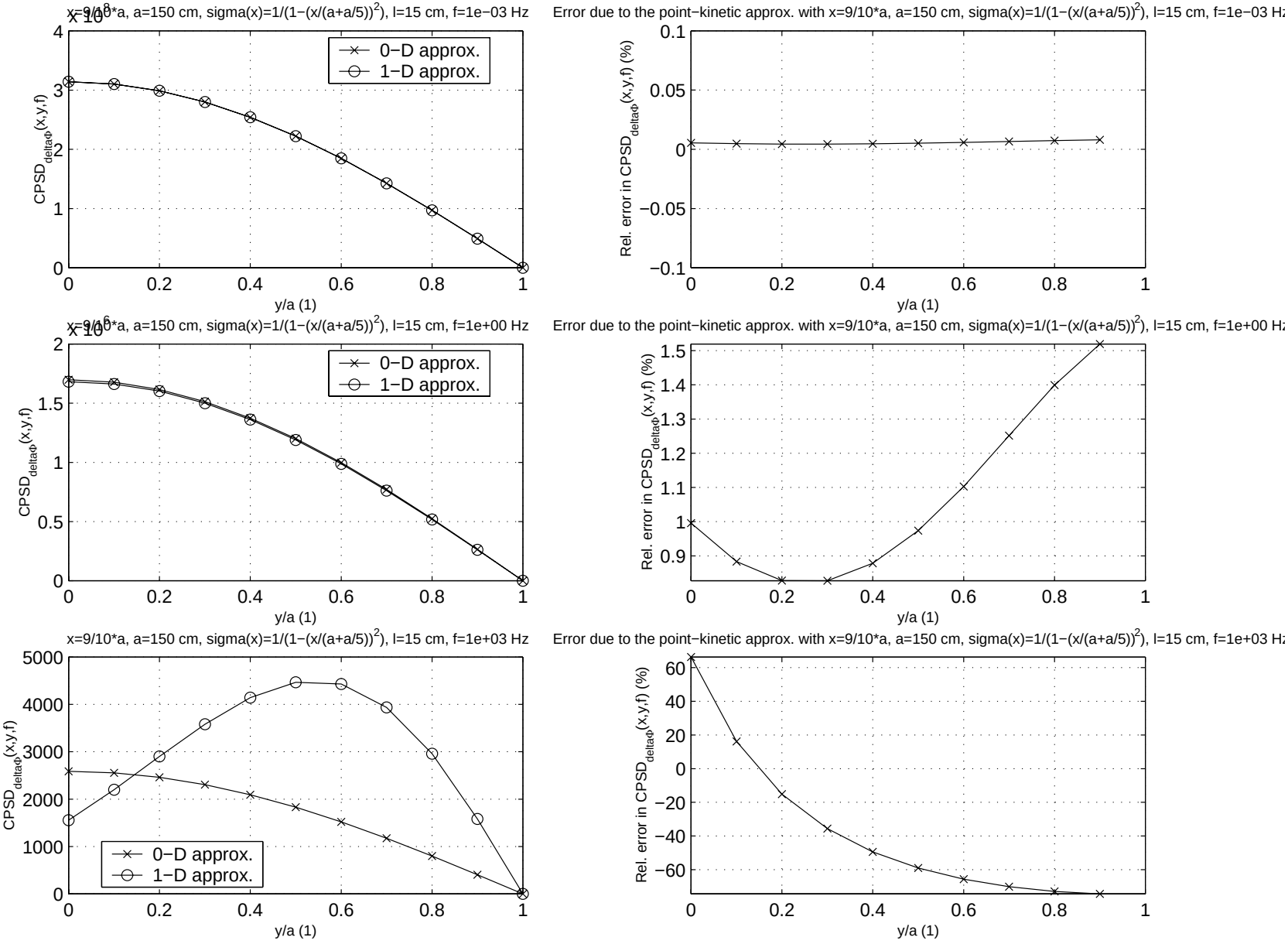
x=9/10*a, a=150 cm, sigma(x)=1/(1−(x/(a+a/5))^2), l=15 cm, f=1e−03 Hz
x 10^8
CPSD_deltaΦ(x,y,f)
0−D approx.
1−D approx.
y/a (1)
Error due to the point−kinetic approx. with x=9/10*a, a=150 cm, sigma(x)=1/(1−(x/(a+a/5))^2), l=15 cm, f=1e−03 Hz
Rel. error in CPSD_deltaΦ(x,y,f) (%)
y/a (1)
x=9/10*a, a=150 cm, sigma(x)=1/(1−(x/(a+a/5))^2), l=15 cm, f=1e+00 Hz
x 10^6
CPSD_deltaΦ(x,y,f)
0−D approx.
1−D approx.
y/a (1)
Error due to the point−kinetic approx. with x=9/10*a, a=150 cm, sigma(x)=1/(1−(x/(a+a/5))^2), l=15 cm, f=1e+00 Hz
Rel. error in CPSD_deltaΦ(x,y,f) (%)
y/a (1)
x=9/10*a, a=150 cm, sigma(x)=1/(1−(x/(a+a/5))^2), l=15 cm, f=1e+03 Hz
CPSD_deltaΦ(x,y,f)
0−D approx.
1−D approx.
y/a (1)
Error due to the point−kinetic approx. with x=9/10*a, a=150 cm, sigma(x)=1/(1−(x/(a+a/5))^2), l=15 cm, f=1e+03 Hz
Rel. error in CPSD_deltaΦ(x,y,f) (%)
y/a (1)

Fig. 6f

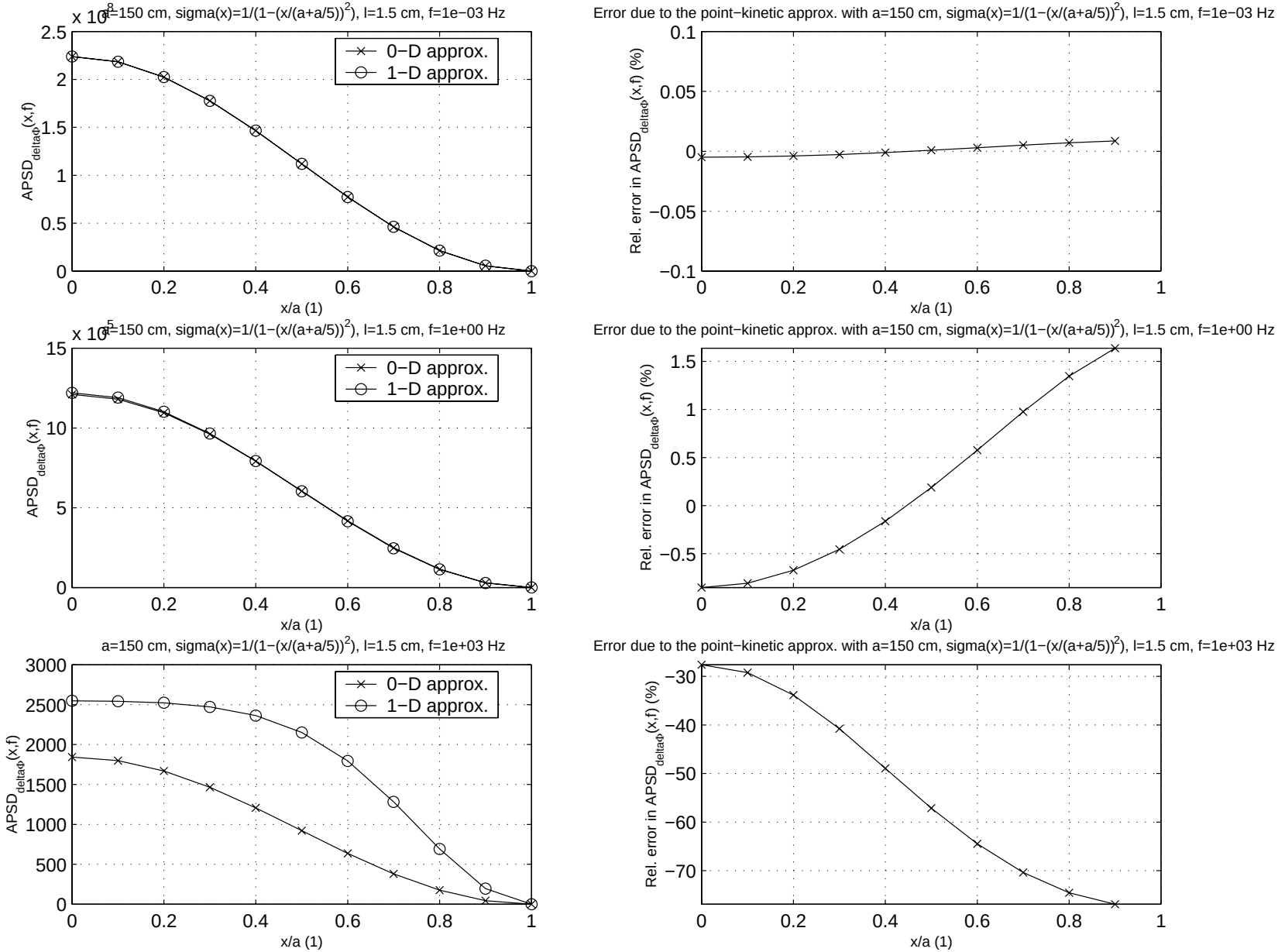
a=150 cm, sigma(x)=1/(1−(x/(a+a/5))^2), l=1.5 cm, f=1e−03 Hz
x 10^8
0−D approx.
1−D approx.
APSD_deltaΦ(x,f)
x/a (1)
Error due to the point−kinetic approx. with a=150 cm, sigma(x)=1/(1−(x/(a+a/5))^2), l=1.5 cm, f=1e−03 Hz
Rel. error in APSD_deltaΦ(x,f) (%)
x/a (1)
a=150 cm, sigma(x)=1/(1−(x/(a+a/5))^2), l=1.5 cm, f=1e+00 Hz
x 10^5
0−D approx.
1−D approx.
APSD_deltaΦ(x,f)
x/a (1)
Error due to the point−kinetic approx. with a=150 cm, sigma(x)=1/(1−(x/(a+a/5))^2), l=1.5 cm, f=1e+00 Hz
Rel. error in APSD_deltaΦ(x,f) (%)
x/a (1)
a=150 cm, sigma(x)=1/(1−(x/(a+a/5))^2), l=1.5 cm, f=1e+03 Hz
0−D approx.
1−D approx.
APSD_deltaΦ(x,f)
x/a (1)
Error due to the point−kinetic approx. with a=150 cm, sigma(x)=1/(1−(x/(a+a/5))^2), l=1.5 cm, f=1e+03 Hz
Rel. error in APSD_deltaΦ(x,f) (%)
x/a (1)

Fig. 7a

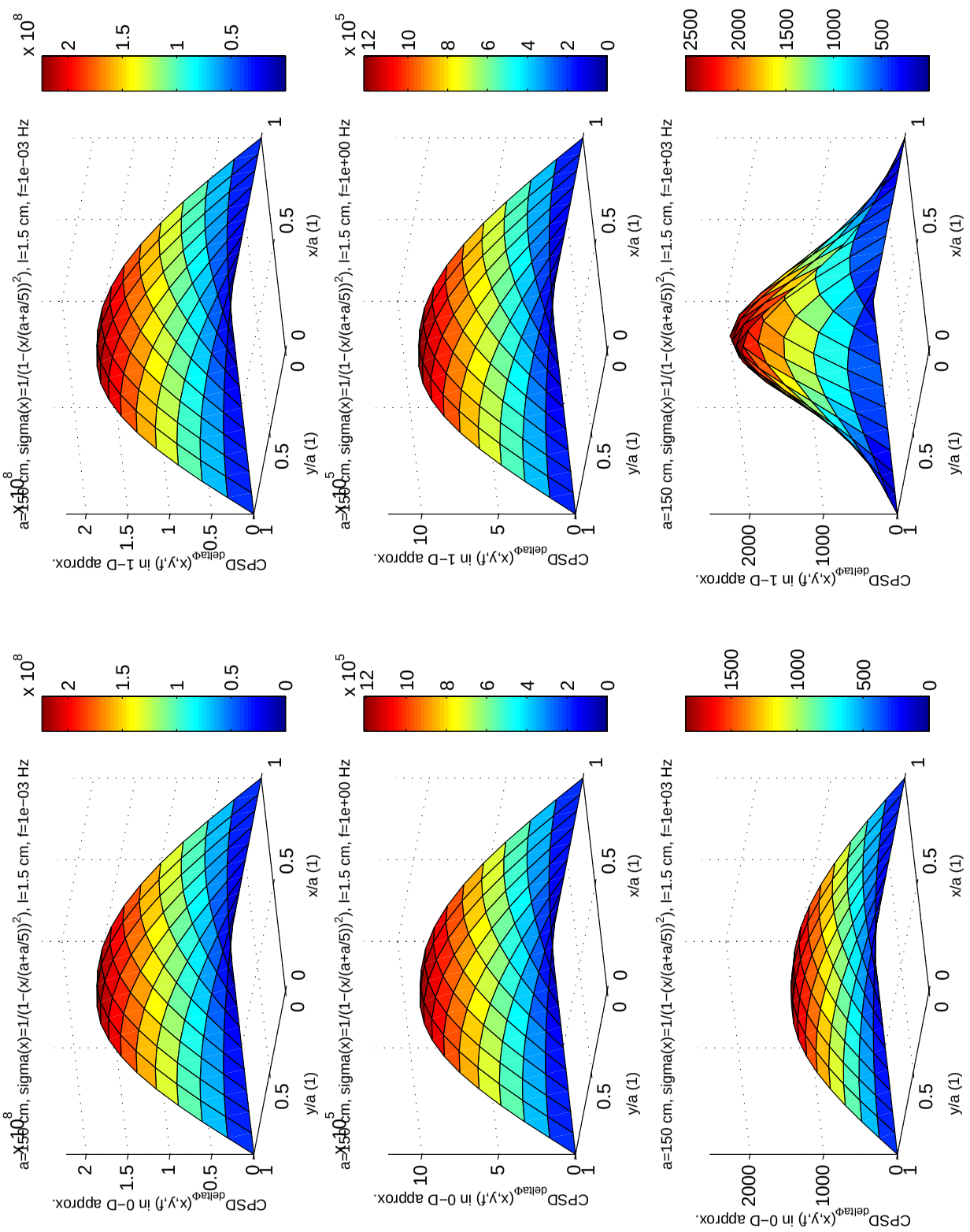
a=150 cm, sigma(x)=1/(1−(x/(a+a/5))^2), l=1.5 cm, f=1e−03 Hz
a=150 cm, sigma(x)=1/(1−(x/(a+a/5))^2), l=1.5 cm, f=1e+00 Hz
a=150 cm, sigma(x)=1/(1−(x/(a+a/5))^2), l=1.5 cm, f=1e+03 Hz
CPSD_deltaΦ(x,y,f) in 0−D approx.
CPSD_deltaΦ(x,y,f) in 1−D approx.
x/a (1)
y/a (1)
x 10^8
x 10^5

Fig. 7b

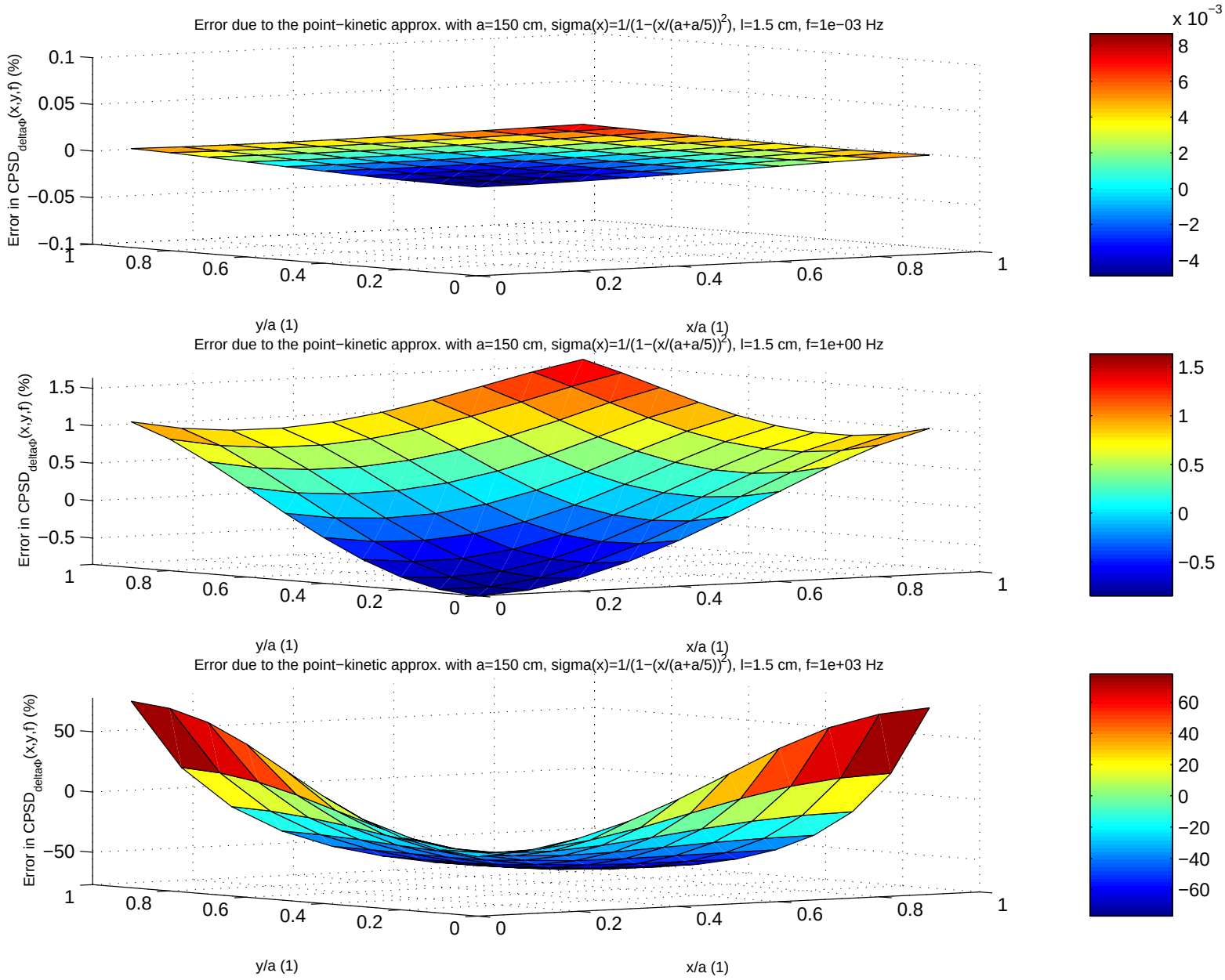
Error due to the point−kinetic approx. with a=150 cm, sigma(x)=1/(1−(x/(a+a/5))^2), l=1.5 cm, f=1e−03 Hz
Error in CPSD_deltaΦ(x,y,f) (%)
0.1
0.05
0
−0.05
−0.1
x 10^−3
8
6
4
2
0
−2
−4
y/a (1)
x/a (1)
Error due to the point−kinetic approx. with a=150 cm, sigma(x)=1/(1−(x/(a+a/5))^2), l=1.5 cm, f=1e+00 Hz
Error in CPSD_deltaΦ(x,y,f) (%)
1.5
1
0.5
0
−0.5
y/a (1)
x/a (1)
Error due to the point−kinetic approx. with a=150 cm, sigma(x)=1/(1−(x/(a+a/5))^2), l=1.5 cm, f=1e+03 Hz
Error in CPSD_deltaΦ(x,y,f) (%)
50
0
−50
60
40
20
0
−20
−40
−60
y/a (1)
x/a (1)

Fig. 7c

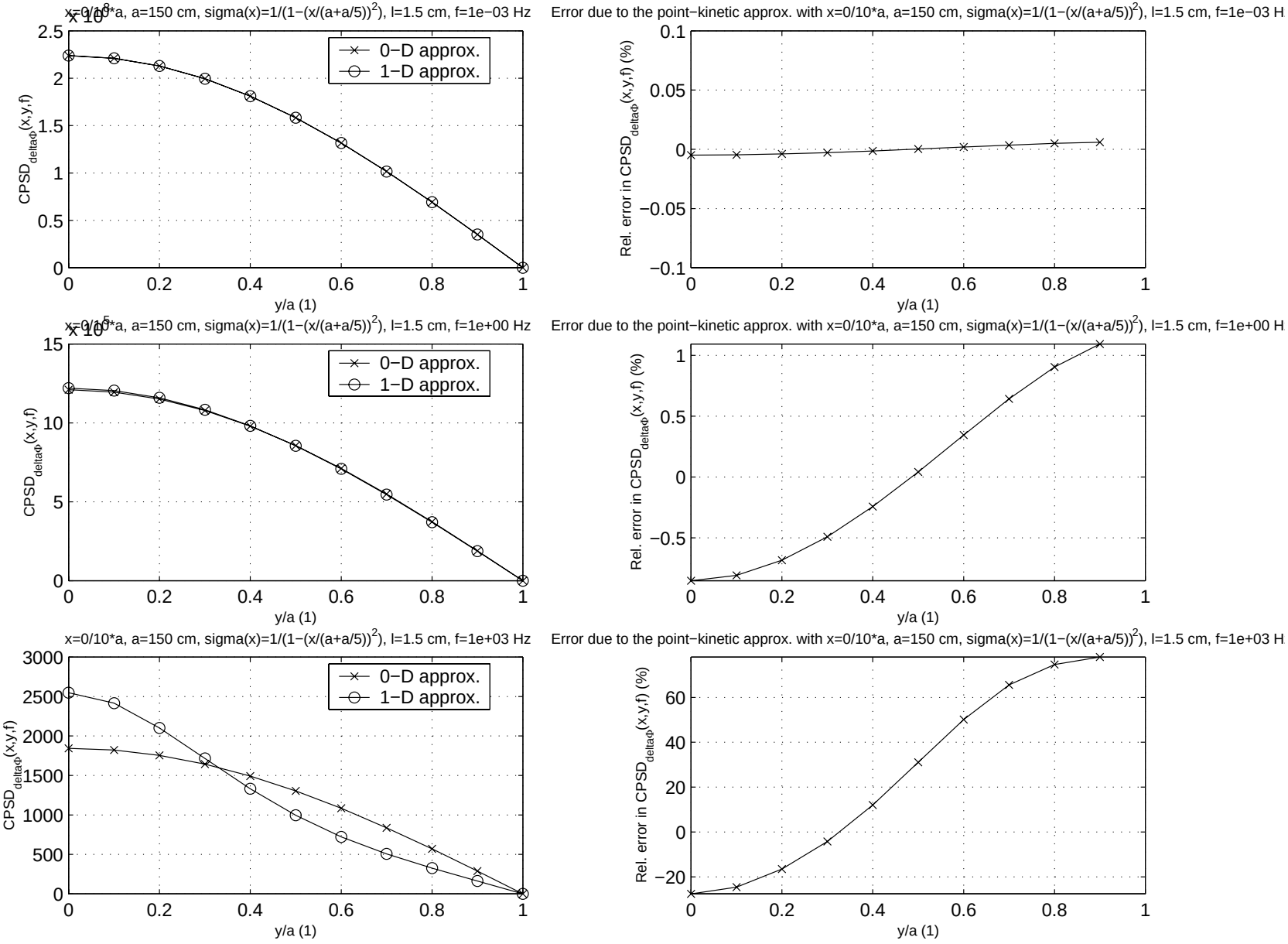
x=0/10*a, a=150 cm, sigma(x)=1/(1−(x/(a+a/5))^2), l=1.5 cm, f=1e−03 Hz
x 10^−8
0−D approx.
1−D approx.
CPSD_deltaΦ(x,y,f)
y/a (1)
Error due to the point−kinetic approx. with x=0/10*a, a=150 cm, sigma(x)=1/(1−(x/(a+a/5))^2), l=1.5 cm, f=1e−03 H
Rel. error in CPSD_deltaΦ(x,y,f) (%)
x=0/10*a, a=150 cm, sigma(x)=1/(1−(x/(a+a/5))^2), l=1.5 cm, f=1e+00 Hz
x 10^−5
Error due to the point−kinetic approx. with x=0/10*a, a=150 cm, sigma(x)=1/(1−(x/(a+a/5))^2), l=1.5 cm, f=1e+00 H
x=0/10*a, a=150 cm, sigma(x)=1/(1−(x/(a+a/5))^2), l=1.5 cm, f=1e+03 Hz
Error due to the point−kinetic approx. with x=0/10*a, a=150 cm, sigma(x)=1/(1−(x/(a+a/5))^2), l=1.5 cm, f=1e+03 H

Fig. 7d

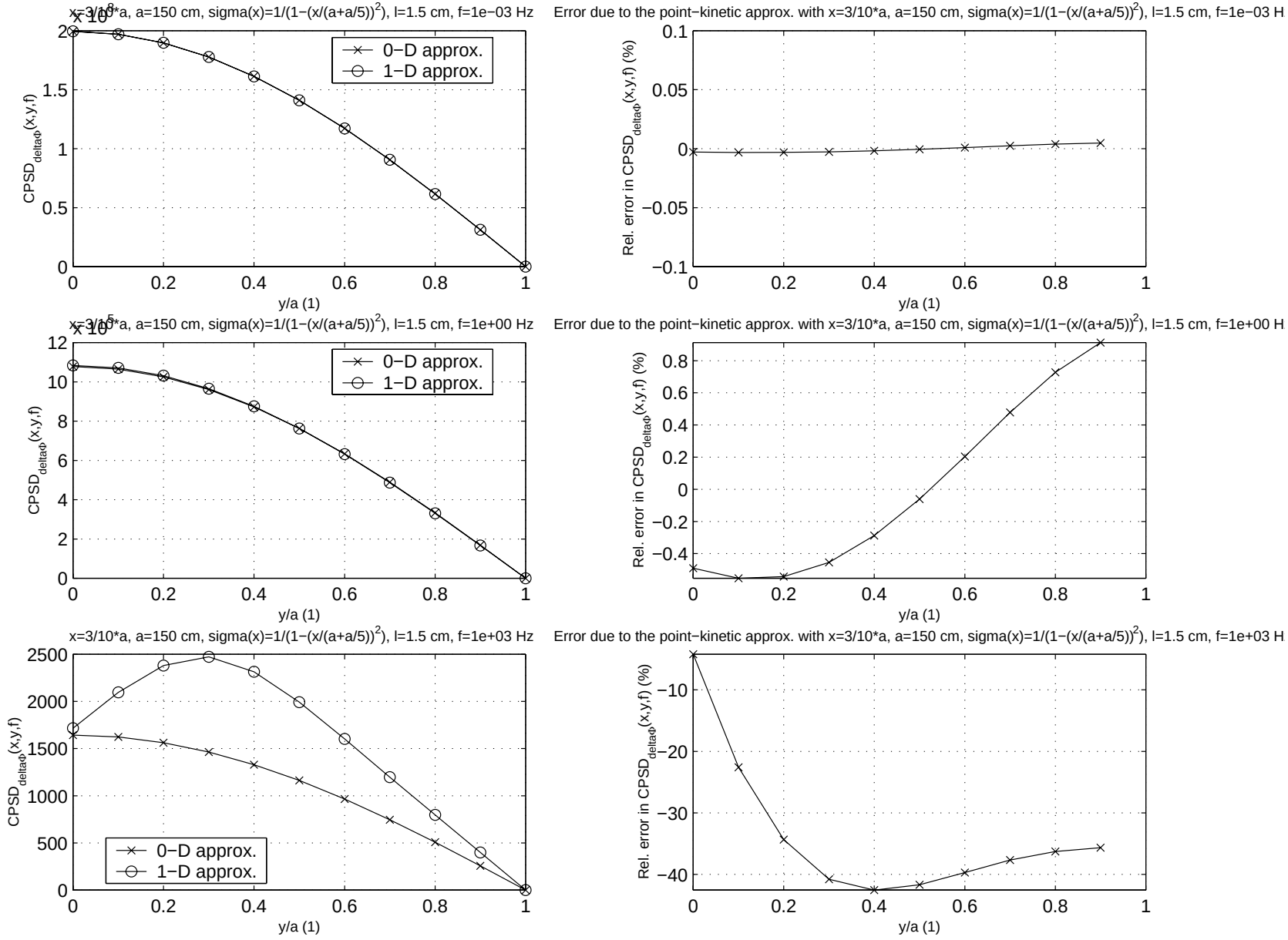
x=3/10*a, a=150 cm, sigma(x)=1/(1−(x/(a+a/5))^2), l=1.5 cm, f=1e−03 Hz
x 10^8
0−D approx.
1−D approx.
CPSD_deltaΦ(x,y,f)
y/a (1)
Error due to the point−kinetic approx. with x=3/10*a, a=150 cm, sigma(x)=1/(1−(x/(a+a/5))^2), l=1.5 cm, f=1e−03 H
Rel. error in CPSD_deltaΦ(x,y,f) (%)
y/a (1)
x=3/10*a, a=150 cm, sigma(x)=1/(1−(x/(a+a/5))^2), l=1.5 cm, f=1e+00 Hz
x 10^5
0−D approx.
1−D approx.
CPSD_deltaΦ(x,y,f)
y/a (1)
Error due to the point−kinetic approx. with x=3/10*a, a=150 cm, sigma(x)=1/(1−(x/(a+a/5))^2), l=1.5 cm, f=1e+00 H
Rel. error in CPSD_deltaΦ(x,y,f) (%)
y/a (1)
x=3/10*a, a=150 cm, sigma(x)=1/(1−(x/(a+a/5))^2), l=1.5 cm, f=1e+03 Hz
0−D approx.
1−D approx.
CPSD_deltaΦ(x,y,f)
y/a (1)
Error due to the point−kinetic approx. with x=3/10*a, a=150 cm, sigma(x)=1/(1−(x/(a+a/5))^2), l=1.5 cm, f=1e+03 H
Rel. error in CPSD_deltaΦ(x,y,f) (%)
y/a (1)

Fig. 7e

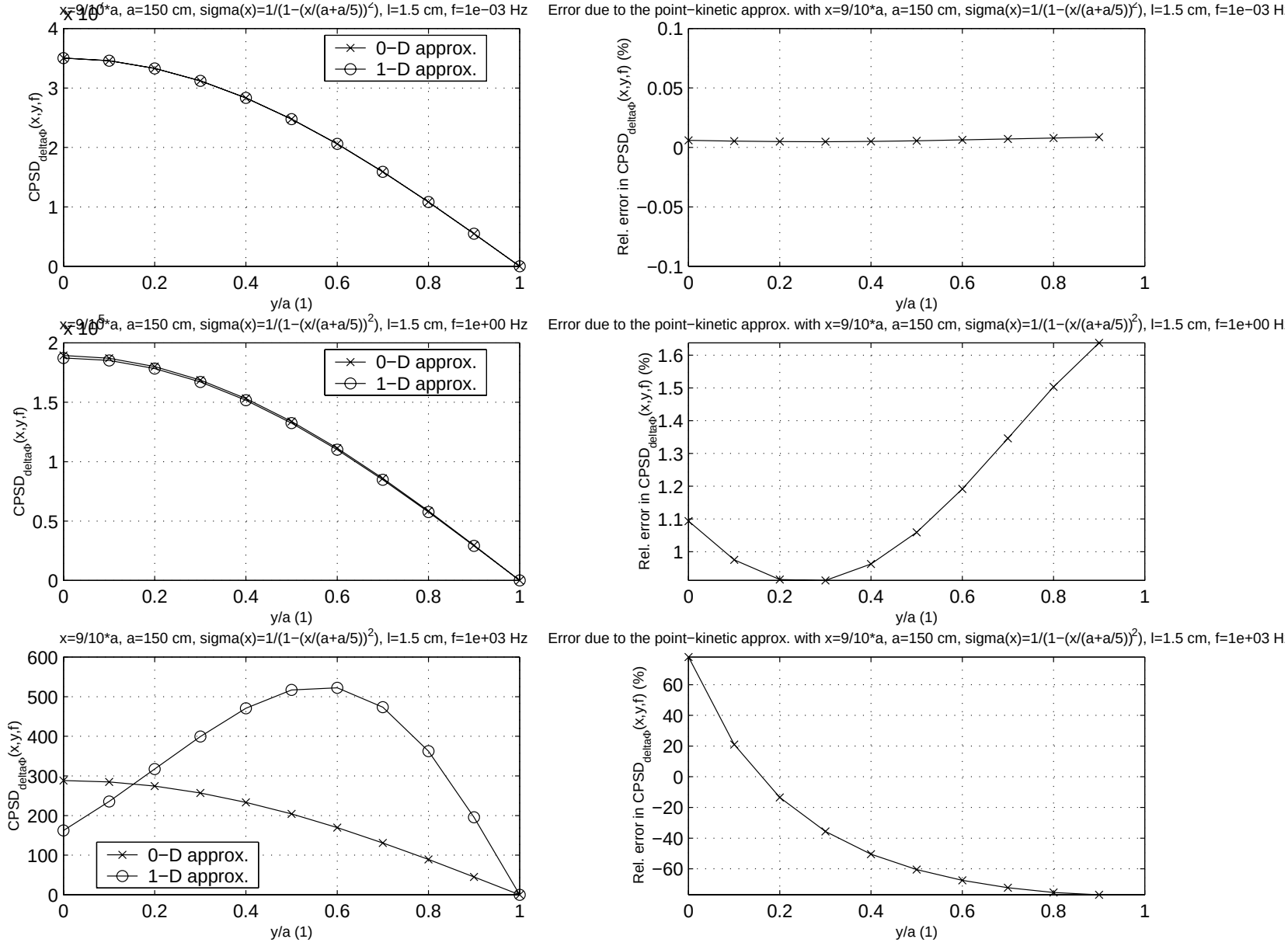
x=9/10*a, a=150 cm, sigma(x)=1/(1−(x/(a+a/5))^4), l=1.5 cm, f=1e−03 Hz
x 10^4
0−D approx.
1−D approx.
CPSD_deltaΦ(x,y,f)
y/a (1)
Error due to the point−kinetic approx. with x=9/10*a, a=150 cm, sigma(x)=1/(1−(x/(a+a/5))^4), l=1.5 cm, f=1e−03 H
Rel. error in CPSD_deltaΦ(x,y,f) (%)
y/a (1)
x=9/10*a, a=150 cm, sigma(x)=1/(1−(x/(a+a/5))^2), l=1.5 cm, f=1e+00 Hz
x 10^5
0−D approx.
1−D approx.
CPSD_deltaΦ(x,y,f)
y/a (1)
Error due to the point−kinetic approx. with x=9/10*a, a=150 cm, sigma(x)=1/(1−(x/(a+a/5))^2), l=1.5 cm, f=1e+00 H
Rel. error in CPSD_deltaΦ(x,y,f) (%)
y/a (1)
x=9/10*a, a=150 cm, sigma(x)=1/(1−(x/(a+a/5))^2), l=1.5 cm, f=1e+03 Hz
0−D approx.
1−D approx.
CPSD_deltaΦ(x,y,f)
y/a (1)
Error due to the point−kinetic approx. with x=9/10*a, a=150 cm, sigma(x)=1/(1−(x/(a+a/5))^2), l=1.5 cm, f=1e+03 H
Rel. error in CPSD_deltaΦ(x,y,f) (%)
y/a (1)

Fig. 7f